



저작자표시-비영리-변경금지 2.0 대한민국

이용자는 아래의 조건을 따르는 경우에 한하여 자유롭게

- 이 저작물을 복제, 배포, 전송, 전시, 공연 및 방송할 수 있습니다.

다음과 같은 조건을 따라야 합니다:



저작자표시. 귀하는 원저작자를 표시하여야 합니다.



비영리. 귀하는 이 저작물을 영리 목적으로 이용할 수 없습니다.



변경금지. 귀하는 이 저작물을 개작, 변형 또는 가공할 수 없습니다.

- 귀하는, 이 저작물의 재이용이나 배포의 경우, 이 저작물에 적용된 이용허락조건을 명확하게 나타내어야 합니다.
- 저작권자로부터 별도의 허가를 받으면 이러한 조건들은 적용되지 않습니다.

저작권법에 따른 이용자의 권리는 위의 내용에 의하여 영향을 받지 않습니다.

이것은 [이용허락규약\(Legal Code\)](#)을 이해하기 쉽게 요약한 것입니다.

[Disclaimer](#)

Doctor of Philosophy

**An Investigation on Spray Combustion Characteristics of
Gasoline Compression Ignition Engine using Constant Volume
Combustion Chamber system**

**The Graduate School of
the University of Ulsan
Department of Mechanical Engineering
Nguyen Ho Xuan Duy**

**An Investigation on Spray Combustion Characteristics of
Gasoline Compression Ignition Engine using Constant Volume
Combustion Chamber system**

Supervisor: Prof. Ock Taeck Lim

A Dissertation

Submitted to

The Graduate School of the University of Ulsan

In partial Fulfillment of the Requirements

for the Degree of

Doctor of Philosophy

by

Nguyen Ho Xuan Duy


Department of Mechanical Engineering

University of Ulsan, Republic of Korea

June 2024

An Investigation on Spray Combustion Characteristics of Gasoline Compression Ignition Engine using Constant Volume Combustion Chamber system

This certifies that the dissertation of Nguyen Ho Xuan Duy is approved.



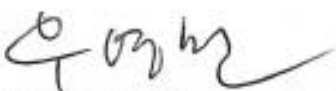
Committee Chair Prof. Kyu Yeol Park



Committee Member Assoc. Prof. Kyoung Sik Chang



Committee Member Assist. Prof. Yoon Ho Lee



Committee Member Dr. Young Min Woo



Committee Member Prof. Ock Taek Lim

Department of Mechanical Engineering
University of Ulsan

June 2024

ABSTRACT

An Investigation on Spray Combustion Characteristics of Gasoline Compression Ignition Engine using Constant Volume Combustion Chamber system

Department of Mechanical Engineering

Nguyen Ho Xuan Duy

The research of multiphase spray combustion in the gasoline compression ignition (GCI) engine conditions is carried out under constant volume combustion system (CVCC). Experiments were performed on a CVCC system to investigate the phenomena of the combustion process through simulated conditions of a diesel engine. In addition, the optical system is applied with the CVCC system to collect images of the combustion process with high data acquisition speed. The GB fuel mixtures applied in this study included varying the volume of biodiesel content in the mixture from 0, 10%, 20% and 40%. The main goal of the research is to provide comprehensive parameters for the GCI engine research process and consider the stable application of gasoline-biodiesel mixtures with the operating conditions of GCI engines in different levels.

The non-vaporizing spray process has proven that the trends and rules of the spray formation process are not much different from those of basic fuels. At the same time, it also determines the influence of injection pressure and ambient density on spray morphology. Besides, the influence of chamber temperature is also mentioned and evaluated to affect the spray characteristics. Temperature has a special impact on spray cone angle when varying at high levels. It also shows the opposite trend for the effect on spray angle in studies related to the spray combustion process.

In the next stage, the spray vaporization process is applied to evaluate the characteristics of the spray more thoroughly in a high temperature environment up to 1000K. The trends of liquid and vapor areas are determined to be inversely proportional to each other when the spray impinge on the wall.

Finally, the combustion process is carried out with the change of important boundary conditions. The injection break time and ignition delay are identified to have a close relationship to determine the diffusion combustion process taking place under normal conditions. The results across the non-vaporizing spray, vaporization and combustion processes also indicate that gasoline fuel mixtures with high octane ratings will give more favorable results with the biodiesel component in the mixture less than 20%.

Keywords: Gasoline-biodiesel, Injection pressure, Spray characteristics, Spray penetration length, spray cone angle, spray area, CVCC, Temperature, Oxygen concentration, Heat released rate, Ignition delay, flame development, high-octane fuel.

ACKNOWLEDGEMENT

First of all, I would like to express my deep gratitude to my supervisor, Professor Ock Taeck Lim, who has always supported and created many opportunities for me throughout this research process. His contributions and encouragement helped me a lot to complete my doctoral research. I have always appreciated his professionalism, warmth and sympathy for me and all members of the laboratory. I will always remember throughout my life this beautiful time. I would like to thank the Graduate School of Mechanical and Automotive Engineering, University of Ulsan.

I would like to thank Prof. Huynh Thanh Cong who created opportunities and supported me during my PhD program at the University of Ulsan.

I would like to express my sincerest thanks to my colleagues at Smart Powertrain Laboratory who have been with me on this journey. Special thanks to Ho Chi Minh City University of Technology for providing the opportunity, approval and support for me to pursue my doctor program at the University of Ulsan.

I would like to express my gratitude to those who have been by my side and encouraged me during difficult times in my life. Thank you to my beautiful love for her patience and understanding and the inevitability to support me until this path becomes a reality.

Finally, I would like to thank my family for their great sacrifices for my life and my growth. Thank you to my father in heaven, he has had an honorable life and has tried to educate me to be a kind person. Thank you to my mother for giving me the dream and tenacity to be able to walk until today. Thank you to my brother for trying to take care of my family while I pursued my career path. Thank you to my sister and my nieces for motivating me so much.

I cannot find the right words to fully express my appreciation for everyone's support, belief, and hope in my ability to achieve my goals. Thanks for this journey that has given me many lessons to be able to walk firmly and have a good soul in the present and the future.

TABLE OF CONTENTS

LIST OF TABLES	ix
LIST OF FIGURES	x
ABBREVIATION AND NOMENCLATURES.....	xiii
1. Introduction	1
1.1 Motivation.....	1
1.2 Approach.....	4
1.3 Objective.....	5
1.4 Thesis outline.....	6
2. Literature review.....	9
2.1 GCI engine technology	9
2.1.1 GCI concept	9
2.1.2 Opportunities and challenges associated with GCI	11
2.2 Macroscopic spray	13
2.2.1 Schlieren method	13
2.2.2 Shadowgraph method.....	14
2.3 Ignition delay and flame development.....	15
2.3.1 Ignition delay	15
2.3.2 Measurement of ignition delay	17
2.3.3 Factors affecting ignition delay	18
2.3.4 Natural luminosity for flame development.....	20
2.4 Fuel	21
2.4.1 Overview of existing transportation fuel options.....	21
2.4.2 Alternatives to conventional fuels	22
2.4.3 Biodiesel fuel	23
2.5 Summary.....	24
3. Experiment setup and methodology	26
3.1 CVCC System.....	26
3.1.1 Constant Volume Combustion Chamber	26
3.1.2 Supply and Exhaust System.....	30
3.2 Data acquisition and control system	31
3.2.1 Control system	32
3.2.2 Data acquisition system	33
3.2.3 Control program.....	34

3.3	Fuel supply system.....	38
3.4	Pressure trace	38
3.5	Optical diagnostic system	40
3.6	Image processing	40
4.	A study on spray characteristic of gasoline-biodiesel blended under GCI engines condition performed on constant volume combustion chamber system.....	42
4.1	Spray development.....	42
4.2	Spray tip penetration	44
4.3	Spray cone angle	46
4.4	Spray area.....	52
4.5	Summary	54
5.	An investigation of the effect of chamber temperature on macroscopic spray characteristic under GCI engine conditions.....	56
5.1	Spray evolution process of gasoline-biodiesel fuel blended.....	57
5.2	Spray penetration length	58
5.3	Spray penetration rate	63
5.4	Spray cone angle	66
5.5	Spray area.....	70
5.6	Summary	72
6.	Experimental analysis of high-temperature effects on vaporization spray characteristics in GCI engine conditions	74
6.1	Methodology	74
6.2	Spray morphology.....	76
6.3	Liquid penetration length.....	77
6.4	Liquid area	79
6.5	Vaporization area	81
6.6	Summary	82
7.	Experimental study of spray combustion phenomena in gasoline-biodiesel blends for GCI engine conditions	83
7.1	Spray evolution	83
7.2	Pressure and heat released rate	85
7.3	Ignition delay	86
7.4	Flame development.....	87
7.5	Summary	88
8.	Conclusions	90

References.....	94
Appendices.....	103
List of Publications	103
List of conferences.....	104
Image processing code.....	105

LIST OF TABLES

Table 2.1: Biodiesel standards around the world.....	23
Table 3.1: An overall information of the test system and additional equipment.....	30
Table 3.2: Technical data of pressure sensor.....	39
Table 3.3: Technical data of pressure sensor.....	39
Table 3.4: Camera specifications.....	40
Table 5.1: Experimental boundary conditions and error.....	59
Table 5.2: Spray breakup time for GB20 under ambient densities of 15kg/m^3 and 30kg/m^3 ..	59
Table 6.1: Experimental test matrix.....	75
Table 6.2: Experimental boundary conditions and error.....	75

LIST OF FIGURES

Figure 2.1: Advantages of GCI engine technology	12
Figure 2.2: Challenges for GCI engine technology	12
Figure 2.3: Principle of Schlieren technique.....	14
Figure 2.4: Schematic of the experimental setup for Shadowgraph of dense sprays in a CVCC [44].....	14
Figure 2.5: Ignition delay of reference fuels of varying cetane number.....	19
Figure 2.6: Effect flowchart of the potential parameters on spray combustion with engines fueled with gasoline-biodiesel blends	25
Figure 3.1: Assembled CVCC with different test equipment	27
Figure 3.2: Exploded view of the CVCC with quartz.....	28
Figure 3.3: Schematic of the CVCC apparatus implemented in the experiments	29
Figure 3.4: Pictorial layout of experimental test bench	29
Figure 3.5: Schematic diagram of supply and exhaust system	31
Figure 3.6: Schematic of control and data acquisition system.....	32
Figure 3.7: Schematic diagram of control system	33
Figure 3.8: Schematic diagram of data acquisition system.....	33
Figure 3.9: Control-flow diagram	34
Figure 3.10: Schematic diagram of sequence of filling gases	35
Figure 3.11: Pressure in the combustion chamber when knocking	36
Figure 3.12: Sequence of diagnosis	36
Figure 3.13: Pictorial representation of fuel injection system	38
Figure 3.14: Optical arrangement for the broadband natural luminosity technique.....	40
Figure 3.15: Definition of spray vaporization characteristics.....	41
Figure 4.1: Spray development of fuel GB10, GB20, and GB40 at injection pressure of 80 Mpa, injection duration 1500 μ s with chamber density of 20 kg/m^3	43
Figure 4.2: Comparison of spray penetration length temporal evolution of all tested fuels at 10 kg/m^3 , 20 kg/m^3 , and 30 kg/m^3 under injection pressure of 40, 60, 80, and 100 MPa with 1200-1500 μ s injection duration.	45
Figure 4.3: Comparison of spray cone angle temporal evolution of all tested fuels at 10 kg/m^3 , 20 kg/m^3 , and 30 kg/m^3 under injection pressure of 40 MPa with 1200-1500 μ s injection duration.	48
Figure 4.4: Comparison of spray cone angle temporal evolution of all tested fuels at 10 kg/m^3 , 20 kg/m^3 , and 30 kg/m^3 under injection pressure of 60 MPa with 1200-1500 μ s injection duration.	49

Figure 4.5: Comparison of spray cone angle temporal evolution of all tested fuels at 10 kg/m ³ , 20 kg/m ³ , and 30 kg/m ³ under injection pressure of 80 MPa with 1200-1500 μs injection duration.	50
Figure 4.6: Comparison of spray cone angle temporal evolution of all tested fuels at 10 kg/m ³ , 20 kg/m ³ , and 30 kg/m ³ under injection pressure of 100 MPa with 1200-1500 μs injection duration.	51
Figure 4.7: Comparison of spray area temporal evolution of all tested fuels at 10 kg/m ³ , 20 kg/m ³ , and 30 kg/m ³ under injection pressure of 40, 60, 80 and 100 MPa with 1200-1500 μs injection duration.	53
Figure 5.1: Comparison of spray evolution for injector angles of 90° and 180° at chamber temperatures of 323K and 473K, injection pressure of 110 MPa and gas ambient density of 30 kg/m ³	58
Figure 5.2: Temporal evolution in spray penetration length for injector angles of 90° and 180° at 15 kg/m ³ with 50, 80, and 100 MPa of injection pressure and chamber temperatures of 323K-398K and 423K.	61
Figure 5.3: Temporal evolution in spray penetration length for injector angles of 90° and 180° at 30 kg/m ³ with 50, 80, and 100 MPa of injection pressure and chamber temperatures of 323K-398K and 423K.	62
Figure 5.4: Temporal evolution in spray penetration rate for injector angles of 90° and 180° at 15 kg/m ³ with 50, 80, and 100 MPa of injection pressure and chamber temperatures of 323K-398K and 423K.	64
Figure 5.5: Temporal evolution in spray penetration rate for injector angles of 90° and 180° at 30 kg/m ³ with 50, 80, and 100 MPa of injection pressure and chamber temperatures of 323K-398K and 423K.	65
Figure 5.6: Temporal evolution in spray cone angle for injector angles of 90° and 180° at 15 kg/m ³ with 50, 80, and 100 MPa of injection pressure and chamber temperatures of 323K-398K and 423K.	68
Figure 5.7: Temporal evolution in spray cone angle for injector angles of 90° and 180° at 30 kg/m ³ with 50, 80, and 100 MPa of injection pressure and chamber temperatures of 323K-398K and 423K.	69
Figure 5.8: The trade-off of spray penetration length and spray cone angle during the spray process at 90° and 180° injector angle and 30 kg/m ³ under 50, 80 and 100 MPa of injection pressure at 423K chamber temperature.	70
Figure 5.9: Temporal evolution in spray area for injector angles of 90° and 180° at 30 kg/m ³ with 50, 80, and 100 MPa of injection pressure and chamber temperatures of 323K-398K and 423K.	71
Figure 5.10: Temporal evolution in spray area for injector angles of 90° and 180° at 30 kg/m ³ with 50, 80, and 100 MPa of injection pressure and chamber temperatures of 323 K-398 K and 423 K.	72
Figure 6.2: Definition of spray vaporization characteristics.	76

Figure 6.3: Schlieren image sequences for different ambient temperature of GB20 and GB40 at 110 MPa injection pressure and 10 kg/m ³ ambient density	77
Figure 6.4: Liquid penetration length for GB20 and GB40 at 600 K to 1000 K ambient temperature and 10 kg/m ³ ambient gas density under 50, 80 and to 110 MPa injection pressures.....	78
Figure 6.5: Spray angle for GB20 and GB40 at 600 K to 1000 K ambient temperature and 10 kg/m ³ ambient gas density under 50, 80 and to 110 MPa injection pressures.....	Error!
Bookmark not defined.	
Figure 6.6: Liquid area for GB20 and GB40 at 600 K to 1000 K ambient temperature and 10 kg/m ³ ambient gas density under 50, 80 and to 110 MPa injection pressures.....	80
Figure 6.7: Vapor for GB20 and GB40 at 600 K to 1000 K ambient temperature and 10 kg/m ³ ambient gas density under 50, 80 and to 110 MPa injection pressures.	81
Figure 7.1: Spray evolution under 70 MPa injection pressure of GB00, GB10 and GB20 with 10 kg/m ³ of gas density.....	84
Figure 7.2: Spray evolution under 70 MPa injection pressure of GB00, GB10 and GB20 with 15 kg/m ³ of gas density.....	85
Figure 7.5: Heat release rate for GB blends fuel at 900 K and 1000 K ambient temperature under ambient density 15 kg/m ³ and 90 MPa injection pressure.....	86
Figure 7.6: Ignition delay of GB fuel blend at 900 K and 1000 K of ambient temperature and 90 MPa injection pressure under 15 kg/m ³ ambient density.....	87
Figure 7.7: Flame development of GB00, GB10 and GB20 under the temperature of 900K and 90MPa of injection pressure under 15kg/m ³ ambient density	88
Figure 7.8: Flame development of GB00, GB10 and GB20 under the temperature of 1000K and 90MPa of injection pressure under 15kg/m ³ ambient gas density	88

ABBREVIATION AND NOMENCLATURES

CI. Compression ignition

CO. Carbon monoxide

NO_x. Nitrogen oxide

HC. Hydrocarbons

PM. Particulate matter

LTC. Low-temperature combustion

DGC. Dilute gasoline combustion

CDC. Clean diesel combustion

EGR. Exhaust gas recirculation.

GCI. Gasoline compression ignition

GB. Gasoline-biodiesel

ID. Ignition delay

HRR. Heat release rate

CVCC. Constant volume combustion chamber

TDC. Top dead center

CN. Cetane number

PRR. Pressure rise rate

HCCI. Homogeneous charge compression ignition

PRR. Pressure rise rate

GTL. Gas to liquid

1. Introduction

1.1 Motivation

Since their inception, compression ignition (CI) engines have been recognized for their robustness and high fuel efficiency [1] [2] [3] [4]. Advances in control technology have mitigated the early issues of elevated noise and maintenance expenses, making CI engines widely used for mobile propulsion in vehicles, power generation, and construction machinery. To comply with stricter emission standards and address the rising fuel demand and diminishing fuel supplies, ongoing research is essential to enhance engine emissions without compromising performance and power [5] [6]. Currently, some after-treatment methods are employed to reduce harmful emissions such as carbon monoxide (CO), nitrogen oxides (NO_x), hydrocarbons (HC), and particulate matter (PM) in the short term [7]. However, the economic barrier posed by the high costs of after-treatment devices restricts their broader application in IC engines. In the long term, exploring innovative combustion concepts and diversifying combustion strategies present potential solutions to reduce pollutants in engine emissions.

New combustion strategies have emerged to enhance and optimize internal combustion engines. Among these, low-temperature combustion (LTC), dilute gasoline combustion (DGC), and clean diesel combustion (CDC) are particularly significant. LTC involves staging the combustion at lower temperatures and maintaining sufficiently lean conditions to avoid high soot and NO_x formation zones in CI engines. This approach can improve engine efficiency by 20% compared to traditional diesel engines. The reduction in combustion temperature is achieved by using substantial exhaust gas recirculation (EGR) along with a lean fuel-air mixture [8] [9]. In DGC, a minimal amount of fuel is combusted in the engine's chamber under an excess of air or with recirculated exhaust gases, which can improve fuel efficiency by up to 35% compared to conventional spark-ignition engines. This improvement is attributed to the more moderate combustion temperatures, reducing heat losses during medium and low loads [10] [11]. In CDC, the combustion sequence resembles that of standard diesel engines, but with more of the air-fuel mixture prepared prior to the start of combustion. This allows the mixture to burn under cleaner conditions, resulting in less soot production. Implementing CDC requires advanced technical components such as a high-speed controller, sophisticated injection strategy, high-pressure injection, EGR, and high air flow within the cylinder.

In addition to the previously discussed strategies, alternative fuels such as biodiesel, dimethyl ether, biogas, and bioethanol are also being explored for use in conventional or modified internal combustion engines to reduce pollution emissions. Biodiesel, in particular, stands out as a viable option for most diesel engines, as it emits fewer air pollutants and greenhouse gases. It offers several benefits, including excellent lubrication properties, biodegradability, non-toxicity, and a composition largely free of sulfur and aromatic compounds, which contribute to its environmental friendliness. Notably, biodiesel combined with high injection pressure can significantly lower soot formation, a major issue in diesel engines, as demonstrated by Wang et al. [20] [21]. Additionally, biodiesel can be produced from a wide range of feedstocks, resulting in varied chemical structures and oxygen contents. Given the depletion of fossil fuels, biodiesel is increasingly viewed as a green and sustainable alternative.

Recent studies have highlighted the promising potential of gasoline-biodiesel blended fuels in advancing Gasoline Compression Ignition (GCI) engine technology, an advanced form of Low-Temperature Combustion (LTC) that mitigates issues typical of diesel engines. This blend leverages the advantages of biodiesel, such as its superior lubricity, renewability, environmental benefits, and high ignitability, enhancing cold starts and preventing misfires at low engine loads. Simultaneously, it retains gasoline's benefits of high volatility and extended ignition delay, which aid in the mixing process and help reduce pollutant emissions. Adams et al. [22] explored GB blends with 5% and 10% biodiesel content using a partially premixed, split-injection combustion strategy, improving the engine's operating range, achieving stable combustion, and lowering intake temperature requirements. Yanu et al. [23] [24] experimented with GB blends containing 5% and 20% biodiesel, adjusting injection timing, exhaust gas recirculation (EGR), and boosting pressure to optimize the performance of GB blends. They reported remarkable outcomes, including a combustion efficiency increase to 93% and a 50% reduction in total hydrocarbons (THC) and CO emissions compared to conventional diesel fuel.

GCI engine technology evolves from modern compression ignition (CI) engines and operates using a mixing-controlled combustion process. In this approach, multiple high-pressure fuel jets are directly injected into the engine's combustion chamber near the top dead center. As the fuel jets penetrate the chamber, they atomize, entrain, and mix with the surrounding air. This entrainment of hot ambient gases raises the temperature of the fuel-air mixture, leading to vaporization and subsequent auto-ignition once the equivalence ratio,

temperature, and residence time of the mixture are favorable for rapid chain reactions. The liquid fuel reaches a maximum penetration distance downstream of the injector, while the vaporized fuel continues to penetrate further. After ignition, a quasi-steady, lifted, and mixing-controlled flame is formed. The combustion process concludes when all the fuel has been combusted. The fuel-air mixing, auto-ignition, and mixing-controlled combustion are governed by injection parameters, fuel chemical properties, and the conditions of the charge gas.

Spray behavior significantly impacts mixture formation and ignition delay, which are crucial for understanding the mixing processes in CI engines. Auto-ignition, a key driver in compression ignition combustion, determines the ignition delay (ID) by influencing the time from fuel injection to the onset of combustion based on fuel characteristics. Ignition delay affects combustion phasing in the engine cycle and the degree of fuel-air pre-mixing needed to form the primary mixture before combustion. This, in turn, substantially shapes the heat release rate (HRR) and the formation of pollutants like NO_x and particulate matter (PM) [13]. An improper ignition delay can lead to negative outcomes, such as reduced engine power output and increased knocking, which causes combustion instability and can significantly shorten engine life [25] [26]. The ID period is influenced by various factors, including fuel type, engine design, operating conditions, and fuel injection strategy. These interrelated combustion processes also affect the level of soot produced during combustion [27][28].

Therefore, to better understand the impact of biodiesel composition on ignition delay and spray behavior of its mixture with gasoline in GCI engines is an important issue. Optical research with many different methods is applied to each process compatible with different spray combustion conditions. It is guaranteed to observe in detail the behavior of the spray as well as the moment of flame appearance. It combines spray combustion experiments on the constant volume combustion chamber (CVCC) system to make assessments about the results, which is the main topic of this thesis. The authors believe that the experimental studies on the spray combustion process that have been carried out provide a better overview of the conditions applied on GCI engines with high-octane gasoline fuels and provide the necessary injection control strategies as well as the limitations that must be avoided to achieve high engine performance.

1.2 Approach

This thesis presents research on the spray combustion process of Gasoline Compression Ignition (GCI) engines. This study stands out due to its utilization of gasoline-biodiesel fuel blends alongside high-octane gasoline in GCI engine conditions. The spray combustion processes are investigated across a broad range of experimental conditions, including variations in ambient temperature corresponding to the conditions of mixture formation. These environmental conditions range from non-vaporizing to non-vaporizing with high chamber temperature, vaporization, and combustion. The primary focus of this research is to evaluate the phenomena of spray combustion and study the intricate relationships between operating injection system parameters and ambient conditions when using gasoline-biodiesel fuel blends in various engine operating conditions.

Furthermore, various optical methods are applied to enhance the study of spray combustion on the Constant Volume Combustion Chamber (CVCC) system used to simulate engine experimental conditions. Initially, experiments on the non-vaporizing spray process between different gasoline-biodiesel fuel blends are conducted on the constant volume chamber system, with biodiesel composition varying from 10% to 40% by volume. The experimental matrix is constructed based on variations in injection pressure, injection time, and ambient density to comprehensively evaluate the spray vaporization process. Additionally, theoretical models of spray breakup time are applied to assess the breakup time of fuel blends under different experimental conditions. The spray process is intimately related to combustion chamber design, cold start processes, and mixture formation before and during combustion. Hence, these initial experiments provide an overall understanding of spray characteristics when applying high-octane fuel blends in GCI engine conditions, where related studies are not yet fully developed.

Secondly, previous studies have shown that the GB20 fuel blend meets optimal specifications for spray characteristics and ensures the presence of the desired biodiesel component in the mixture. GB20 is selected as the primary fuel for studying the impact of chamber temperature on spray morphology and characteristics. It also contributes to evaluating engine operating conditions, which significantly affect mixture formation inside the combustion chamber for high-octane fuel when used on both CI and GCI engine platforms.

Thirdly, the research focuses on the stages of spray formation under the influence of boundary conditions, including temperature and ambient density. To comprehensively assess the phases required for combustion, the vaporization process acts as an intermediate between

the non-vaporizing spray process and combustion. In this objective, experiments are controlled to activate the spray in a high-temperature environment ranging from 600-1000 K without combustion occurring, with oxygen levels ensured at 0%. The results of the vaporization process will complement the overall picture of how thermodynamic effects influence harsh spray conditions.

Finally, combustion is the culmination of the entire research process under similar boundary conditions to the spray experiments outlined earlier. In this section, evaluations of the impact of biodiesel content in the fuel on ignition delay characteristics and flame development are conducted. Additionally, the relationships between the non-vaporizing spray process and combustion process are closely examined. Furthermore, the differentiation in determining the value of ignition delay through pressure curve methods and optical methods is also addressed.

Additionally, various optical methods are refined and applied to observe the phenomena of spray combustion of gasoline-biodiesel blends. Alongside this, the CVCC system, with its high level of refinement and almost fully automated control through the LABVIEW program, has been operated. The control modes did not experience any anomalies during the pre-combustion process.

1.3 Objective

The primary aim of this study is to examine the spray combustion characteristics of blended fuels comprising gasoline and biodiesel. Specifically, the thesis aims to focus on:

Evaluating the applicability of gasoline-biodiesel fuel blends in the operating conditions of GCI engines at low and moderate loads.

Providing a comprehensive study from the initiation of spray formation to the formation and reaction of the mixture through combustion processes. The characteristics of spray combustion are discussed and analyzed in detail corresponding to the operating conditions of GCI engines. Combustion spray models are established to propose appropriate control modes and mitigate the shortcomings existing in GCI engines to enhance their applicability and achieve better engine performance and emissions.

Improving optical methods corresponding to the experimental conditions of the combustion process. For spray experiments, Schlieren and Shadowgraph methods are employed to measure

spray characteristics, including spray penetration length, spray cone angle, spray area, liquid length, liquid area, and vapor area. For combustion experiments, ignition delay and flame development are captured through high-speed camera data and pressure data directly recorded from pressure transducers.

The research involves preparing and configuring a constant volume combustion chamber (CVCC) system to replicate high temperature and pressure conditions akin to those found in engines. A model for the premixed combustion process will be developed to forecast the generation of reactive species at the start of injection (SOI). Prior to experimentation, the CVCC system and optical setup will be validated using pure diesel fuel under standard conditions. The outcomes will be analyzed and compared with existing research to verify the precision of both the CVCC system and optical configuration.

Gasoline-biodiesel blends with varying ratios of 10%, 20%, and 40% by volume are applied in combustion spray experiments at temperature ranges from 298 K to 1000 K with different ambient densities and varied conditions of the fuel injection system. The experimental conditions focus on enhancing the auto-ignition characteristics of gasoline direct-injection compression ignition (GDCI) combustion strategies under low load and cold start conditions.

1.4 Thesis outline

Chapter 1 outlines the scope of the thesis, providing a concise introduction to the research topic and situating it within the context of previous studies. It briefly discusses the enhancements made, along with detailing the research aims and objectives.

Chapter 2 aims to provide an overview of the literature related to GCI engines and the combustion spray process in cases using gasoline and gasoline-like fuels. The first part will provide an assessment of GCI engines, an efficient method to reduce soot and NO_x emissions in CI engines while improving the efficiency of using gasoline fuel. Secondly, the characteristics of the spray and combustion processes as well as associated phenomena will be discussed. Subsequently, theoretical models of the spray process will be provided, along with macroscopic spray methods. Theories and methods for measuring ignition delay will also be presented to enhance the overall assessment of the combustion spray process. Finally, an evaluation of the energy demand for transportation and the role of alternative fuels in climate change mitigation and reduction of harmful emissions will be provided.

Chapter 3 details the configuration of the constant volume chamber experiment system, including the setup of the gas supply and fuel delivery systems. It also provides an overview of the optical diagnostic methods employed. The chapter introduces the experimental test procedures and outlines the analysis methods used. Furthermore, it includes a detailed explanation of the image processing techniques applied to study the spray combustion process.

Chapter 4 evaluates the influence of biodiesel composition on the spray process of gasoline-biodiesel blends under GCI engine operating conditions. The non-vaporizing spray process is applied as a fundamental platform to assess spray characteristics along with the application of shadowgraph optical method. The physical characteristics of the spray are presented through an experimental matrix of injection pressure (40 MPa-100 MPa), injection duration (1200-1500 μ s), ambient density (10 kg/m^3 - 30 kg/m^3), and different fuel compositions (GB10-GB20-GB40). The combination of results from these characteristics shows that GB20 neutralizes common factors in spray characteristics and ensures stable injector operation conditions under harsh conditions due to the increased fuel viscosity.

Chapter 5 presents the evaluation of chamber temperature (323 K – 498 K) influence on the spray formation process of GB20 blend. The experimental matrix is constructed based on variations in chamber temperature, injector angle, injection pressure, and ambient density. The non-vaporizing spray process is applied to compare the phenomenon of spray behavior in high-temperature chamber environments. Remarkable results show that the cone spray angle tends to decrease as the chamber temperature increases. Additionally, the injector spray angle at 180 degrees is influenced by gravity, causing disturbances to the spray. The Schlieren optical method is applied to capture images of the spray process, clearly showing shockwaves when the spray enters high-pressure environments.

Chapter 6 presents the vaporization spray characteristics of GB20 and GB40 fuel blends in high-temperature environments, ranging from 600 K, 800 K, and 1000 K. The spray process is controlled so that the injection timing is activated at 0% oxygen concentration, ensuring that combustion is prevented to easily observe spray phenomena in high-temperature environments. The liquid and vapor phases are clearly identified when the spray exceeds the 600 μ s threshold. The structure and morphology of the vaporization spray add to the overall research picture for the application of high-octane gasoline fuels in GCI engines.

Chapter 7 presents the spray combustion process of gasoline fuels, GB10, and GB20. This means that the non-vaporizing spray process and combustion process are conducted to investigate spray combustion behaviors and characteristics in this chapter. Combustion characteristics including ignition delay, heat release rate, and flame development are discussed to determine their close relationship as well as their relationship with the initial spray process. It is noted that the injection cut-off time and ignition delay are closely related to each other to determine the normal diffusion combustion process.

Chapter 8 serves as the culmination of this thesis, presenting the summary and conclusions drawn from the experimental studies. It integrates insights gained from various diagnostic methods to provide a comprehensive understanding of spray combustion. The chapter highlights significant findings derived from the research.

2. Literature review

The purpose of this part is to provide an outline of the background information relevant to current research. In the first section, the GCI engine technology is given. Also, the opportunities and challenges of this kind of engine are presented. The second part of this chapter covers macroscopic spray in detail, including the optical methods involved and the various spraying processes. It demonstrates a clear influence on the engine design process, as well as the level of mixture mixing for the combustion process. Furthermore, the third part presents the characteristics of the combustion process, including ignition delay and flame development, to clearly illustrate their relationship. This process is complex and has a strong impact on combustion efficiency, engine performance, and emissions. Finally, the review of the demand for transport energy and the role of alternative fuel in terms of climate change and harmful gas emission are presented.

2.1 GCI engine technology

The Compression Ignition (CI) engine operates on high cetane fuels, igniting due to the elevated air temperature from mechanical compression within the cylinder. Known for its high thermal efficiency stemming from a substantial expansion ratio, CI engines typically run on diesel fuel, which auto-ignites quickly but poses challenges with high soot and NO_x emissions. Controlling these pollutants in diesel engines is complex and costly. Additionally, the potential for ignition knock limits the efficiency of Spark Ignition (SI) engines, constrained by compression ratios.

Looking forward, higher-octane gasoline is crucial to prevent knocking and enhance SI engine efficiency, though lower-octane gasoline may become more prevalent. In this context, Gasoline Compression Ignition (GCI) engine technology emerges as promising. GCI engines capitalize on gasoline's high volatility under high compression ratios [29][30], offering a solution to diesel engine challenges such as soot and NO_x emissions while maintaining diesel-like efficiency [31]. GCI engines are designed to operate efficiently with gasoline having a Research Octane Number (RON) between 70 and 85 [32], combining the benefits of high compression ratios from CI engines with favorable gasoline characteristics.

2.1.1 GCI concept

Gasoline Compression Ignition (GCI) is an advanced combustion technology characterized by high thermal efficiency and reduced emissions, requiring minimal modifications to standard

diesel engines. GCI can operate in various combustion modes, spanning fully premixed homogeneous combustion to diffusion-controlled modes. Partially premixed combustion, blending aspects of Homogeneous Charge Compression Ignition (HCCI) and diesel combustion, significantly enhances fuel efficiency by auto-igniting the fuel-air mixture through a combination of diffusion and premixing mechanisms. Under different load conditions, GCI engines utilize distinct strategies: at lower loads, homogeneous mixtures are achieved through early injection timing, whereas at higher loads, direct injection near top dead center (TDC) promotes diffusion-controlled combustion. Effective management of fuel stratification is crucial, particularly under high loads where ignition delay lengthens. This approach ensures optimal combustion efficiency with a small portion of the mixture igniting via auto-ignition, while the majority undergoes combustion through the diffusion process.

Kalghatgi et al. [33] initiated interest in utilizing higher octane fuels with increased volatility, comparing the performance of diesel fuel with a cetane number (CN) of 56 against gasoline with 84 RON and 95 RON using a single late fuel injection pulse of fixed width to maintain consistent fueling. Their study revealed that under low speed and load conditions, gasoline-like fuels exhibited longer ignition delays, effectively reducing NO_x emissions from light-duty engines. However, challenges arose due to overly advanced ignition timing and combustion instability attributed to lean local in-cylinder mixtures. Optimal fuel distribution or stratification was identified as crucial for achieving both combustion stability and emissions performance. At higher loads, issues such as excessive pressure rise rate (PRR) and increased NO_x formation were mitigated by employing Exhaust Gas Recirculation (EGR) to suppress premixed combustion effects. Dec et al. [34] [35] [36] investigated the benefits of partial fuel stratification (PFS) on equivalence ratio distribution, PRR, and extending high-load operating limits. Their findings demonstrated that PFS facilitated advanced combustion phasing, resulting in a 1% increase in thermal efficiency with IMEP_g below 2.4%, combustion efficiency between 96.8% and 97.8%, and indicated gross thermal efficiency ranging from 44.1% to 45.3%, while maintaining low NO_x and soot emissions. Additionally, their study on intake boost effects in gasoline HCCI engines revealed that increasing intake boost pressure from 5 bar to 16.34 bar of IMEP_g allowed for higher maximum loads. They attributed this success to their ability to retard combustion phasing while ensuring stable combustion with intake boost.

Adams et al. [37] explored the effects of biodiesel-gasoline blends on Gasoline Compression Ignition (GCI) combustion, focusing on 5% and 10% biodiesel blends using a

partially premixed, split-injection approach. Their findings highlighted that these biodiesel additions notably lowered the intake temperature requirement while also increasing NO_x emissions and reducing CO and unburned hydrocarbons (UHC), attributed to gasoline's higher average bulk temperature.

Meanwhile, Yanuandri [23] conducted studies comparing GB20 (80% gasoline, 20% biodiesel) and conventional diesel fuel modes in a single-cylinder diesel engine. Their investigation encompassed parameters such as peak pressure rise rate (PRR), combustion phasing, ignition delay, and emissions of NO_x and hydrocarbons (HC). The research revealed that GB20 exhibited shorter ignition delays and lower HC emissions, demonstrating biodiesel's potential to mitigate challenges in GCI applications, including enhancing lubricity when blended with gasoline. Additionally, Yanuandri [23] examined a 5% biodiesel blend with gasoline under different injection strategies, finding that GB05 provided improved combustion stability. As blended biodiesel-gasoline fuels become more prevalent, understanding the spray development process across varying biodiesel concentrations becomes increasingly important for optimizing engine performance and emissions control in GCI technologies.

2.1.2 Opportunities and challenges associated with GCI

Due to its specific operational strategies such as optimized gas exchange at part-load conditions, utilization of a low-pressure fuel pump, high volatility fuel properties, extended ignition delay, and high compression ratios, the newly developed Gasoline Compression Ignition (GCI) combustion process achieves fuel efficiency comparable to diesel engines with lower exhaust emissions. Particularly under Low Temperature Combustion (LTC) conditions, GCI engines can achieve extremely low NO_x emissions. Additionally, CO emissions are significantly reduced due to an overly stoichiometric air-fuel ratio and effective mixture preparation, contrasting with spark-ignited modes. Successful commercialization of GCI vehicles could pave the way for more efficient automotive solutions in regions where diesel fuel availability for passenger cars is limited. Figure 2.1 illustrates the main advantages of GCI technology.

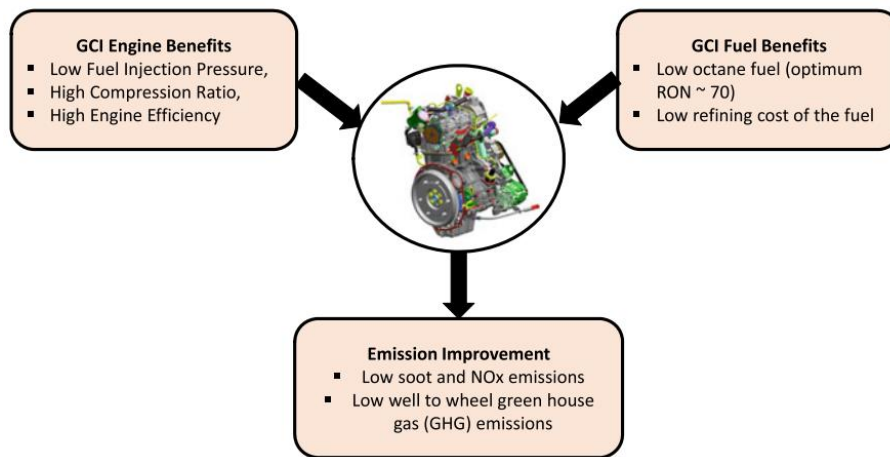


Figure 2.1: Advantages of GCI engine technology

Gasoline typically has a cetane number (CN) in the market of less than approximately CN15, which poses challenges for auto-ignition in Gasoline Compression Ignition (GCI) engines, especially during low-load and cold starting conditions. The very low CN of gasoline significantly extends ignition delay, necessitating earlier injection in the compression stroke compared to conventional diesel injection. At these low temperature and pressure conditions, achieving ignition becomes even more challenging. Consequently, further research is necessary to address these challenges before widespread adoption of GCI technology in commercial vehicles. Figure 2.2 [38] illustrates the primary challenges associated with GCI technology. Despite these challenges, most issues can be resolved through optimized combustion processes, which are generally simpler compared to diesel engines. Therefore, the implementation of GCI technology holds potential benefits for both the automotive industry and oil companies, helping to balance the demand between light and heavy fuel oils in future fuel scenarios.

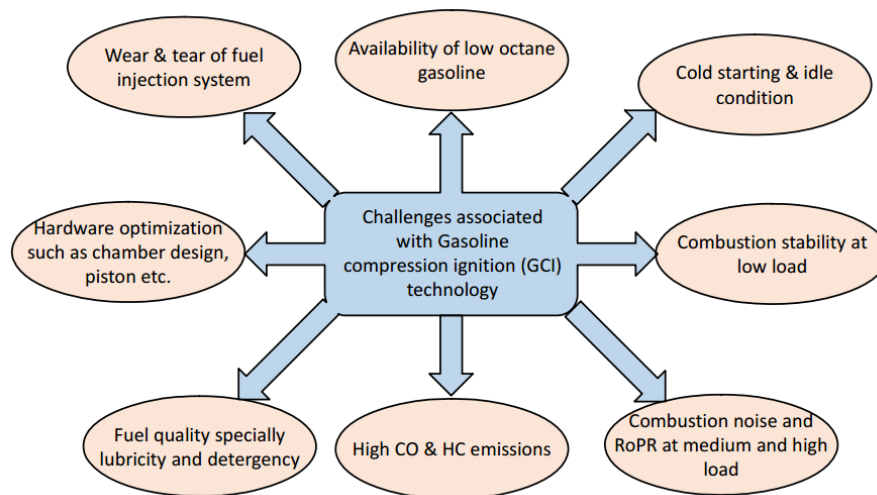


Figure 2.2: Challenges for GCI engine technology

2.2 Macroscopic spray

In recent years, the pursuit of cleaner and more efficient internal combustion engines has led to the emergence of innovative technologies such as Gasoline Compression Ignition (GCI) engines. GCI engines combine the high efficiency of compression ignition engines with the lower emissions of gasoline engines, offering a promising solution for reducing both fuel consumption and pollutant emissions in the transportation sector.

At the heart of GCI engine operation lies the process of fuel injection and mixing, which plays a pivotal role in achieving optimal combustion performance. Macroscopic spray, a key aspect of fuel injection, refers to the bulk behavior of the fuel spray as it interacts with the surrounding air within the combustion chamber. Unlike microscopic spray characteristics, which focus on the atomization and vaporization of individual fuel droplets, macroscopic spray parameters encompass the spatial distribution, penetration, and mixing of the fuel spray on a larger scale.

Understanding and optimizing macroscopic spray characteristics are crucial for enhancing the combustion process in GCI engines. Efficient mixing of fuel and air within the combustion chamber promotes homogenous combustion, leading to improved thermal efficiency and reduced emissions. Moreover, precise control of macroscopic spray parameters can influence combustion phasing, combustion stability, and pollutant formation, thereby shaping the overall performance and environmental impact of GCI engines.

2.2.1 Schlieren method

The Schlieren technique operates similarly to the Shadowgraph method. When a light beam passes through the test section, denser regions deflect the beam, resulting in a shift in the image observed on the viewing plane. Unlike Shadowgraph, Schlieren measures the first derivative of fluid density and utilizes a knife-edge for cutoff, as illustrated in Fig. 2.3. The position of this knife-edge influences the image projected on the screen and is typically oriented perpendicular to the nozzle, facilitating visualization of density variations along the spray length [39][40]. Both techniques are essential for quantifying integral quantities along the path of the light beam and are indispensable for imaging across a broad spectrum of density gradients[41][42].

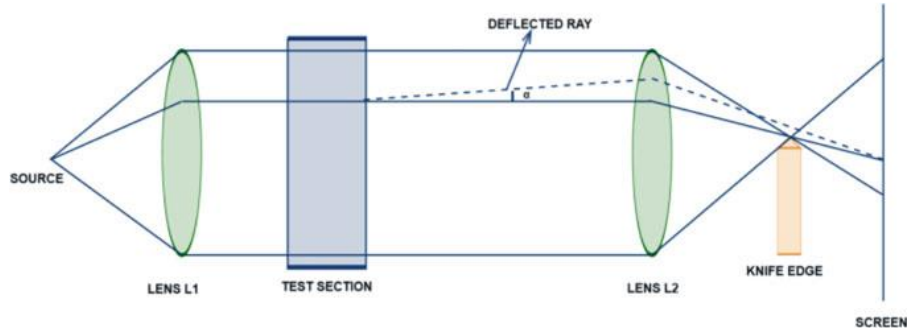


Figure 2.3: Principle of Schlieren technique

2.2.2 Shadowgraph method

The Shadowgraph technique is widely favored for spray visualization due to its simplicity and relatively low cost. Variations in density across the spray area, caused by gradients in pressure, temperature, and mixture, create non-uniform refractive index regions. As light passes through these regions, it undergoes refraction and phase shifts, resulting in variations in refracted light intensity. These intensity variations cast shadows on a screen, forming what is known as a 'shadowgraph'. Light, emitted from a source such as a laser or non-laser, is captured by a camera, typically a high-speed camera, after passing through the test section. The shadowgraph method measures the second derivative of fluid density. Figure 2.4 illustrates a schematic of the experimental setup for the Shadowgraph technique. While particularly suited for studying flows from two-dimensional nozzles, it also provides reasonable qualitative insights into three-dimensional nozzle flows [43].

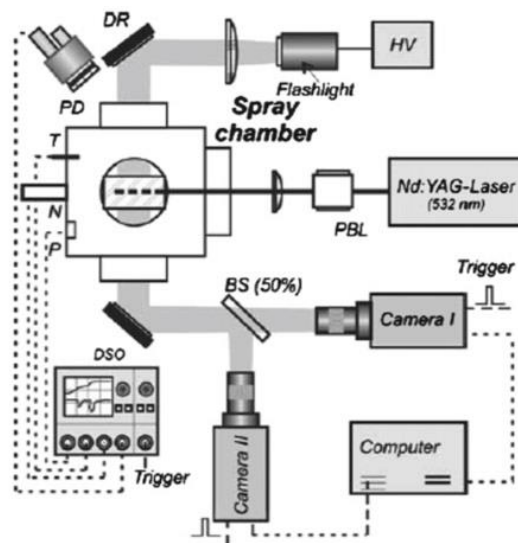


Figure 2.4: Schematic of the experimental setup for Shadowgraph of dense sprays in a CVCC [44]

2.3 Ignition delay and flame development

In the pursuit of cleaner and more efficient internal combustion engines, Gasoline Compression Ignition (GCI) technology has emerged as a promising solution. Central to the optimization of GCI engines is the intricate relationship between ignition delay and flame development. Ignition delay, the time interval between fuel injection and the onset of combustion, profoundly influences the timing and characteristics of flame propagation within the combustion chamber. Understanding this relationship is pivotal for optimizing combustion phasing, thermal efficiency, and emissions in GCI engines. In this context, a comprehensive exploration of the interplay between ignition delay and flame development is essential for advancing the development of GCI engine technologies.

2.3.1 Ignition delay

Ignition delay (ID) is the interval between the start of liquid fuel injection and the onset of ignition. It is commonly described by an Arrhenius-type equation (Equation 2.1), encompassing the time required for liquid breakup, vaporization, and the accumulation of radicals to a critical level necessary for rapid chain branching essential for ignition [45][46]. Therefore, ID is influenced by both the physical properties of the fuel and charge gas, as well as the chemical reactivity of the fuel [47][48]. ID plays a crucial role in determining the proportion of heat released during the premixed combustion phase versus the mixing-controlled combustion phase, directly impacting combustion timing and pressure rise rates within an engine [49]. Moreover, ID significantly affects engine emissions and performance [50]. Engines operating with fuels exhibiting short ID tend to produce higher particulate matter (PM) emissions due to incomplete mixing, whereas fuels with longer ID durations often result in increased nitrogen oxides (NO_x) and noise levels. Excessive ID compared to engine design specifications can also lead to issues such as fuel impingement. Injection pressure, ambient density, temperature, oxygen concentration, and nozzle diameter are factors known to affect ID, with higher injection pressures and temperatures generally reducing ID while larger nozzle diameters tend to increase it.

$$\tau_{id} = a\Phi^{-k^*}P^{-n^*} \exp\left(\frac{E_a}{R_u T_{cyl}}\right) \quad (2.1)$$

Where, τ_{id} = Ignition delay time

Φ = Equivalence ratio

E_a = Activation energy

T_{cyl} = Gas temperature in cylinder

R_u = Gas constant value

a, k^* and n^* = Empirical constants

Asanas et al. [51], the pressure and temperature are measured to predict ignition delay time. The pressure and temperature at injection timing are calculated as following equations.

$$T_{cyl} = T_m \cdot \varepsilon_{eff}^{c-1} \quad (2.2)$$

$$P_{cyl} = P_m \cdot \varepsilon_{eff}^c \quad (2.3)$$

Where, $\varepsilon_{eff} = \frac{V_{disp}}{V_{soi}}$ Effective compression ratio (2.4)

c = Polytropic constant

P_{cyl} = Cylinder charge pressure

P_m = Manifold pressure

T_{cyl} = Gas temperature in cylinder

T_m = Manifold temperature

V_{disp} = Cylinder displacement

V_{soi} = Cylinder volume at injection timing

Polytropic exponent is calculated by expression of Hardenberg and Hase [52] as below.

$$c = k^+ - \frac{k^+ - 1}{f \cdot u_p + 1} \quad (2.5)$$

Where, K^+ = Specific heat ratio of a gas, $c_p / c_v = 1.4$

f = Constant 1.1

u_p = Average speed of the piston

In the context of the ignition delay correlation discussed earlier, oxygenated fuels present a different consideration. Lahiri et al. [53] proposed using the fuel-to-oxygen ratio instead of equivalence ratio, which adjusts ignition delay as a function of the oxygen content in the fuel. The Cetane number remains a fundamental indicator of fuel's compression ignition quality. Hardenberg and Hase [54] developed a correlation that effectively incorporates Cetane number in such analyses.

$$E_A = \frac{B}{CN + 25} \quad (2.6)$$

Where, B = a constant

CN = Cetane number

The ignition delay time for diesel fuels is influenced by several factors including the Cetane number, viscosity of the fuel, nozzle hole-size, injected quantity, and injection pressure. Wolfer [55] provides a method to calculate ignition delay specifically for diesel fuels, taking into account these contributing factors.

$$ID = 3.45 \exp(2100 / T_m) p_m^{-1.02} \quad (2.7)$$

2.3.2 Measurement of ignition delay

There are two primary methods for defining ignition delay in internal combustion engines. One approach involves monitoring the pressure inside the combustion chamber using a high-frequency response pressure transducer. Before ignition, fuel spray vaporization causes a slight decrease in ambient gas temperature and a corresponding dip in pressure. Autoignition subsequently increases temperature and pressure until ignition occurs, defined as the point where pressure returns to its initial ambient level or slightly exceeds it.

Alternatively, ignition delay can be measured through combustion luminosity. OH luminescence has shown poor correlation with pressure-based methods for ignition delay measurement. Instead, soot luminescence, indicating the start of diffusion flame, has demonstrated better consistency across different fuel types. Luminosity measurements can be conducted using a CCD camera, photodiode, or photo transistor.

In practical terms, ignition delay is the interval between fuel injection into the combustion chamber via the injector and the moment ignition occurs. The time of fuel injection is determined by the electrical signal that triggers the injector, adjusted by subtracting the injection delay, which accounts for the nozzle tip's inertia. This delay is quantified through macroscopic spray images [56].

In this work, the pressure is recorded throughout the combustion process using the pressure transducer until the combustion process gradually ends. The heat-release rate is calculated based on the pressure increase of the combustion process and is calculated according to the formula:

$$\frac{dQ}{dt} = \frac{1}{1-\gamma} V \frac{dP}{dt}$$

where Q is the heat released in Joules (J), t is time in seconds (s), V is the volume in cubic meters (m³), P is pressure in Pascals (Pa), and γ is the specific heat capacity, 1.4 in this study. Ignition delay was defined as the period from opening the injector until release of 1% of the cumulative heat release [57].

2.3.3 Factors affecting ignition delay

2.3.3.1 Ambient Conditions

Ambient temperature significantly impacts ignition delay in combustion processes. Higher temperatures accelerate both the physical processes contributing to ignition delay and the chemical reaction rates involved [58][59]. For instance, Fuller et al. [60] observed a 50% reduction in ignition delay when ambient temperatures increased from 950 K to 1038 K, and an 80% reduction when temperatures rose further to 1125 K. Similar trends were reported by Kobori et al. [61], showing a nearly 90% decrease in diesel fuel ignition delay as temperatures increased from 625 K to 1000 K. Additionally, Ramesh et al. [62] found that even low concentrations of NO (100 PPM) could significantly alter ignition characteristics, with the magnitude and direction of change dependent on temperature and fuel type. For example, an increase from 0 PPM to 50 PPM of NO reduced ignition delay by about 35%, whereas an increase from 50 PPM to 100 PPM resulted in only a 10% reduction. Other components such as CO₂, CO, and H₂O also affect ignition delay, albeit to a lesser extent. Ignition delay is also influenced by ambient pressure, with Hoogterp et al. [26] demonstrating a 20-30% decrease in ignition delay for diesel fuel as pressure increased from 60 bar to 80 bar. This reduction is

attributed to higher gas density increasing air entrainment collision and the molar concentration of oxygen in the spray zone.

2.3.3.2 Fuel Injection

Air entrainment into the spray zone plays a crucial role in influencing the ignition delay of fuel sprays. Parameters related to fuel injection significantly impact how quickly air enters the spray zone, thereby affecting droplet sizes and injection velocity, which in turn increase or decrease ignition delay. For instance, increasing the orifice diameter of the injector from 0.1 mm to 0.2 mm can increase ignition delay by 30%, attributed to larger droplet sizes, reduced injection velocity, and slower air entrainment, thereby prolonging the physical delay in total ignition delay [61]. Similarly, Schihl and Hoogterp [26] observed a 25% increase in ignition delay when the orifice diameter increased from 0.176 mm to 0.212 mm, indicating a threshold beyond which the physical delay dominates due to larger droplet sizes. However, minimal effects were noted with smaller increases in diameter, such as from 0.025 mm to 0.05 mm. Nguyen et al. [63] found that orifice diameter had a moderate impact on ignition delay. Moreover, increasing injection pressure can slightly increase ignition delay by enhancing injection velocity, which leads to smaller fuel droplet sizes and faster vaporization rates. Nonetheless, the effect diminishes at higher pressures; for instance, increasing injection pressure from 60 MPa to 100 MPa results in nearly constant ignition delay.

2.3.3.3 Fuel Properties

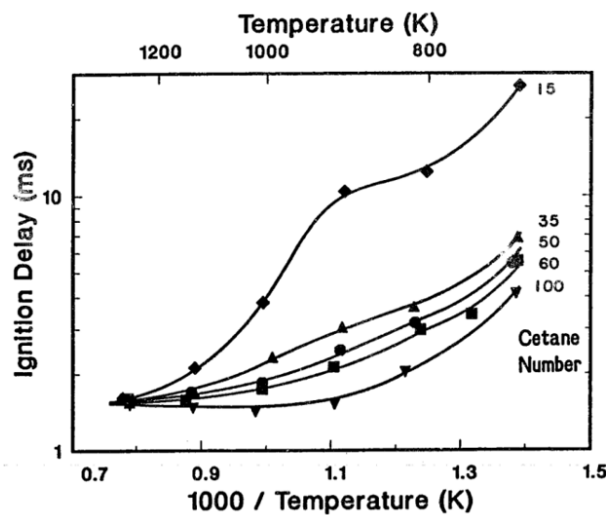


Figure 2.5: Ignition delay of reference fuels of varying cetane number

In assessing fuel properties affecting ignition delay, the cetane number emerges as the primary determinant. Lee and Bae [64] underscored its significance, finding that ignition delay

is more strongly influenced by cetane number compared to density, volatility, and viscosity. Their study compared fuels with cetane numbers of 39 and 46, showing a decrease in ignition delay of 5% to 13% (0.1 to 0.2 ms) as the cetane number increased. This aligns with findings by Pickett and Hoogterp [65], who observed that jet propellant, despite evaporating faster than diesel fuel, exhibited a longer ignition delay due to its lower cetane number. The authors concluded that while physical properties like evaporation rate, viscosity, and density influence fuel injection dynamics, they exert minor effects on ignition delay compared to cetane number. This assertion is supported by Siebers' study, which characterized ignition delay for reference fuels with varying cetane numbers in a CVCC setup, as depicted in Figure 2.5.

2.3.4 Natural luminosity for flame development

Natural luminosity serves as a crucial tool for visualizing the combustion process in GCI engines simulated within constant volume combustion chambers [66]. The emission of light during combustion allows researchers to directly observe flame development, propagation, and interaction with surrounding air and fuel mixture [67]. This visual feedback aids in understanding the dynamics of combustion, including ignition timing, flame stabilization, and the influence of operating conditions on combustion behavior.

Natural luminosity provides valuable information for quantifying flame characteristics in GCI engines [68]. By capturing the intensity, duration, and spatial distribution of luminous emissions, researchers can analyze parameters such as flame speed, flame front curvature, and flame structure [69]. These quantitative insights facilitate the evaluation of combustion performance and the validation of computational models simulating GCI engine combustion processes.

The intensity and temporal evolution of natural luminosity in GCI engines correlate with combustion kinetics, providing indirect indicators of ignition delay and reaction rates [70]. Observations of luminous emissions can reveal variations in combustion timing and progression under different operating conditions, offering insights into the complex interplay between fuel injection, air-fuel mixing, and chemical kinetics [71]. This correlation enhances our understanding of ignition mechanisms and aids in refining combustion strategies for improved efficiency and emissions control.

Natural luminosity provides unique insights into combustion phenomena occurring within GCI engines [72], including pre-mixed combustion, mixing-controlled combustion, and

transition regimes between compression ignition and flame propagation [73]. By analyzing the spatial and temporal evolution of luminous regions, researchers can identify dominant combustion modes, assess the effectiveness of combustion strategies, and explore opportunities for enhancing combustion efficiency and reducing emissions in GCI engines [74].

2.4 Fuel

2.4.1 Overview of existing transportation fuel options

Liquid fuels offer distinct advantages due to their high energy density per volume, ease of storage, and efficient transport compared to solid or gaseous alternatives [75] [76] [77]. These attributes have solidified liquid fuels as the predominant choice for transportation over the past century, resulting in a robust global infrastructure valued in trillions of dollars for their production and distribution. In contrast, gaseous fuels require compression or liquefaction to reduce their specific volume before they can effectively power transportation vehicles, necessitating additional energy inputs and infrastructure development, which can be barriers to widespread adoption [78] [79] [80]. Despite efforts to diversify energy sources, the transportation sector remains heavily reliant on crude oil, with approximately 95% of transport energy derived from petroleum in the early 2000s. Projections suggest this dependency will persist, with petroleum maintaining around 90% of the market share by 2040 [81].

Liquid fuels for transportation are primarily produced in oil refineries, starting from crude oil and undergoing various processing stages. Crude oil consists of a mixture of chemical compounds with differing boiling points. Initially, crude oil is distilled to separate it into fractions with distinct boiling ranges. Approximately 2% of crude oil is converted into gases at higher temperatures, yielding liquid petroleum gas (LPG) consisting predominantly of propane. Lighter fractions from this refining process, typically boiling in the gasoline range (with carbon atom counts ranging from 20 to 200), are termed "straight run gasoline" (SRG). The term "naphtha" encompasses products within this boiling range that undergo further processing to enhance resistance to auto-ignition, serving as both blended components for gasoline and primary feedstock for petrochemicals.

The demand for transportation fuels necessitates processes that convert heavier and less valuable fractions into lighter fractions suitable for use in fuel components. Complex refining processes aim to improve the anti-knock quality of different fraction streams. The anti-knock quality of fuel under specific engine operating conditions is influenced by its molecular

structure. Detailed chemical reaction mechanisms governing ignition properties typically involve hundreds of species and thousands of elementary reactions, particularly in low-temperature regimes. Petroleum refining involves various chemical engineering processes and facilities within refineries to convert crude oil into valuable products such as LPG, gasoline (petrol), kerosene, jet fuel, diesel oil, and fuel oils.

2.4.2 Alternatives to conventional fuels

The use of fossil fuels poses significant challenges, primarily due to their CO₂ emissions contributing to climate change, which has become a pressing global concern in recent decades. As societal awareness of environmental issues grows, there is increasing scrutiny on energy sources, prompting the emergence of alternative fuels. These alternatives offer various advantages over fossil fuels, including lower emissions, reduced pollution, and potentially lower fuel prices. Currently, biofuels account for approximately 4% of global transport energy, with compressed natural gas (CNG), LPG, and liquefied natural gas (LNG) contributing around 1%. In contrast, electricity and hydrogen play negligible roles in global transport energy supply.

Governments worldwide incentivize biofuels through subsidies such as tax breaks, grants, loans, and loan guarantees. These measures aim to reduce oil imports, support agriculture, and stimulate rural employment. However, biofuels generally incur higher costs than fossil fuels. The production of biofuels may also intensify competition for land between the food production and energy sectors, leading to increased land prices, heightened water and energy demands for crop irrigation, and transportation. Moreover, the environmental benefits of biofuels remain uncertain and vary across different aspects. Increased biofuel production could necessitate substantial agricultural land restructuring. For instance, the International Energy Agency (IEA) projects that achieving a 27% share of transportation energy from biofuels by 2050 would require an additional 100 million hectares, impacting between 12 to 165 million hectares of land [82]. Managing such demands becomes increasingly challenging in a world facing population growth and rising food demands.

Hydroelectric energy offers numerous advantages as a clean and renewable energy source, devoid of pollution issues associated with fossil fuels. Hybrid electric vehicles (HEVs) like the Toyota Prius exemplify this technology, utilizing both an internal combustion engine and electric motor to optimize fuel efficiency, particularly effective in city driving with frequent stops and starts. Modern HEVs employ regenerative braking to enhance efficiency by converting kinetic energy into stored electric energy. Battery electric vehicles (BEVs) rely

solely on rechargeable battery packs for power, while plug-in hybrid electric vehicles (PHEVs) can recharge their batteries from an external power source, combining electric and internal combustion power for extended range, albeit limited by battery size and weight constraints.

Natural gas, facilitated by advanced compression techniques, has emerged as a cleaner alternative in transportation, notably through compressed natural gas (CNG) and gas-to-liquids (GTL) technologies. CNG powers modified gasoline engines or dedicated CNG vehicles, while GTL produces liquid fuels compatible with existing infrastructure. Despite higher initial costs, natural gas vehicles offer lower maintenance and safety benefits compared to gasoline counterparts, contributing to their increasing adoption in the transport sector. Projected growth in global shale gas reserves and advancements in extraction technology suggest natural gas could comprise about 5% of global transportation energy by 2040, up from 1% currently, albeit subject to regional cost variations and infrastructure constraints.

2.4.3 Biodiesel fuel

Table 2.1: Biodiesel standards around the world.

Properties (units)	Malaysia	Korea	Thailand	USA	EU	Brazil
Flash point (°C)	182 ↑	120 ↑	120 ↑	130 ↑	120 ↑	100 ↑
Viscosity at 40°C (cSt)	4.415	1.9-5.0	3.5- 5	1.9- 6	3.5- 5	-
Sulphated Ash (% mass)	0.01 ↓	0.01 ↓	0.02 ↓	0.02 ↓	0.02 ↓	0.02 ↓
Sulphur (% mass)	0.001 ↓	0.001	0.001 ↓	0.001↓.	0.001 ↓	-
Cloud point (°C)	15.2	-	-	-	-	-
Cu corrosion (3hr, 50°C)	Class 1	Class 1	Class 1	Class 3	Class 1	Class 1
Cetane number	-	-	51 min.	47 min.	51 min.	-
Water & Sediment (vol.%)	0.05 ↓	0.05 ↓	-	0.05 ↓	-	0.05 ↓
Carbon residue (wt%)	-	0.1 ↓	0.3 ↓	0.05 ↓	-	0.1 ↓
Acidity (mg, KOH/gm)	-	0.5 ↓	-	0.05	0.05	0.08
Free glycerin (% mass)	0.01 ↓	0.02 ↓	0.02 ↓	0.02 ↓	0.02 ↓	0.02 ↓
Total glycerin (% mass)	0.01 ↓	0.16 ↓	0.25 ↓	0.24 ↓	0.25 ↓	0.38 ↓
Phosphorus (% mass)	-	0.001 ↓	0.001 ↓	0.001 ↓	0.001 ↓	-
Distillation temperature	-	-	-	<360°C	-	<360°C
Oxidation stability, hrs	-	6 ↑	6 ↑	3 ↑	6 ↑	6 ↑

Biodiesel, a clean, biodegradable, and renewable fuel, has garnered significant interest in the engine community for its potential benefits. It effectively reduces particulate matter (PM) emissions in diesel engines by enhancing combustion through the oxygen content present in biodiesel, which inhibits soot formation. Biodiesel is chemically similar to conventional diesel fuel and can be derived from various sources such as vegetable oils, animal fats, tallow, and used cooking oil through a process known as transesterification. Currently, biodiesel is primarily produced from oils like palm, soybean, rapeseed, and used cooking oils due to their

availability and suitability for production. While straight agricultural oils hold promise as a biodiesel source, their high cost currently limits commercial production. Biodiesel is commonly used as a blend with petroleum diesel, with B20 (20% biodiesel, 80% petroleum diesel) being the most prevalent blend used in diesel vehicles worldwide without requiring engine modifications. International biodiesel standards are summarized in Table 2.1 [85][86].

2.5 Summary

This literature review highlights studies on CI engines fueled with gasoline or blended with other fuels, particularly focusing on GCI mode or similar combustion strategies. Research covers various fuel types including gasoline and biodiesel blends, and explores methods to extend engine operation range such as using boost pressure, controlling intake temperature, managing local air-fuel stratification through injection strategies, and modifying fuel properties. Despite these advancements, challenges persist in GCI engine technology due to the inherent complexity of CI engines operating in GCI combustion mode. Further studies are needed to address these complexities and optimize the performance of GCI engines.

In a GCI engine, controlling the final injection timing is crucial for governing combustion phasing, which in turn affects local air-fuel stratification, driving combustion and emission characteristics. The characteristics of fuel spray have been demonstrated to have a close relationship with determining the fuel mixture and stratification. Identifying the timing of spray formation, the length of liquid under different environmental conditions will determine the ignition timing and influence the combustion process in the engine. Therefore, combining the investigation of spray characteristics with ignition delay quantifies the necessary properties and avoids inappropriate controls affecting the efficiency of the combustion process in the engine. Additionally, if the spray process is not executed perfectly, it will have a significant impact on emission performance in the engine, especially in GCI engine conditions.

Furthermore, definitions and measurement methods for ignition delay and natural flame luminosity are also discussed. It demonstrates the synergy in determining combustion process characteristics. There exists a direct correlation between ignition delay and natural flame luminosity, where longer ignition delays often lead to a more pronounced luminous flame. This relationship is attributed to the extended duration of low-temperature combustion associated with longer ignition delays, allowing more time for the formation of soot particles and subsequent increase in flame luminosity.

The methods applied to the combustion process are also mentioned to provide a detailed comparison of results. Additionally, it highlights appropriate methods for each process and the influence of each method on the respective processes.

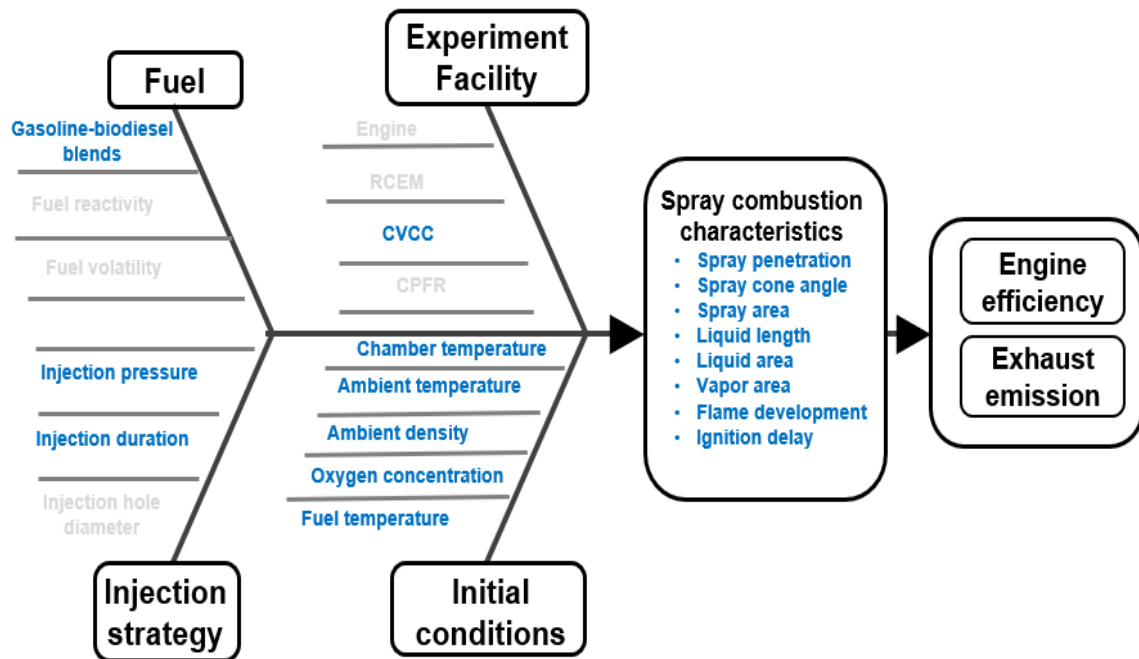


Figure 2.6: Effect flowchart of the potential parameters on spray combustion with engines fueled with gasoline-biodiesel blends

To deepen the understanding of fuel-air mixing, auto-ignition, and combustion processes, it is crucial to study the fuel vaporization rate, entrainment rate of charge gases, and fuel reactivity. Previous research has highlighted several key measurable variables that offer insight into these processes: spray penetration, spray dispersion, liquid length, flame development, and ignition delay. Sequential experimental studies are essential to identify significant parameters and phenomena related to spray combustion in compression ignition (CI) engines fueled with gasoline-biodiesel blends. The methodology to achieve these targets is summarized in the flowchart presented in Figure 2.6.

3. Experiment setup and methodology

To investigate spray and combustion processes in Gasoline Compression Ignition (GCI) engines, laboratory experiments were conducted using a custom-designed constant volume combustion chamber (CVCC). This setup replicated the chemical and thermodynamic conditions of modern diesel engines, including variations in Exhaust Gas Recirculation (EGR) levels. The CVCC, outfitted with advanced instrumentation, enabled precise control over ignition delay and other critical parameters. Key features included a high-speed, high-resolution data acquisition system for real-time pressure measurements, a high-pressure common-rail fuel injection system for accurate fuel delivery, an exhaust gas sampling system for emissions analysis, and an optical system for detailed spray combustion analysis. This controlled environment facilitated a thorough examination of both non-vaporization and vaporization processes of fuel spray and subsequent combustion phenomena, providing valuable insights into the dynamics of GCI engine operation.

3.1 CVCC System

3.1.1 Constant Volume Combustion Chamber

The Constant Volume Combustion Chamber (CVCC) is a fundamental tool in investigating various combustion and spray phenomena under conditions that emulate those found in diesel engines, characterized by high temperatures and pressures. Originally introduced by Oren et al. in their 1984 study, CVCCs consist of high-strength hollow chambers with ports for operation and instrumentation access. These chambers achieve the necessary pressure and temperature through a controlled chemical heating process, allowing the isolation of injection and combustion processes from other engine influences. Optical access to the chamber enables visualization of internal events, facilitating the use of high-speed cameras and image analysis tools to enhance understanding of injection and combustion dynamics.

In operation, the CVCC is first evacuated and then filled with a mixture of fuel, oxidizer, and inert gas, known as the premixed charge. This mixture is designed to create specific ambient conditions and is homogenized through either a mixing fan or turbulent mixing induced by directional gas intake ports. Ignition of the premixed charge is initiated by one or more spark plugs, leading to a rapid increase in temperature and pressure within the chamber due to heat release. As the products of the premixed charge gradually cool through heat transfer to the chamber walls, the pressure decreases correspondingly, allowing for a range of ambient

densities and temperatures to be explored. For ignition delay measurements, liquid fuel is injected as the desired conditions are achieved, with the assumption that autoignition occurs at constant ambient conditions due to the rapid ignition of fuel sprays compared to the cooling rate of the premixed charge products. CVCCs can have either spherical or cylindrical interiors, with typical volumes ranging from 0.13 to 2.3 liters for cylindrical designs and 1.8 to 4.2 liters for spherical ones.

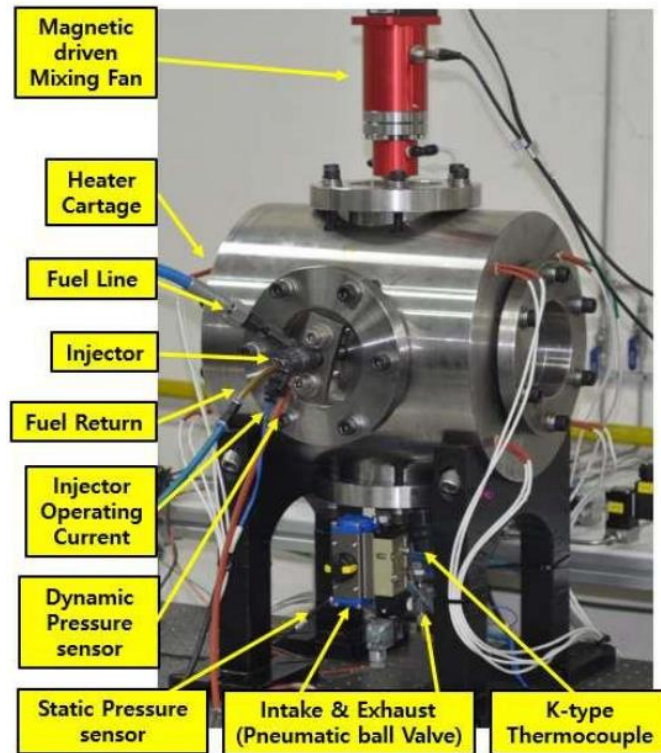


Figure 3.1: Assembled CVCC with different test equipment

The Smart Powertrain Lab’s Constant Volume Combustion Chamber (CVCC) features a cubic design with two configurations: a fully solid-sided internal volume of 1.3 liters and a partially optically accessible version with a 1.5-liter volume, incorporating quartz windows on two sides. These quartz windows are 120 mm in diameter and 50 mm thick, providing essential optical access for high-speed diagnostics. For safety, the chamber is equipped with a relief valve that caps the maximum pressure at 120 bar, with operational pressures typically below 100 bar.

Internally, the CVCC is equipped with a variety of instruments for data collection. These instruments are mounted both vertically and horizontally to facilitate comprehensive monitoring of combustion events, as depicted in Figure 3.1. A magnetically driven fan ensures a homogenous gas mixture and uniform temperature distribution during pre-combustion by

stirring the internal gases. Ignition of the premixed charge is achieved using a spark plug, strategically placed to facilitate the longest possible fuel travel path before impinging on the chamber walls, promoting thorough combustion analysis.

To mimic real engine conditions, where successive combustion cycles heat the cylinder walls, the chamber walls can be heated up to 100°C using integrated heater cartridges. This heating not only simulates engine thermal effects but also prevents condensation on the quartz windows during pre-combustion, maintaining optical clarity.

Recent modifications to the CVCC enhance the control and automation of experimental parameters via LabVIEW. These modifications include automatic and direct control of intake and exhaust valves, as well as a magnetically driven stirrer to ensure consistent gas mixing. The spark ignition system can now be precisely timed and adjusted on a microsecond scale, with automatic triggering after a preset duration. Fuel injection occurs under specific thermodynamic conditions, and the National Instruments Data Acquisition (NI DAQ) system records data from the onset of pre-combustion through to the conclusion of spray combustion, allowing detailed analysis of combustion phenomena.

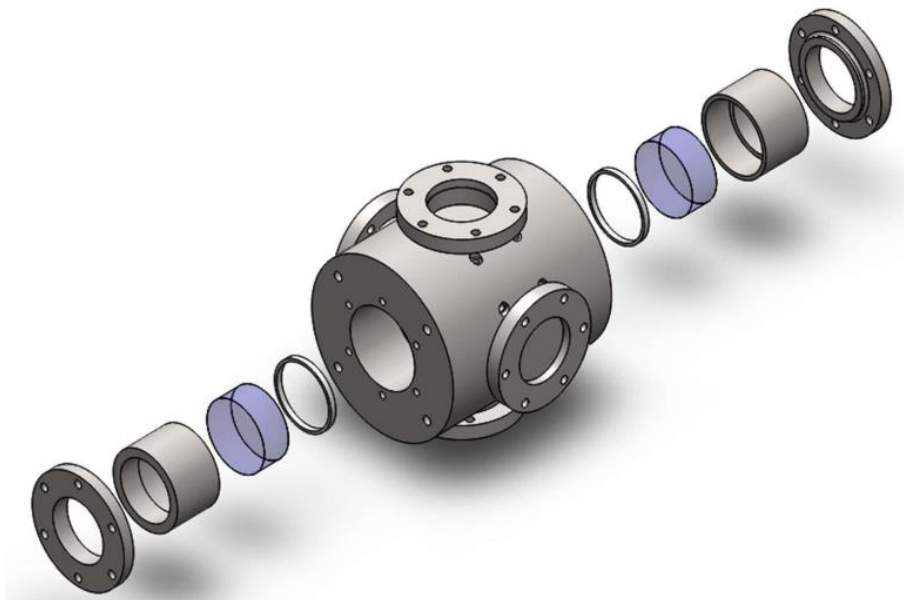


Figure 3.2: Exploded view of the CVCC with quartz

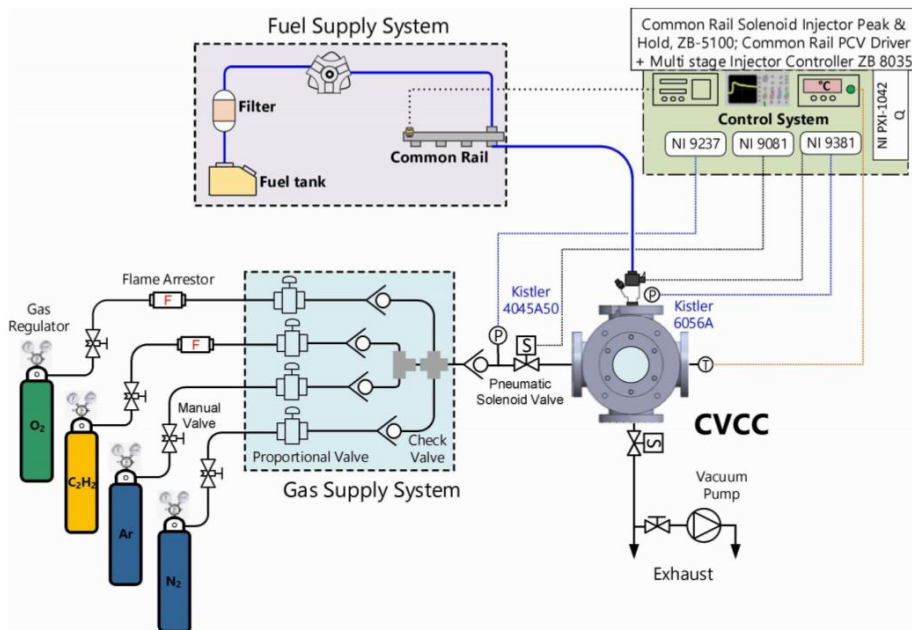


Figure 3.3: Schematic of the CVCC apparatus implemented in the experiments

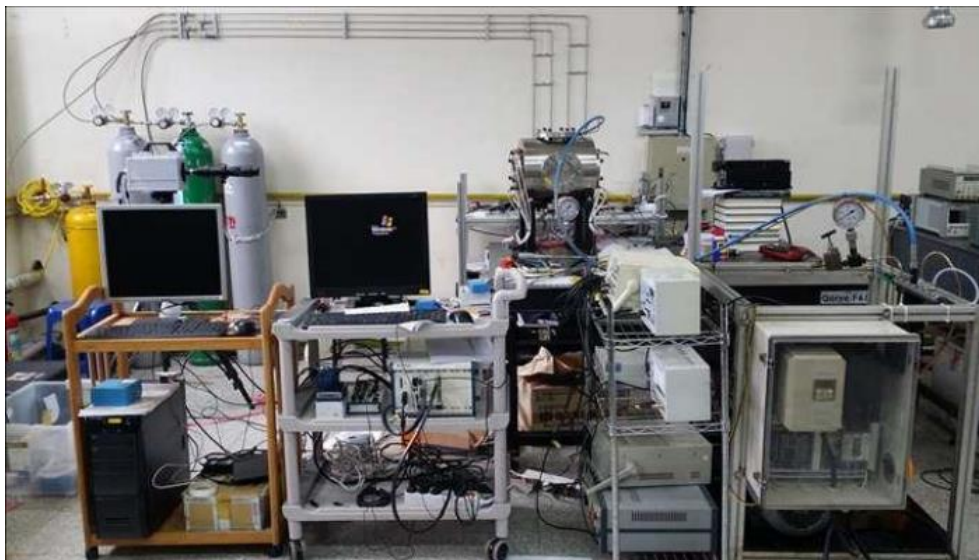


Figure 3.4: Pictorial layout of experimental test bench

Figures 3.2 to 3.4 present both a schematic and a photograph of the experimental test facility. The CVCC is a cube-shaped vessel with a combustion chamber offering extensive optical access from all sides, each measuring 110 mm, enabling thorough visualization of the fuel spray before it impacts the chamber walls. The top window supports a mixing fan for turbulence generation, while inlet and exhaust valves regulate the introduction and expulsion of gases. A dynamic pressure transducer (Kistler 6001) with a range of 0 to 250 bar is installed at the bottom corner of the vessel for pressure measurements. This facility is uniquely designed

to investigate the physics of combustion, including spark-ignition and spray combustion. Key dimensions, sensors, and acquisition systems are detailed in Table 3.1.

Table 3.1: An overall information of the test system and additional equipment

Basic Parameter		Unit
Shape of the internal chamber	115 × 115 × 115	mm
Window aperture	110	mm
Injector mounting	Side Window	
Number of spark plugs	1	
Spark plug position	Bottom Window	
Combustible gas fill	Sequential	
Mixing fan location	Top window	

Measurement Condition			
	Minimum	Maximum	Unit
Ambient density	5	20	bar
Ambient temperature	298	1000	K
Oxygen concentration	0	0.21	vol fraction
Wall temperature	293	443	K
Fuel temperature	Ambient	NA	K
Common rail pressure	300	1350	bar
Injection duration	800	2000	μs

Auxiliary system		
Proportional valve	Burkert 2875(only N ₂), Burkert 2873	0-25, 0-16 bar
Intake Valve	Pneumatic ball Valve	0- 10 bar
Exhaust Valve	Pneumatic ball Valve	0- 10 bar
Vacuum pump	Spaemax Rocker 400	.5mbar Hg
Ignition coils driver	Mobiq Ignition Coil Driver	
Sprak Plug	Denso IRIDIUM(SK16PR-A11)	
Mixing Fan	Propeller type magnetic driven fan	

Sensor & Data Acquisition		
DAQ & control software	NI PXI 1042Q & LabVIEW	
Static gas pressure sensor	Peizo resistive Kristler 4045A50	0 - 50 bar
High Pressure calibrator	Sensys PSHHC020BCPG	0- 20 bar
Low pressure calibrator	Sensys PSHHC002BCPG	0- 2 bar
Dynamic gas pressure sensor	Peizo resistive Kristler 6056A	0 -250 bar
Vessel temperature sensor	Thermocouple K type **mm	
Module for Pressure measuement	NI 9237	
Module for Proportional Valve	NI 9238	

3.1.2 Supply and Exhaust System

Figure 3.5 illustrates the schematic diagram of the supply and exhaust system used in the experiment. The premixed charge consists of acetylene, argon, oxygen, and nitrogen gases. These gases are introduced into the constant volume combustion chamber (CVCC) sequentially using promotional valves (Burkert 8605) until the desired partial pressure targets are achieved.

The filling procedure is controlled by a Labview program using the Proportional-Integral-Derivative (PID) method, functioning as a filling program. A pressure transducer (4045A50) measures the in-chamber pressure during the filling process and provides feedback to the filling program. This automated filling procedure ensures stable test conditions throughout the experiment. This setup allows for precise control and manipulation of the gas composition and pressure within the CVCC, enabling the investigation of specific combustion conditions relevant to the study of GCI engine operation.

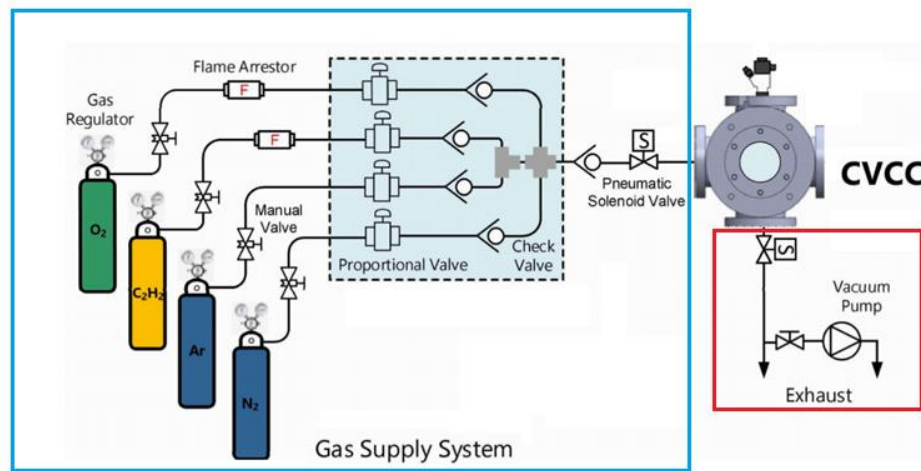


Figure 3.5: Schematic diagram of supply and exhaust system

3.2 Data acquisition and control system

The control and data acquisition system schematic, shown in Figure 3.6, outlines the automated management of all control and data collection tasks by the main computer. This computer operates a custom-designed LabView interface, facilitating the control of gas filling, exhaust flushing, and the initiation of the combustion sequence. The LabView interface also allows for the adjustment of various operating parameters. Additionally, a second computer manages the high-speed camera, enabling the modification of camera settings. The ignition signal from LabView triggers the high-speed camera recording.

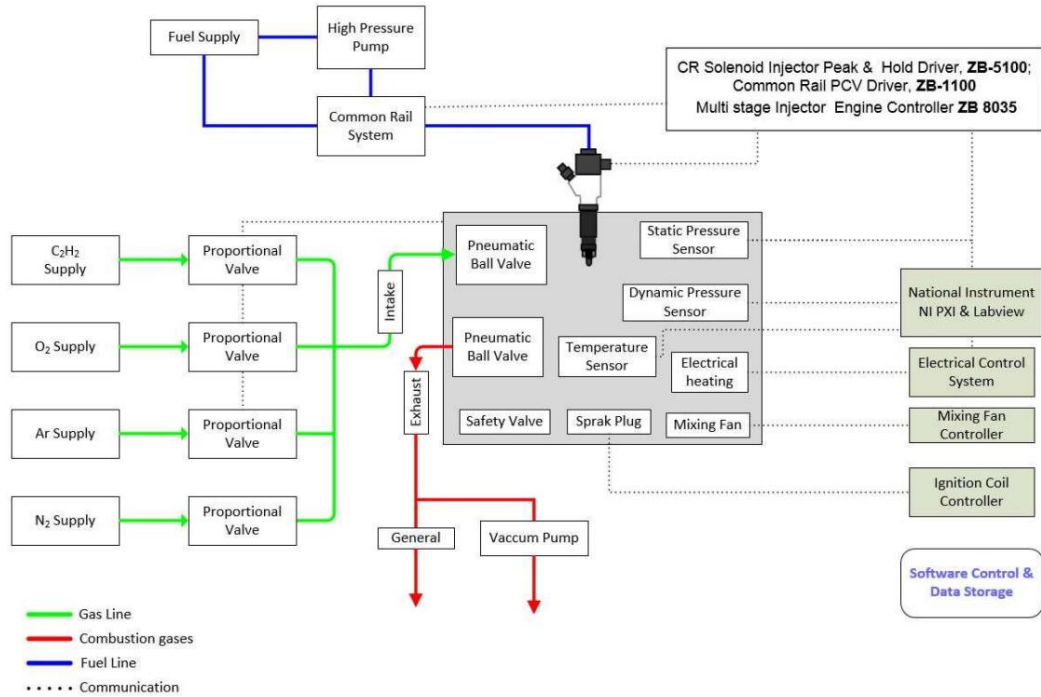


Figure 3.6: Schematic of control and data acquisition system

3.2.1 Control system

Figure 3.7 depicts the schematic of the control system utilized in the present study, categorized into high-speed, high-resolution, mid-speed, low-speed, and digital tasks. Experimental operations were overseen by a National Instruments (NI) PXI-7813R, which was linked to NI 9472, NI 9237, NI 9381, and NI 4910 via a cRIO 9515 expansion chassis. The NI 9472 module was responsible for managing intake valves, exhaust valves, sensor valves, bump valves, total valves, a mixing fan, and a vacuum pump. NI 9237 connected to two pressure sensors for measuring combustion chamber pressure during filling. Four promotional valves controlling charged gases were coordinated by NI 9381, while NI 9410 handled tasks such as triggering the spark plug and injector. High-speed analog data (vessel pressure, injection command, spark command, injection pressure) was captured at 24-bit resolution and 50 kHz frequency. Additionally, oxidizer inlet pressure, acetylene inlet pressure, and mixing fan speeds were monitored using a 16-bit, 50 Hz NI 9237 module. Hydraulic cylinders were employed for actuating the intake and exhaust valves.

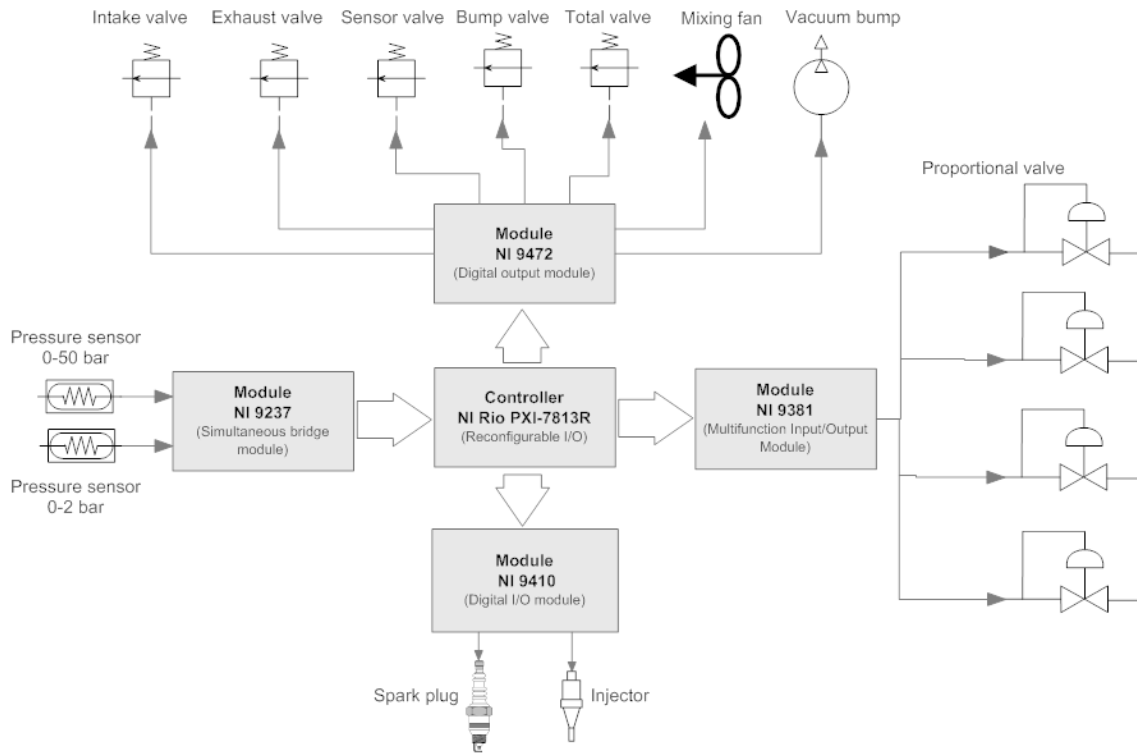


Figure 3.7: Schematic diagram of control system

3.2.2 Data acquisition system

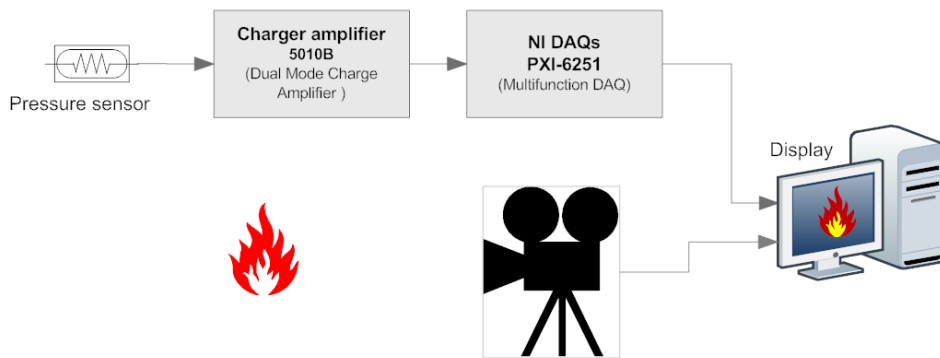


Figure 3.8: Schematic diagram of data acquisition system

Figure 3.8 depicts both a schematic and a photograph of the data acquisition system utilized in this study. The system employs the NI PXI 6251 multifunction DAQ in conjunction with the BNC-2120 module to gather data. Tasks are categorized into two main areas: monitoring pressure history in the combustion chamber and imaging the combustion flame of the fuel sample.

For capturing the combustion process, a high-speed camera equipped with PFV software is utilized to acquire a sequence of images. Simultaneously, a high dynamic pressure transducer records pressure variations resulting from the heat release during fuel combustion. The charge

amplifier 5010B and NI PXI 6251 are employed to amplify and convert signals from the pressure sensor into suitable digital formats, which are automatically saved to an Excel file.

3.2.3 Control program

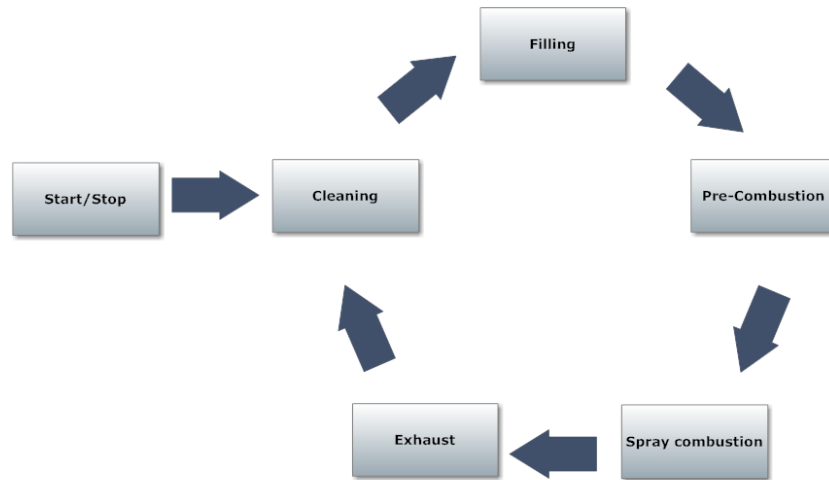


Figure 3.9: Control-flow diagram

The operation of the CVCC follows a structured sequence, outlined in Figure 3.9. Initiating with the start/stop button, which activates or deactivates the CVCC, the process commences with gas cleaning throughout the chamber, followed sequentially by gas filling. Subsequently, other phases ensue until concluding with the exhaust process.

Filling process

The filling process is crucial for achieving precise experimental outcomes, as illustrated in Figure 3.10. Initially, Argon (Ar) is introduced using PID control to reach the desired target pressure. Following this, Acetylene (C_2H_2) is filled, succeeded by oxygen (O_2), and finally Nitrogen (N_2). Throughout this process, two types of pressure sensors are employed to monitor chamber pressure: a high-precision sensor for acetylene and argon, and a standard sensor for nitrogen and oxygen.

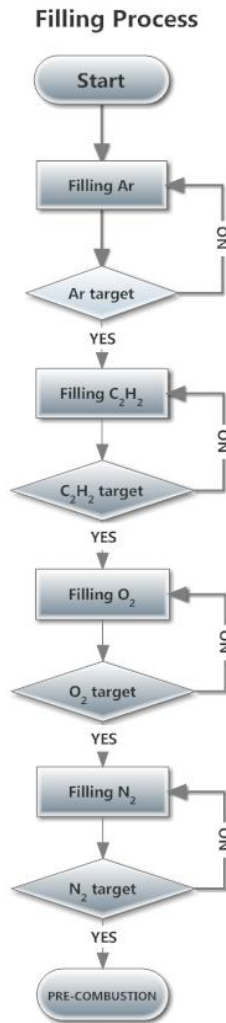


Figure 3.10: Schematic diagram of sequence of filling gases

This process is critical as it significantly impacts the accuracy of test results and the overall stability of the system. Specifically, it can lead to a dangerous phenomenon known as knocking. Knocking occurs when the concentration of Acetylene (C_2H_2) in the combustion chamber becomes excessively rich. When the spark plug ignites the mixture, it burns rapidly, causing a sudden and abnormal rise in chamber pressure. This rapid pressure increase produces a distinct sound similar to an explosion. Figure 3.13 illustrates how in-chamber pressure rises during knocking incidents. Such events pose serious risks, potentially leading to explosions in the chamber or pipes, posing significant danger to human life.

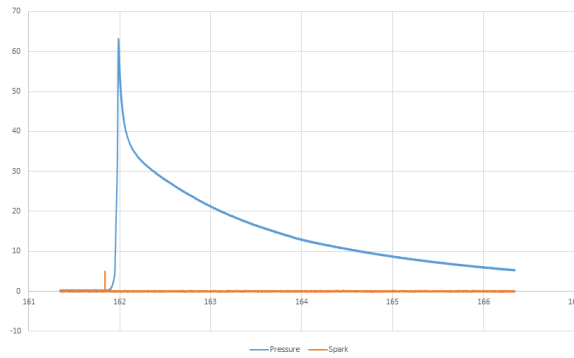


Figure 3.11: Pressure in the combustion chamber when knocking

Diagnostic function

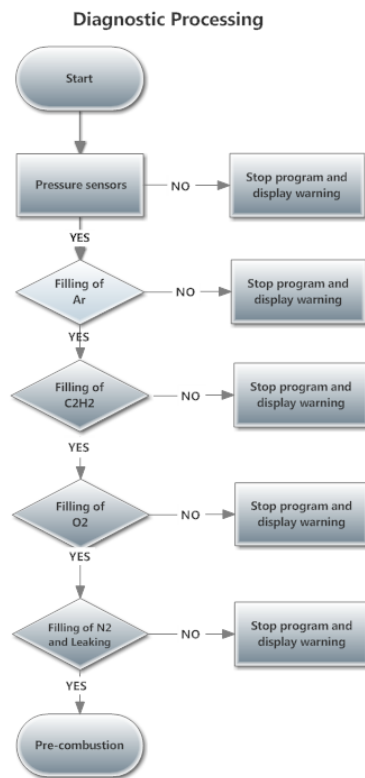


Figure 3.12: Sequence of diagnosis

The CVCC operates fully automatically and is highly reliable; however, unforeseen events can occur during its operation. For instance, over time, a pressure sensor may become inaccurate or disconnect, resulting in data transmission failures to the controller. This can lead to inaccurate signals being sent to control units, potentially causing dangerous situations. For example, misunderstanding the pressure in the combustion chamber might result in overfilling of Acetylene (C₂H₂), leading to knocking and possibly damaging the glass window.

Therefore, a diagnostic program to prevent knocking is essential. Figure 3.12 outlines this diagnostic application, structured into five steps as follows:

Step 1: The program verifies sensor connections and properties under atmospheric conditions. If both pressure sensors return values close to zero, indicating they reflect atmospheric pressure, the sensor and connections are deemed good. Otherwise, a warning message alerts to connection or sensor issues.

Step 2: After the argon filling completes, the program checks chamber pressure against target values. If the error is within 0.001 bar, argon filling is confirmed as successful, proceeding to acetylene filling. If the error exceeds this threshold, a warning is issued, and the program halts.

Step 3: Similar to argon, the program checks the acetylene filling process.

Step 4: Post-oxygen filling, the program uses a less accurate sensor to check pressure. If the error is within 0.01 bar, the filling is accepted. If pressure exceeds the high-precision sensor's range, the sensor valve closes to protect it.

Step 5: Post-nitrogen filling, the program checks for chamber leakage by isolating it for 10 minutes. Pressure is then compared to the target; an error over 0.02 bar triggers a warning for possible filling error or chamber leakage. If below this threshold, the filling process is considered complete, and the next steps, such as pre-combustion, commence.

Exhaust and cleaning process

When the program initiates, it begins with the exhaust and cleaning process as follows:

1. The exhaust valve opens to release gas products to the venting system.
2. The bump valve opens, connecting the vacuum pump to the combustion chamber.
3. The sub-exhaust valve closes to isolate the combustion chamber.
4. The vacuum pump operates for 60 seconds to extract gas products.
5. The intake valve opens to introduce Nitrogen gas (N₂) into the chamber.
6. The fan runs for 30 seconds to ensure thorough mixing.
7. The sub-exhaust valve opens to expel gases to the venting system.

8. The vacuum pump runs again for 60 seconds to remove gas from the combustion chamber.
9. Nitrogen gas (N₂) is filled to reach a pressure of 1 bar in the chamber.
10. The sub-exhaust and exhaust valves open to vent gases until the chamber pressure matches environmental pressure (1 atm).
11. The exhaust valve closes to complete the exhaust and cleaning process.

3.3 Fuel supply system

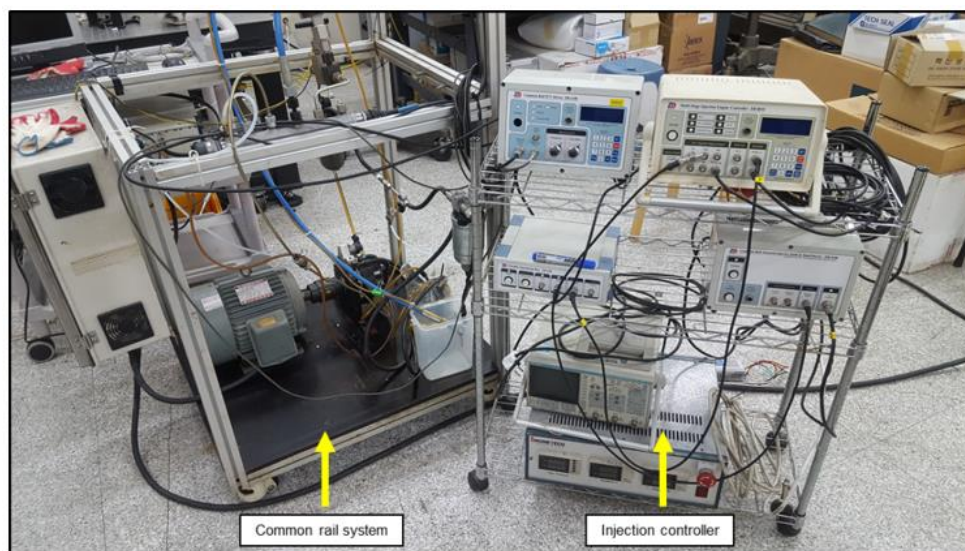


Figure 3.13: Pictorial representation of fuel injection system

The fuel system employs a common-rail direct fuel injection setup comprising several key components: a peak and hold injector driver (ZB-5100), a common-rail injection pressure controller (ZB-1100), a pressure control valve, a rail pressure sensor, a high-pressure pump, a low-pressure pump, and a single-hold injector.

The common-rail injection pressure controller regulates fuel pressure using the pressure control valve, capable of maintaining pressures up to 1800 bar. A LabVIEW program installed on the NI computer controls injection timing and duration. This control is achieved by utilizing feedback from a pressure sensor installed within the chamber, ensuring precise fuel injection synchronization with the combustion process.

3.4 Pressure trace

Table 3.2: Technical data of pressure sensor

Change Input		
Connector Type	BNC neg. or TRIAX neg.	
Measuring range FS	pC	±2 ... 2 200 000
Measurement uncertainty		
Ranges FS <10 pC	%	<±2
Ranges FS <100 pC	%	<±0,6
Ranges FS ≥100 pC	%	<±0,3
Drift, measuring mode DC (Long)		
at 25 °C, max. relative Humidity RH of 60 % (non-condensing)	pC/s	<±0,03
at 50 °C, max. relative Humidity RH of 50 % (non-condensing)	pC/s	<±0,3
Max. common mode voltage between input and output ground	V	<±25
Overload	%FS	≈±110

Table 3.3: Technical data of pressure sensor

Range	bar	0 ... 250
Calibrated partial ranges	bar	0 ... 50
	bar	0 ... 2,5
Overload	bar	300
Sensitivity	pC/bar	≈-25
Natural frequency	kHz	≈90
Linearity, all ranges	% FSO	≤±0,5
Acceleration sensitivity		
axial (with cooling)	bar/g	<0,01
radial (with cooling)	bar/g	<0,001
Operating temperature range		
Cooling water flow	l/min.	0,3 ... 0,5
Sensitivity shift		
50 ±35 °C	%	≤±0,5
50 ... 350 °C	%/°C	≤0,01
Thermo shock		
bei 1 500 1/min, 9 bar p _{mi}		
Δp	bar	<±0,2
Δp _{mi}	%	<±1
Insulation resistance at 20 °C	TΩ	≥10
Shock resistance	g	2 000
Tightening torque	N-m	10
Cooling water pressure	bar	≤6
Capacitance, with cable	pF	110
Weight	g	18
Plug, ceramic insulator	Type	M4x0,35

In the current study, the quartz pressure sensor utilized is the thermo-dynamic quartz pressure sensor (6061B), which employs polystable quartz elements ideal for thermo-dynamic measurements in small combustion engines. This sensor is paired with a single-channel laboratory charge amplifier (Kistler 5018A) and sampled at 200 kHz with 12-bit analog-to-digital (A/D) resolution.

The charge amplifier (Kistler 5018A) is versatile, allowing adjustment via its settings panel to accommodate different sensors and varying test conditions. This flexibility ensures optimal performance and accurate data acquisition tailored to specific experimental requirements.

3.5 Optical diagnostic system

The optical setup is based on the Schlieren approach with a Z-type configuration. Halogen lamps, high-speed cameras, and concave spherical mirrors (diameter 150 mm, focal length 2000 mm) collect spray images from the combustion chamber. A halogen light source is shone at the first concave spherical mirror with a diverging light source to capture spray movement. This diverging light source is then transformed into a parallel light source and shone at the second concave mirror into the converging source and directly at the camera. Using a Photron SA3 high-speed camera, the photos were captured at 10,000 frames per second with a resolution of 512x256 pixels.

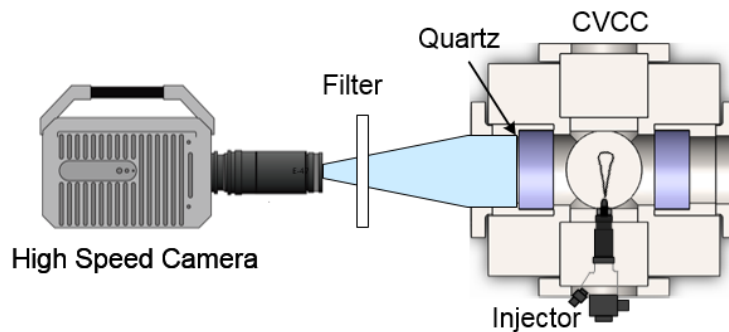


Figure 3.14: Optical arrangement for the broadband natural luminosity technique.

Table 3.4: Camera specifications.

Camera	Photron SA1.1
Lens	AF Micro-Nikkor 60mm f/2.8D
Frame rate	20000 fps
Optical filter	600 nm Shortpass
Exposure time	50 μ s
Resolution	512x256
Scale	0.196 mm/pixel

3.6 Image processing

The experimental process utilizes a Photron high-speed camera Mini AX200 color, recording the spray process at 80000 fps with an exposure time of 1/1500000 seconds. Image resolutions for the Schlieren method in fuel test cases GB20 and GB40 are 0.43 mm/pixel and 0.41 mm/pixel, respectively. To analyze the images efficiently, a custom MATLAB-based image processing technique is employed, aiming for precise data extraction and reduced processing time. The process involves converting RGB images to grayscale, binarizing them, applying filters, removing small particles, and iterating through a processing loop. Fig. 3.15

provides further insight into vaporization spray, defining liquid length as the distance from the image's origin to the farthest point of the black pixel block, and spray angle as the angle within a length $S/2$ on both sides of the liquid region. The liquid area is determined by subtracting background from image frames. Vaporized fuel areas are highlighted with a yellow border. Vapor area calculations are akin to liquid area calculations but require identification and exclusion of the liquid zone. Each experimental case is repeated thrice to average results, minimizing errors and improving reliability through regression analysis.

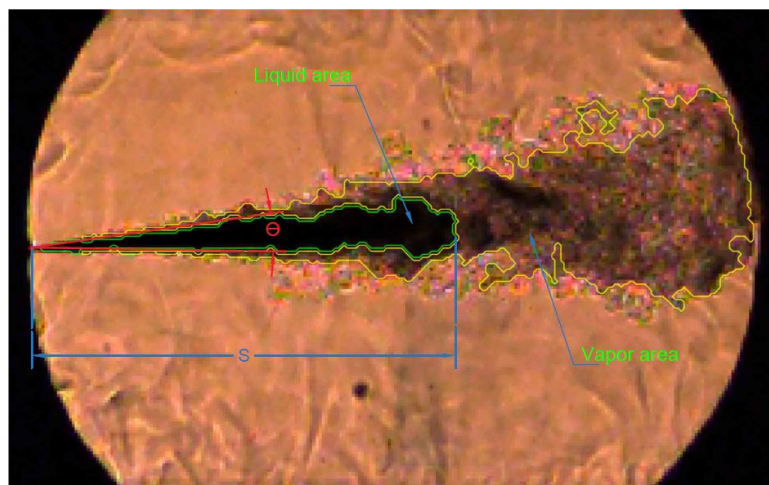


Figure 3.15: Definition of spray vaporization characteristics

4. A study on spray characteristic of gasoline-biodiesel blended under GCI engines condition performed on constant volume combustion chamber system

This chapter presents the study of the spray characteristics of the gasoline-biodiesel fuel mixture at various operating conditions of the GCI (gasoline compression ignition) engine performed in a constant volume combustion chamber (CVCC). Spray development, spray penetration length, spray cone angle and spray area were considered and evaluated under the change of injection pressure, ambient gas density and injection duration with assurance boundary conditions for all experiment cases. The injection pressure affecting the reduction of the spray cone angle was found when being increased from 40 MPa to 100 MPa. In addition, raising the ambient gas density reduces the spray length of the fuels at the same time and slows down the speed at which spray impinges on the wall. Typically in the case of GB40 at pressures of 100 Mpa and 1500 μ s, corresponding to ambient gas density levels from 10-20- 30 kg/m^3 , the penetration rate is 100, 62.5, 47.61 m/s, respectively. Meanwhile, at a pressure of 40 Mpa, with the same conditions, the speed of hitting the wall is 58.82, 42, 40 m/s, respectively. The results clearly show the influence of ambient gas density on the spray formation rate and stability when increasing injection pressure. The fuels had different biodiesel compositions from 10, 20 and 40 % by volume to indicate differences in the viscosity properties of the fuels. In addition, the association between the properties makes the difference in the results of the spray area during the test. Optical modeling was set up according to the shadowgraph method using high-speed cameras to collect images from the spraying process. The method applies an image processing algorithm in MATLAB to analyze the images after the experiment. Overall evaluation of the spray characterization process, the physical properties as well as the theoretical models are reviewed, providing an overview for the study of the bio-fuel mixture to apply to GCI engines with the advantage of longer ignition delay.

4.1 Spray development

The injection development process illustrates the characteristics of the actual injection in the cylinder. This includes spray angle and penetration length results as well as spray area. The injection development of the three tested fuels (GB10, GB20 and GB40) is shown in Table 6 under injection conditions at a pressure of 80 MPa and a chamber density of 20 kg/m^3 . Because the experimental process provides many visual results of the spray over time, in this section

only the representative results are chosen for detailed illustrations. In addition, images are shown under the same testing conditions and timelines for more convenient comparisons. The liquid interacts with the quiescent air charge from the very beginning of the injection phase before atomization takes place, leading to accelerated fuel insertion [89]. The spray shape depends on the direction of the spray and its development. In this argument, results are shown from the start of the spray until impingement on the wall. Spray development under the operation of a small diameter nozzle results in a lower area compared to other large sizes. However, the small diameter injector can push the spray speed faster than usual, resulting in a faster impact on the wall. Real engine performance means that the spray will hit the top of the piston faster and spray impingement then occurs. More in-depth processes will be discussed in the next study. As shown in Table 6, the visual spray shape difference is minimal. However, the spray cone angle and the spray penetration length are different and will be discussed in detail in the next section of this study. The results were found to show the effect of the fuel viscosity on the injection properties. When biodiesel concentration in the fuel increases, the spray penetration length also increases, it cannot be concluded that this increase is linear. But it can be shown that when the spraying process is stable at 700 μs , the spray angle has little fluctuation, and the spray boundaries are more stable. In addition, further steps are needed to analyze the velocity vectors or turbulence in the two-dimensional images of the beam to provide a better analysis and more specific direction.

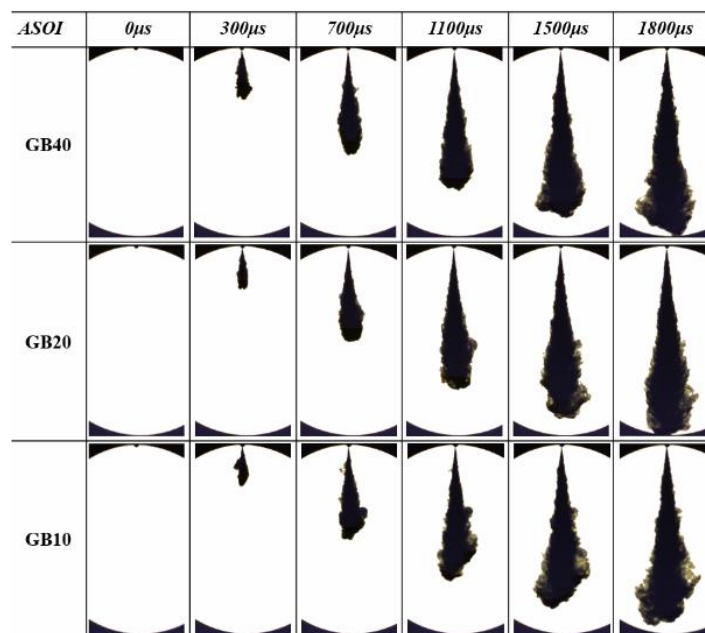


Figure 4.1: Spray development of fuel GB10, GB20, and GB40 at injection pressure of 80 Mpa, injection duration 1500 μs with chamber density of 20 kg/m^3 .

4.2 Spray tip penetration

Fig. 4 shows the time injection penetration of the three tested fuels of this study with injection durations varying from 1200 μs -1500 μs at a chamber density of 10-20-30 kg/m^3 . The left side shows the spray penetration length that varies with the injection pressure from 40-100 MPa provided that the injection duration is 1500 μs , while the right side shows the results of the injection duration of 1200 μs . Time of the results were sequential self-spaced at 100 μs for each photograph. The experiments were carried out sequentially under the same conditions of spray origin, photo frame and light intensity to ensure a homogeneous comparison. However, the first stage of spray development from 0 to below 300 μs was not shown. Given the consistent internal conditions during the test, the results of the spray penetration length clearly show changes in fuel properties, injection pressure and ambient density. The error of the boundary conditions of the test including injection pressure, ambient gas density, fuel temperature, and constant volume chamber temperature do not collectively exceed 2 %. The start and endpoints of spray in this test were defined by the injector tip, respectively, until the injector envelope reaches the opposite wall and dispersion begins. The discrepancy in spray penetration length between fuels is not considerable. This is consistent with the trend of previous research [90]. However, the spray penetration length of all fuels tends to decrease gradually at the same analysis time and the wall hit speed is slower due to the increasing resistance of the pressure from the outside environment within the range tested from 10 to 30 kg/m^3 . This is explained by the increased resistance of the back pressure from the chamber counteracting the impulse flux of the spraying liquid, which reduces the spray penetration. Therefore, the spray penetration length of a higher ambient back pressure will result in a lower ambient gas density condition at the same injection pressure.

Based on the results in Fig. 4, as the injection pressure increases, the spray penetration length also follows the same pattern. Explanation of this can be based on spray property laws [89] [91]. As the injection pressure increases, the kinetic flux is increased causing more fuel flow, resulting in the touch speed becoming the same trend. In addition, at injection pressures of 80 and 100 MPa, almost all fuel impinges on the wall or breaks before touching the wall, but the spray process enters a stable stage. At 40 and 60 MPa, the spray penetration was lower, but the comparison time conditions did not change at 1200 μs and 1500 μs , via images collected from high-speed cameras and image processing. Especially, the injector tends to close the needle before spray impingement on the wall. Typically, in the case of GB40 at pressures of 100 MPa and 1500 μs , corresponding to ambient gas density levels from 10- 20- 30 kg/m^3 , the penetration rate is 100, 62.5, 47.61 m/s, respectively. Meanwhile, at a pressure of 40 MPa, with the same conditions, the speed of hitting the wall is 58.82, 42, 40 m/s, respectively. The results clearly show the influence of ambient gas density on the spray formation rate and stability when increasing injection pressure. However, when comparing the three fuels GB10, GB20 and GB40 at the same ambient gas density of 10 kg/m^3 , the penetration rate are 97.08, 90.09, 90.09 m/s at 100 MPa

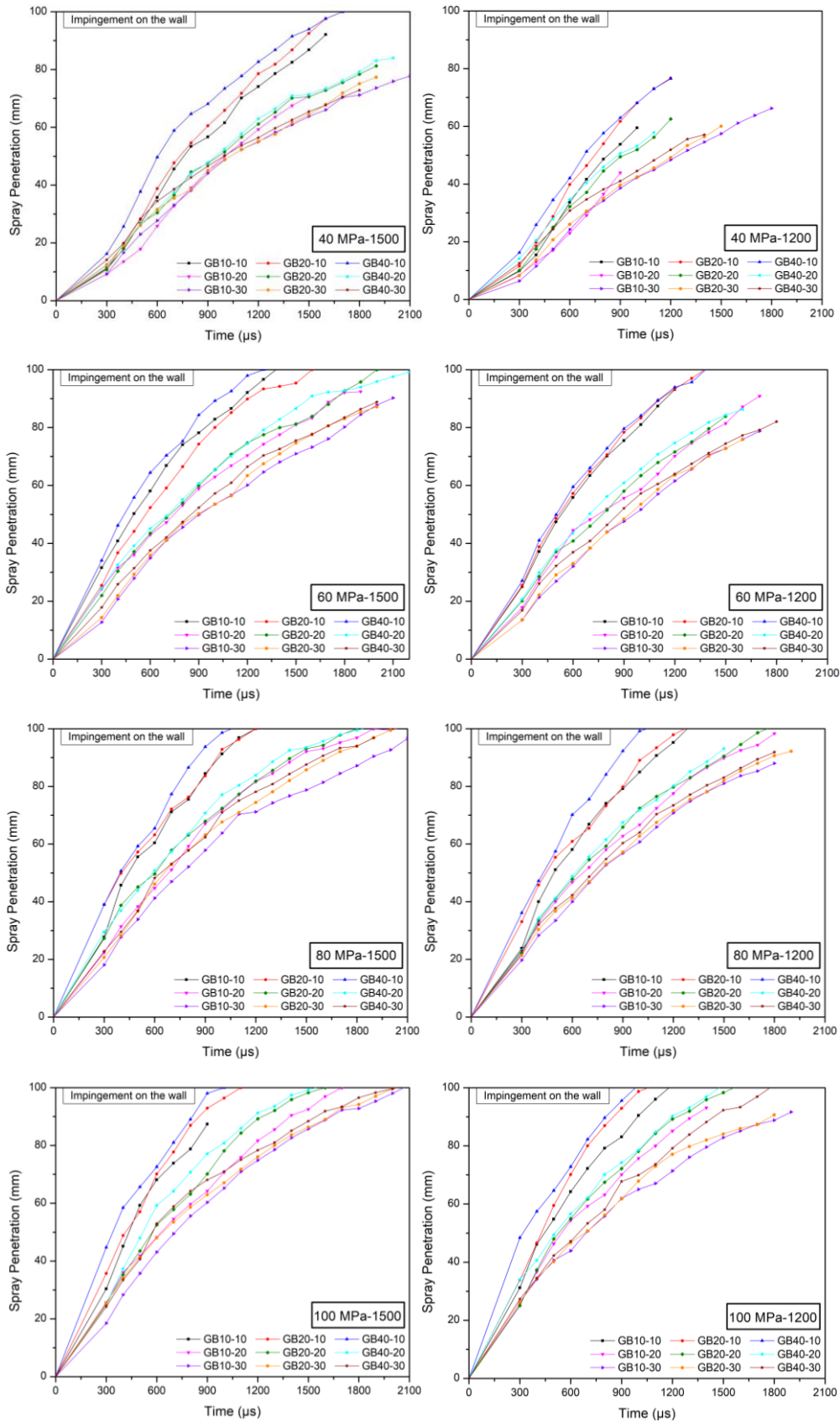


Figure 4.2: Comparison of spray penetration length temporal evolution of all tested fuels at 10 kg/m^3 , 20 kg/m^3 , and 30 kg/m^3 under injection pressure of 40, 60, 80, and 100 MPa with 1200-1500 μs injection duration.

injection pressure and 57.56, 58.82 at injection pressure of 40 MPa. Thereby, it is shown that the difference between GB20 and GB40 under the same conditions is not too large and the percentage of biodiesel in the fuel also contributes to stabilizing the spray process.

Some previous studies have also shown that early penetration of the nozzle is divided into two phases, the initial osmosis phase and then a sudden transition to rapid penetration [92]. But in this study, the experiments for the initial osmosis assessment are not yet complete and will be presented when assessing the vaporization conditions to the next study. Therefore, research can only evaluate through the use of counter equations to give results of spray breakup time based on experimental conditions and the properties of the fuel. Through the value of the spray breakup time, the results characterize that the spray breakup time decreases with increasing ambient gas density, which promotes the stable image of the spray as well as increasing the level of the exposure mixture of air and fuel. In addition, the study also shows that the change in the viscosity of the fuel will also affect the spray breakup time with the assurance of the boundary conditions in the experiments. This leads to the opposite trend of increasing the ambient gas density, which is increasing the viscosity of the fuel leads to an increase in spray breakup time. The results of the spray penetration length presented in the graph in Fig. 4 at injection duration of 1200 μs and 1500 μs all show the same development trend of fuel with higher viscosity. In most injection pressure ranges, the GB40 and GB20 show faster jet growth over time compared to the GB10 because of its fuel properties. Increasing biodiesel content in the fuel results in an increase in the viscosity and density of the test fuel mixture. Since ongoing research is based on GCI engine conditions, a gasoline fuel can be used but over time it will greatly affect the operating conditions of the injector because of its low viscosity. In addition, it shows that there is a trade-off when increasing the biodiesel content in the fuel mixture, which will result in faster penetration of the fuel to the cylinder wall. This is not as good as increasing the level of the mixing of fuel and air inside the combustion chamber. However, with the basic evaluation for this injection process and the previous application studies of gasoline-biodiesel blends for GCI engines still shows the potential applications in real engine high ignition capacity of biodiesel and high volatility from gasoline.

4.3 Spray cone angle

Results of the spray cone angle are shown in Figs. 5-8. The results are presented for 40 MPa to 100 MPa injection pressures with a comparison of different injection times. The tendency of the injection angle at a fixed pressure levels to decrease over time. The results of the spray cone

angle is started at 0 and the next step is 300 μs until the spray is switched off or spray impingement reaches the wall. In the initial stage from 0 to below 300 μs the results of the spray are still recorded but the analysis is not completely accurate. It needs to rely on the microscopic method to get a better overview, which is not included in this study. The reduction of the spray cone angle is a function of the influence between the constant injection pressure and the chamber pressure. The spray cone angle relates directly to the spray development and the area of the spray beam. The best theory is that the spray lasts a long time, the conical injection angle increases, it will give the best mixture for combustion. However, in some cases, if the spray angle is too large, it will cause a collision in the cylinder wall and this is not good for the combustion in the engine. Besides, the spray angle is also an important parameter for improving the spray morphology theory. At the beginning of the spraying process including the injection delay, the needle will slowly open until fully open according to the set injection duration, and the spray following this trend begins to form small spray spots until it grows and goes into steady-state before reaching the wall. There are some cases affected by the ambient density, where the injection duration is not enough to meet the external environment. Spray breakage will occur in such cases, and the spray beam continues to move in the axial direction of the injector until it is dispersed in its surroundings or until walls are reached. The effect of spray beam formation is explained by the low kinetic energy of the fuel mass will result in raised amount of fuel concentrated near the injector that resonates with the pressure compression in the previous injector. It will push the fuel sequence further and further. The point here is that the density outside the injector promotes the growth of fuel droplets forming the spray angle. The spray cone angle depends on the axial velocity and the radial turbulence. A more stable spray beam results in a higher axial velocity which causes the spray angle to decrease its shape. In order to determine the correct spray cone angle, it is observed that the influence lays in the experimental imaging method and the resultant analysis method.

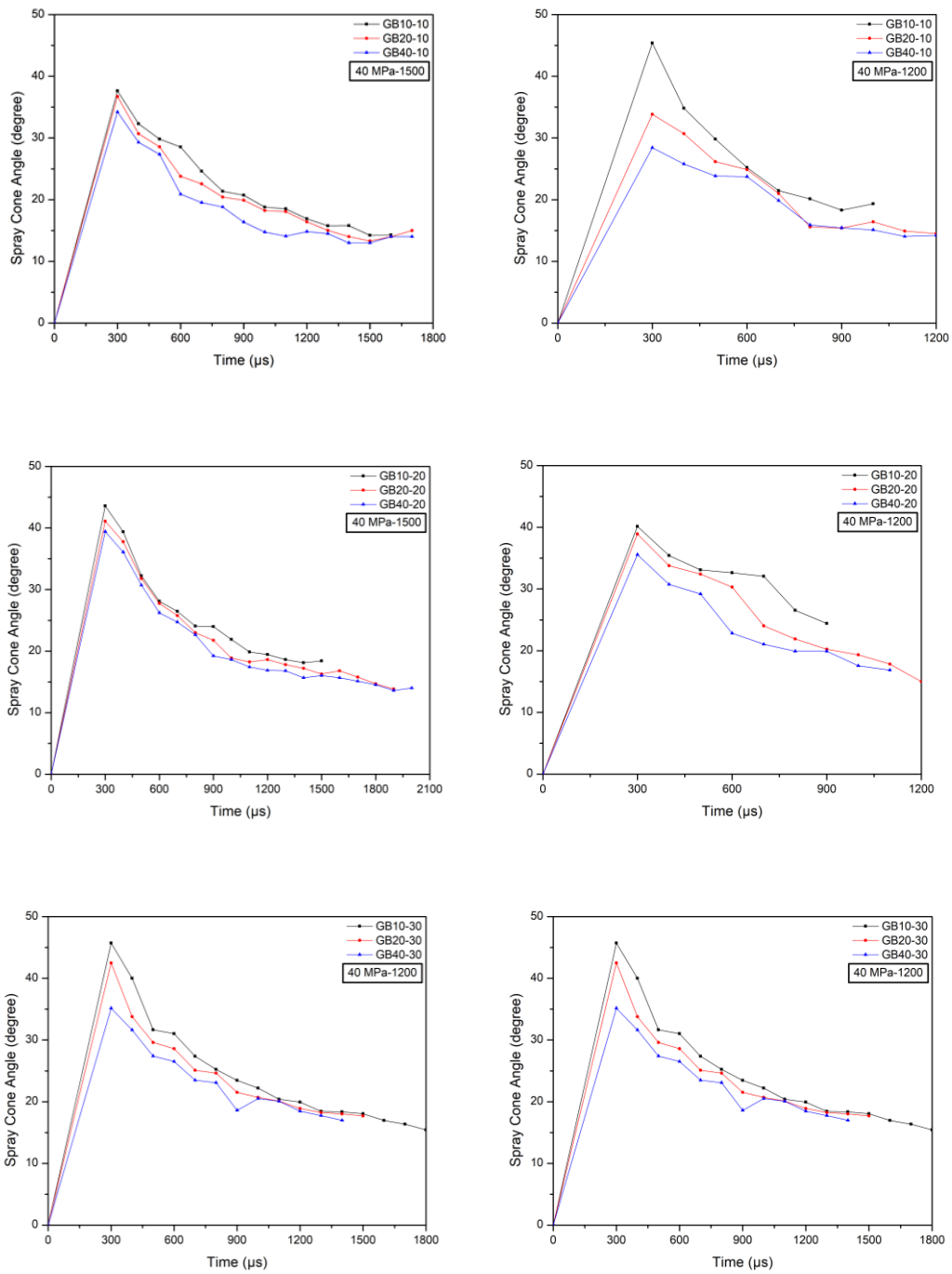


Figure 4.3: Comparison of spray cone angle temporal evolution of all tested fuels at 10 kg/m³, 20 kg/m³, and 30 kg/m³ under injection pressure of 40 MPa with 1200-1500 μs injection duration.

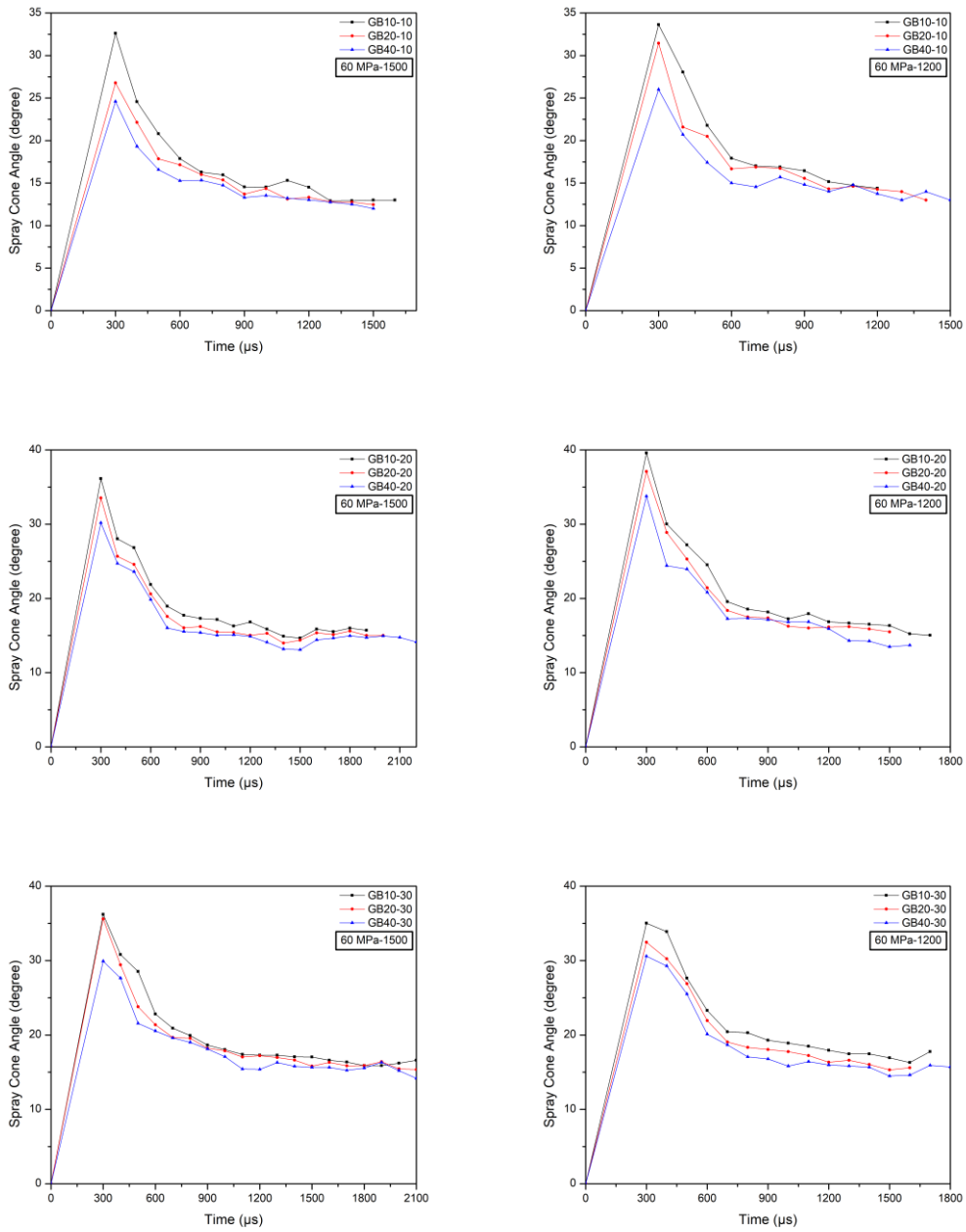


Figure 4.4: Comparison of spray cone angle temporal evolution of all tested fuels at 10 kg/m³, 20 kg/m³, and 30 kg/m³ under injection pressure of 60 MPa with 1200-1500 μs injection duration.

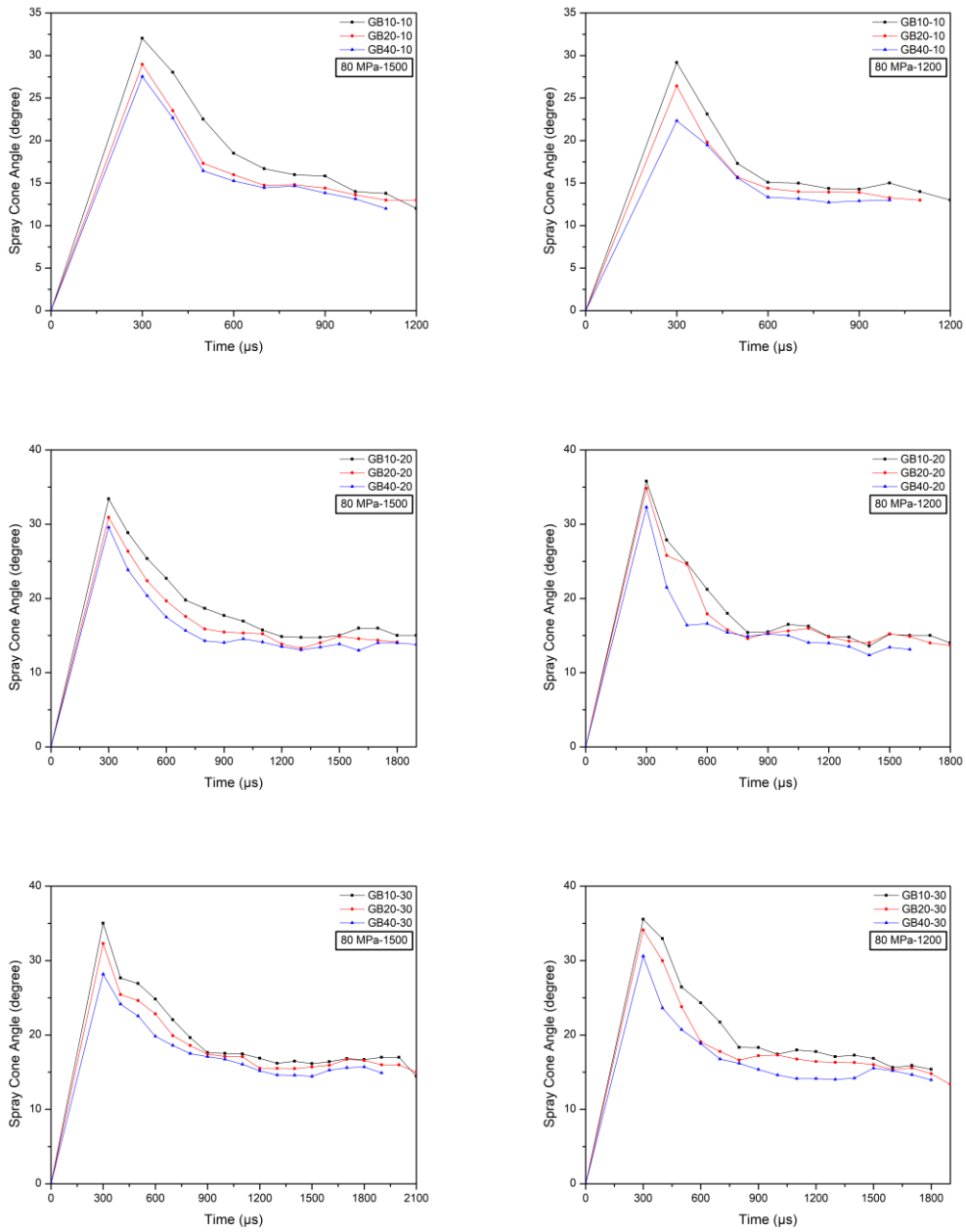


Figure 4.5: Comparison of spray cone angle temporal evolution of all tested fuels at 10 kg/m³, 20 kg/m³, and 30 kg/m³ under injection pressure of 80 MPa with 1200-1500 μs injection duration.

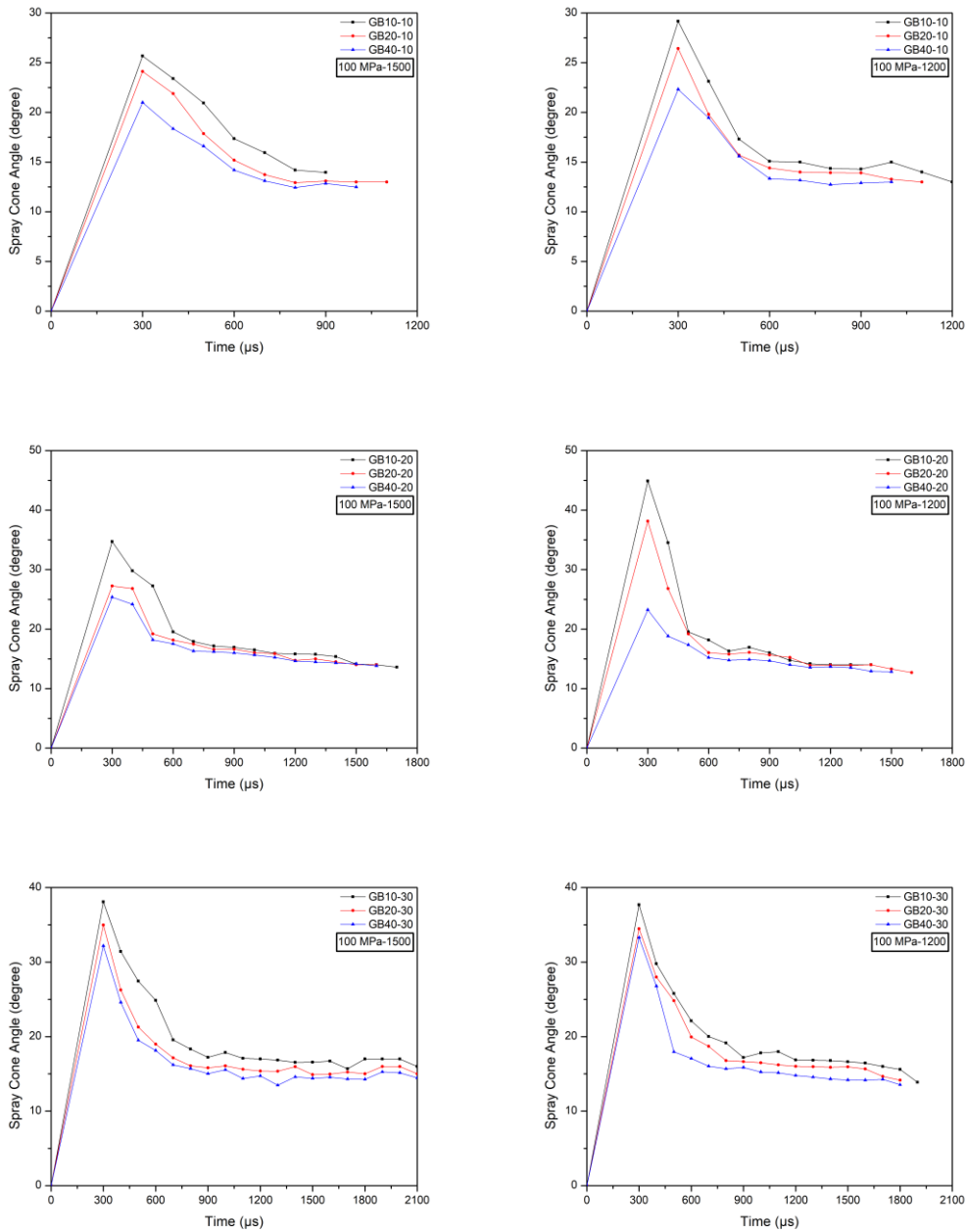


Figure 4.6: Comparison of spray cone angle temporal evolution of all tested fuels at 10 kg/m³, 20 kg/m³, and 30 kg/m³ under injection pressure of 100 MPa with 1200-1500 μs injection duration.

When the stabilization phase is entered, the spray angle will have a small or constant change in the end stages of the spray. If specific methods of analyzing the results are not used, the difference between the spray beam development over time will be very low. Therefore, in this study, the shadowgraph imaging method is used and the image processing algorithms are referenced and modified from ECN to ensure a standard comparison. At the first stage after spray break-up time, the spray angle in all test cases tended to decrease sharply and started to

go into the stable phase from about 600 μs . An increase in injection pressure means an increased jet-speed which leads to a decrease in the injection angle and also shows that the sensitivity between the injection angle and the injection pressure is low sensitive. However, for the same spray pressure conditions, an increase in ambient gas density leads to a larger cone angle and also the duration of the existence of a spray in the chamber before reaching the wall. At the time of stabilization, the change in the spray cone angle becomes smaller and more sensitive to the chamber pressure increase. This is due to increased ambient gas density resulting in a greater spray intrusion resistance which causes the spray to tend to diffuse wider and blend with its surroundings better.

4.4 Spray area

The relationship between spray angle and spray length contributes to spray area formation. The spraying area is an important parameter for evaluating the spraying process and compensate for shortcomings that the parameters should not be clearly shown. Because we can only see the 2D cross-section of the spray beam through the injection area. So, it roughly evaluates how well the fuel is blended with the air around it. The spray area is determined by the pixel difference of the image sprayed into the combustion chamber space and the initial image of the spray development. Spray volume analysis can be performed according to the spray area and the thickness of the spray length, but the spray area is located in three dimensional space and is susceptible to disturbances leading to non-genuine results. Similarly, Fig. 9 depicts the spray beam area under test conditions of injection pressures of 40 MPa to 100 MPa with 1200- 1500 μs injection duration at ambient gas density of 10-20-30 kg/m^3 respectively for GB10, GB20 and GB40 fuel types. Similar to the method shown in the previous section, the results arranged to the left represent the injection time of 1500 μs and the remainder was 1200 μs . At 40 MPa, the resulting trends for the fuels are approximately the same, but as the injection pressure witnesses an increasing pattern, the tendency to influence the chamber pressure is more evident at an injection pressure of 100 MPa. Based on the results from the jet length and the injection angle, the injection area of all 3 fuels tends to stop earliest at 10 kg/m^3 chamber pressure. The experimental results show that the difference compared with the previous study when fueled with high biodiesel content always dominates in the area exposed to the surrounding air. This can be explained by higher jet momentum and differences in test temperature conditions as well as injection duration. Additionally, increasing the ambient gas density inside the chamber reduces the area of the spray beam at the same time compared to

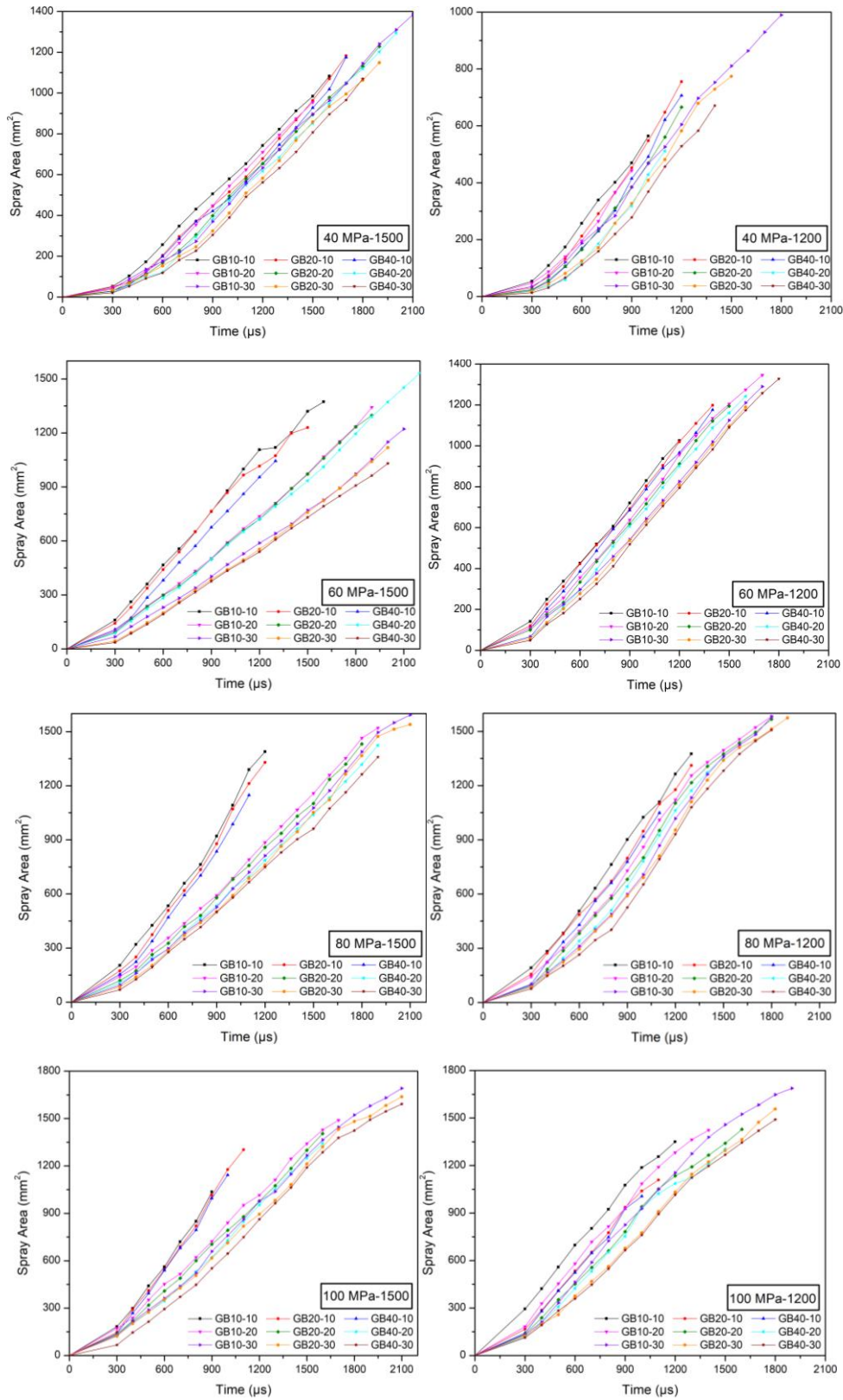


Figure 4.7: Comparison of spray area temporal evolution of all tested fuels at 10 kg/m^3 , 20 kg/m^3 , and 30 kg/m^3 under injection pressure of 40, 60, 80 and 100 MPa with 1200-1500 μs injection duration.

conditions with lower back pressure but it promotes the breakdown of fuel particles for better mixing and a higher steady state.

Some previous studies indicated that the linear trend of spray development is based on the test conditions, which is consistent with the resulting trend of this study [93] [94]. However, at some point with the injection pressures of 60 and 80 MPa, the fuel with the lower reduction in the injection angle at some point after step into the GB40 fuel spray beam stabilization phase. As a whole, with a gradual rise in injection pressure and injection duration, the area of the spray beam tends to increase over time and is affected by ambient gas density, but it increases the degree of blending air and fuel. Increasing the biodiesel composition increases fuel viscosity has been demonstrated in the fuel properties as well as investigated by the injection penetration length but it also shows bonding through the injection angle and injection area. However, the increase in biodiesel composition up to 40 % by volume of the fuel in this study was the basis for showing a clear comparison of its effect on the injection properties but it was not possible to conclude whether its advantage also depends on the flammability characteristics as well as the evaluation processes afterwards.

According to current studies, good evaporation conditions for the gasoline fuel are meant to take advantage of its self-ignition ability and further blend with biodiesel components to ensure the stable operation of the injector. High boiling points and a high cetane index can create a superior fuel mixture. Based on the above factors, GB20 is still promising for future studies because it shows a balance in based on the spray properties.

4.5 Summary

The evaluation process of the injection properties of fuel types GB10, GB20 and GB40 under ambient density conditions of 10, 20, 30 kg/m³ with the injection duration of 1200 μs and 1500 μs can be summarized as follows: ·When the spraying process is stable from the stage at 700 μs, the spray angle has little fluctuation, and the spray boundaries are more stable. The injection penetration length is remarkably influenced by the ambient gas density. In addition, increased biodiesel composition in the fuel leads to enhanced spray penetration length due to the fuel characteristics and the change in injection momentum. ·The trade-off of increasing the biodiesel content in the fuel mixture results in faster penetration of the fuel into the cylinder, which is not as efficient as increasing the degree of mixing between the fuel and internal air in the combustion chamber. ·For the same injection pressure conditions, an increase in the

ambient gas density results in a larger spray cone angle and also the duration of the spray existence in the chamber before it reaches the wall. At the time of stabilization, the change in the injector cone angle becomes smaller and more sensitive to the pressure increase in the spray chamber. ·The relationship between spray angle and spray length contributes to spray area formation. As the injection pressure and injection duration increase, the area of the spray beam also tends to increase over time and is affected by ambient gas density, but it tends to claim up the degree of mixing between the air and the fuel. ·The spray penetration of each type of fuel is considered in this paper, which clearly shows the combination of the experimental matrix between injection pressure, ambient gas density and biodiesel composition in the fuel. For each type of fuel when increasing ambient gas density, the penetration rate will decrease. In the case of the same ambient gas density, the penetration rate of GB20 and GB40 will not be too different, but GB40 is still somewhat higher than GB20. Through that, the article wants to provide a comprehensive data matrix on the spray process so that it can provide parameters for the research of GCI engines for high octane fuel and longer ignition delay. Under the influence of fuel viscosity, the results are normally shown through the test conditions by changes in injection pressure and ambient gas density. However, to consider the most suitable fuel for studies on GCI engines for high octane gasoline fuel, GB20 is still the most suitable. In addition, when applying biofuel through many studies, it has been proved that adding biofuel below 20 % by volume will not affect too much the operating conditions of the engine as well as ensure for stable combustion.

5. An investigation of the effect of chamber temperature on macroscopic spray characteristic under GCI engine conditions

Spray characteristics play an important role in the application of gasoline compression ignition (GCI) engines because it affects engine performance as well as engine design. In this study, the influence of temperature on the non-vaporizing spray process was evaluated through the experimental process on the constant volume chamber (CVC) with simulated conditions of the GCI engine. The experimental matrix was constructed by varying key factors, including chamber temperature, fuel injection pressure, and chamber gas density. The CVC with built-in heaters allows for temperature variations at 323 K, 398 K, and 423 K. To accommodate low load conditions, the fuel injection pressure is varied between 50 MPa and 110 MPa. Simultaneously, chosen variations of gas density, including two levels of chamber density are selected at 15 kg/m^3 and 30 kg/m^3 respectively. In addition, the injector angles are arranged at 90° (vertical) and 180° (horizontal) to create an overview of the spray characteristics for the case study of GCI engine conditions, viable for future studies using a constant-volume combustion chamber (CVCC), or even rapid compression engine machine (RCEM) in which the injector is commonly set horizontally. The gasoline blended with biodiesel by volume percentage consisting of 80% gasoline and 20% biodiesel was used as the main fuel in this study, namely the GB20 blend. The results of the spray characteristics collected through the images of the spray process based on the Schlieren optical method and the highspeed camera, consisting of the spray evolution and penetration length, spray penetration rate, spray area, as well as the spray cone angle are investigated. The difference in the spray process is denoted as the chamber temperature is increased. The spray penetrates to the chamber wall limit more quickly at elevated temperatures. The results were recorded as a decrease in impingement time by 12% and 9.5%, respectively, at the injection pressure of 50 MPa together with an ambient gas density value of 15 kg/m^3 . The cone angle of the spray tends to reduce by approximately around 3° to 10° in all experimental cases when the chamber temperature is high. However, when entering the post-phase at 450–600 μs , cone angle differences are negligible during the injection reaching the stable phase.

5.1 Spray evolution process of gasoline-biodiesel fuel blended

The spray evolution process is the foundation on which other spray characteristics can be analyzed. Based on the spray evolution process, the results recorded through the images can provide the characteristics of the spray penetration length, spray cone angle, spray area and so on. Typical results of the spray evolution in this study are presented for the conditions of injection pressure of 110 MPa, chamber density of 30 kg/m^3 , injector angles of 90° and 180° , chamber temperatures of 323 K and 473 K to evaluate the difference of spray pattern as well as spray behavior under high temperature. The results shown below in Fig. 3 are selected for intervals that give the most intuitive view of the spray development. However, the change in the morphology of the spray is more easily seen when images are placed in the same orientation. Therefore, the image rotation of the injection angle of 180° was performed to facilitate comparison at the same time points of the injector angle of 90° and 180° . According to the images of the spray evolution process displayed, the temperature has a major impact on the spray formation features. The stability of the environment in the chamber is greatly affected because the molecules move faster as the temperature increases from 323 K to 473 K. The spray formation time was also shortened by about $300 \mu\text{s}$ under the same conditions of injection pressure and gas density in the chamber. The shortening of the spray forming time and the impingement process will result in a more uniform mixture and better combustion improvement [95]. In addition, the Schlieren method significantly contributes to the quality of the experimental results compared to previous studies. When the injection pressure is increased, higher-density shock waves are created. However, shock waves are more difficult to observe clearly at 473 K and create noise at the edge of the injector. In addition to the large influence of temperature, the study also compares injector angles of 90° (vertical) and 180° (horizontal). The results show that injector angle of 90° produces a spray pattern that expands more quickly, with a larger spray angle. This means that the spray penetration length of the injector angle of 90° will be higher than that of the injector angle of 180° under the same test conditions. This difference can be explained due to fact that the influence of gravity has had a significant impact on the jet formation process in the case of injector angle of 180° .

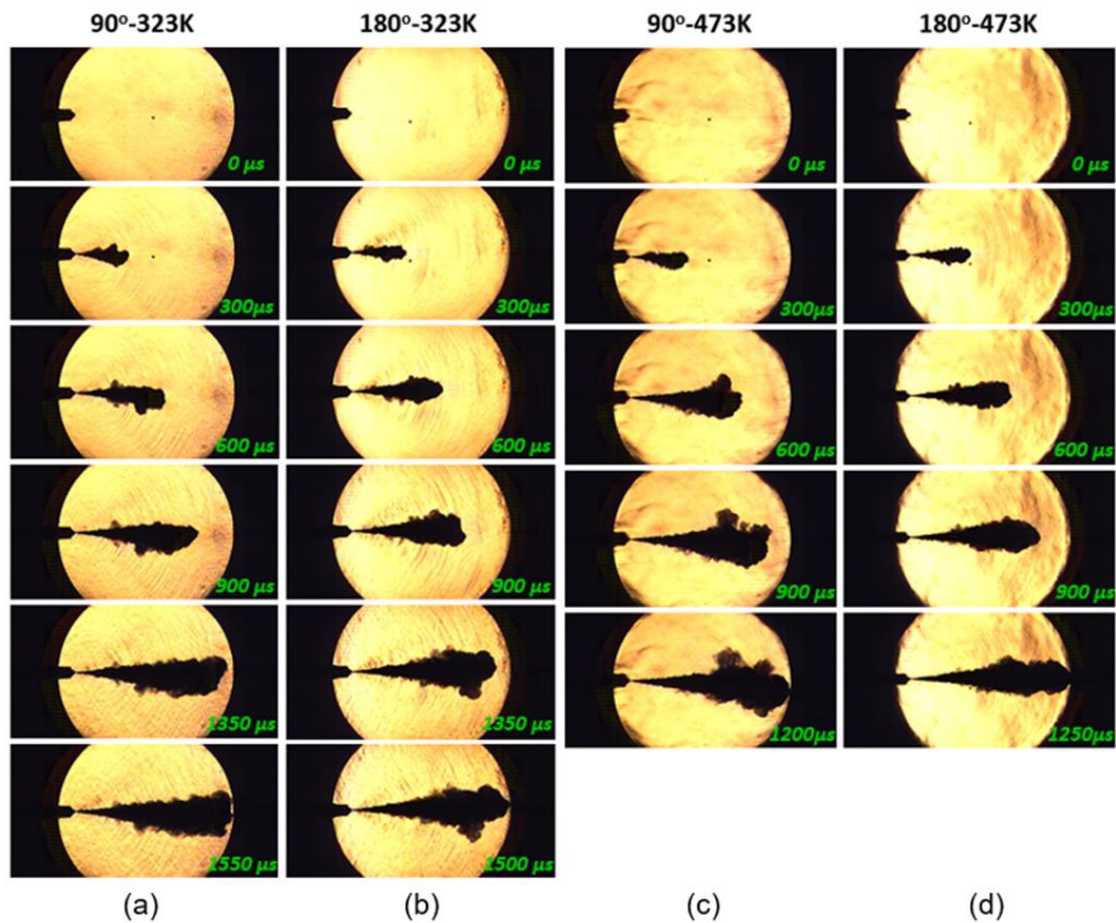


Figure 5.1: Comparison of spray evolution for injector angles of 90° and 180° at chamber temperatures of 323K and 473K, injection pressure of 110 MPa and gas ambient density of 30 kg/m³.

5.2 Spray penetration length

The spray penetration length of GB20 fuel is shown in Figs. 4 and 5 with the experimental conditions listed above. In this study, the injection duration was fixed at 1500 μs. Based on the graph below, the left side represents the 90° injector angle and the right side is the 180° injector angle. The results are presented with a time step of 150 μs. Experimental comparisons are guaranteed under the same conditions of optical setup to avoid the influence of uncertainty. The permissible error in all test cases does not exceed 2% including ancillary equipment. The errors of the main factors in this study are also presented in Table 5. The parameters are calculated based on the real-time experimental process. For each data shown in the error table, it has to go through a lot of testing for the stability of the equipment and record the value according to the max–min amplitude of each factor. In the case of the chamber temperature value, it is controlled by two independent controllers and is checked again through the

temperature data midi logger in various positions before starting the experimental process. To determine the spray penetration length, the start and end points are determined by the position of the injector tip and when the spray impinges on the wall.

Table 5.1: Experimental boundary conditions and error

Experiment conditions	Average value	Error value (%)
Injection pressure (MPa)	50-80-100	0.68-0.625-0.5
Density (kg/m ³)	15-30	0.1-0.15
Chamber temperature	323K-398K-423K	0.95-1.15-1.3
Fuel temperature (K)	323	1.5

Previously proposed theories of spray characteristics suggest that the spray tip penetration time can be separated into two main areas by a key breakup time. The spray breakup time (t_{break}) is based on the equations of Hiroyasu and Arai [96], and is illustrated as follows:

$$t_{break} = 28.65 \frac{\rho_f d_o}{\sqrt{\rho_c \Delta P}}$$

The details of the equation construction process were presented in the previous study with relevant parameters. The results of the t_{break} moment are presented in Table 6 with the respective values of injection pressure in addition to the ambient gas density. T_{break} is defined as an intersection, when $t < t_{break}$ the spray development and remains in the primary breakup region, and the spray penetration length tends to be linear. During this stage, the spray droplets emerge from the nozzle hole with a large spray angle and pointed tip structure before breaking due to the fact that when $t > t_{break}$, the fuel from the injector continues to be molecularized into smaller droplets thanks to the resistance of the external pressure and the density of the liquid and gas. At this time, the fuel enters the secondary injection stage and the spray development is slow due to the influence of the surrounding gas density. The development of spray penetration length is nonlinear and distinct from that of the primary spray stage. Current research also observed this two-stage based spray tip development phenomena, and all of the associated t_{break} values are given in Table 6.

Table 5.2: Spray breakup time for GB20 under ambient densities of 15kg/m³ and 30kg/m³

Ambient density (kg/m ³)	Injection pressure		
	50 MPa	80 MPa	110 MPa
15	160.839μs	126.423μs	106.798μs

Higher injection pressure results in increased spray penetration length, which can be attributed to increased spray momentum flux. This considerable rise is seen following the secondary breakup stage (t_{break}). The t_{break} values decrease from 160 μ s to 106 μ s respectively as the injection pressure increases from 50 MPa to 110 MPa at 15 kg/m³. This result is completely in line with the growing trend of spray penetration length. The imaging results of macroscopic spray can be obtained at the pre-t_{break} and post-t_{break} stages. However, the appearance of the spray beam is very small and can cause errors if the results are recorded in this case. Therefore, the limitation of the optical method applied in the present study is that it cannot be compared explicitly with the t_{break} value. To be able to accurately assess this stage, near-nozzle and microscopic spray experiments need to be applied to provide a more objective assessment. The introduction of a spray penetration length calculation equation based on fuel density and related pressure values provides a faster method of predicting injection pressure variation. In addition, this study's lowest injection pressure case was 50 MPa, which resulted in a complete absence of spray breakup before impingement on the wall. It seems to have overcome the drawback described in the previous study [97] [98].

Temperature variation was recorded from a low of 323 K to a high of 473 K. The gas supplied to the inside of the chamber is heated due to the high temperature of the chamber. This leads to a faster diffusion of the molecules inside. The faster movement of molecules will promote the spray beam to grow faster. With increased temperature, the process completes more quickly and the touching time decreases to a maximum of 400 μ s. This phenomenon completely obeys the laws of thermodynamics and molecular diffusion. The above phenomenon is recorded through a comparison between the injector angles of 90° and 180°, at an injection pressure of 50 MPa and gas density of 15 kg/m³, in which the impingement time decreases by 12% and 9.5%, respectively, when the temperature is increased from 323 K to 473 K. Under different conditions, when increasing the injection pressure to 110 MPa and the density of 30 kg/m³, the impingement time decreased by 22.5% and 16.6%, respectively. However, in Figs. 4 and 5 for the period from start to finish, the effect of temperature did not seem to be so great in the case of spray penetration properties. Spray penetration length increases neither much nor linear in most test cases. At the last stage, the change of temperature affected this characteristic. Note that, there is a clear difference between the injector angles of

90° and 180°, with the impingement speed of injector angle of 90° always being higher. Through the results, it can be determined that the injector angle of 90° always prevails for the injection and mixture formation inside the combustion chamber.

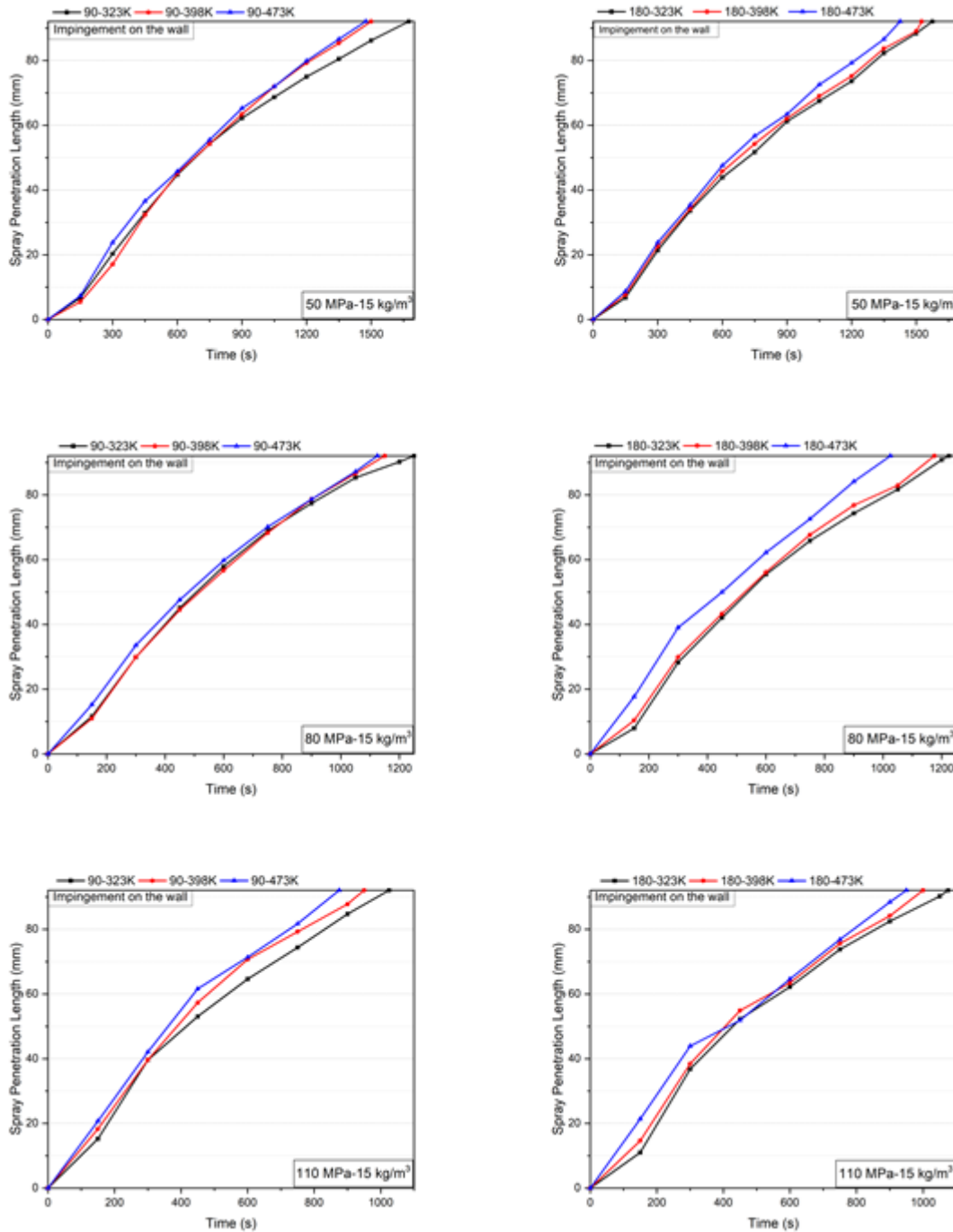


Figure 5.2: Temporal evolution in spray penetration length for injector angles of 90° and 180° at 15 kg/m³ with 50, 80, and 100 MPa of injection pressure and chamber temperatures of 323K-398K and 423K.

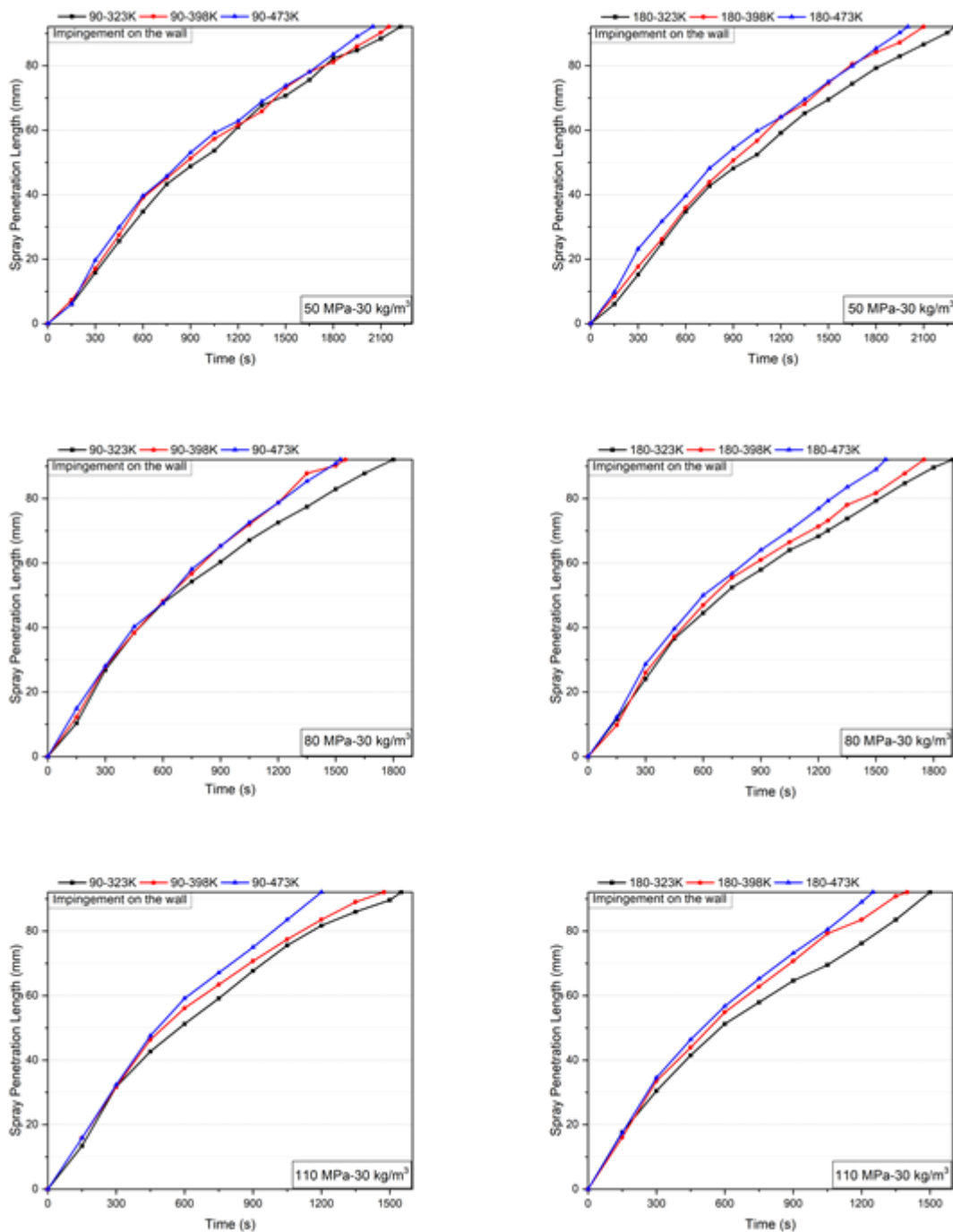


Figure 5.3: Temporal evolution in spray penetration length for injector angles of 90° and 180° at 30 kg/m^3 with 50, 80, and 100 MPa of injection pressure and chamber temperatures of 323K-398K and 423K.

The addition of biodiesel to the fuel ensures stable operating conditions of the injectors and directly affects the spray formation process due to increased fuel volume. Moreover, it also enables some of the fundamental disadvantages of high-octane gasoline fuel in the case of GCI

engines to be overcome. Indeed, it also shows the potential of GCI engines to use commercial fuel directly when the combustion modes and injection strategies are improved.

5.3 Spray penetration rate

The spray penetration rate results are shown in Figs. 6 and 7. Although the spray penetration rate results are mainly based on the spray penetration length, it helps to show the specific development process more clearly. The spray penetration rate is calculated based on spray penetration length over time. As shown in the results, the spray penetration rate peaks at about 300 μs after the spray starts to appear and decreases over time until the spray's wall impingement. The fluctuation in spray penetration rate over time can be explained by the fact that during the injection phase, the fuel injected in the previous stage undergoes acceleration due to the large pressure difference between the nozzle inside and outside gas density. Then, because of the promotion of the amount of the fuel in the next phase, the volume of the spray beam increases, as does the diffusion due to temperature, and the surrounding environment hinders the axial force of the spray to make the velocity decrease and cause a strong deceleration. After the spray beam enters the steady state, it means that the fuel is continuously supplied, causing the kinetic energy of the spray beam to increase to achieve a balance between the main thrust of the spray beam and the drag force of the outside ambient density. At this point, the spray penetration rate is still decelerating but with a slower amplitude until impingement on the wall. All test cases showed penetration rates within the allowable range and similar trends to related studies [99] [100]. The penetration rate values are recorded at 66, 130 and 146 m/s at 50, 80, and 110 MPa of pressure respectively in the 473 K-30 kg/m³ case at an injector angle of 90°. In addition, the effect of temperature is almost pronounced when compared under the same experimental conditions of injection pressure and ambient gas density. For example, in the case of 80 MPa, the penetration rate result was reported to increase by 9.4% and 12.6% for the 398 K and 473 K temperatures respectively compared to the 323 K chamber temperature. Meanwhile, a significant upward trend for the highest injection pressure was recorded at 22% for the 473 K case at the injector angle of 90°. However, the influence of the injector angle also affects the penetration rate results. At 110 MPa injection pressure and 473 K temperature, the penetration rate of the 90° injector angle is 3.6% higher than that of 180° injection angle. Meanwhile, the number was recorded 4.5% higher at 398 K temperature with 80 MPa injection pressure, also inclined to 90° injector angle. The results also suggest that the 90° injection angle will have an advantage because it is not affected by the effect of gravity.

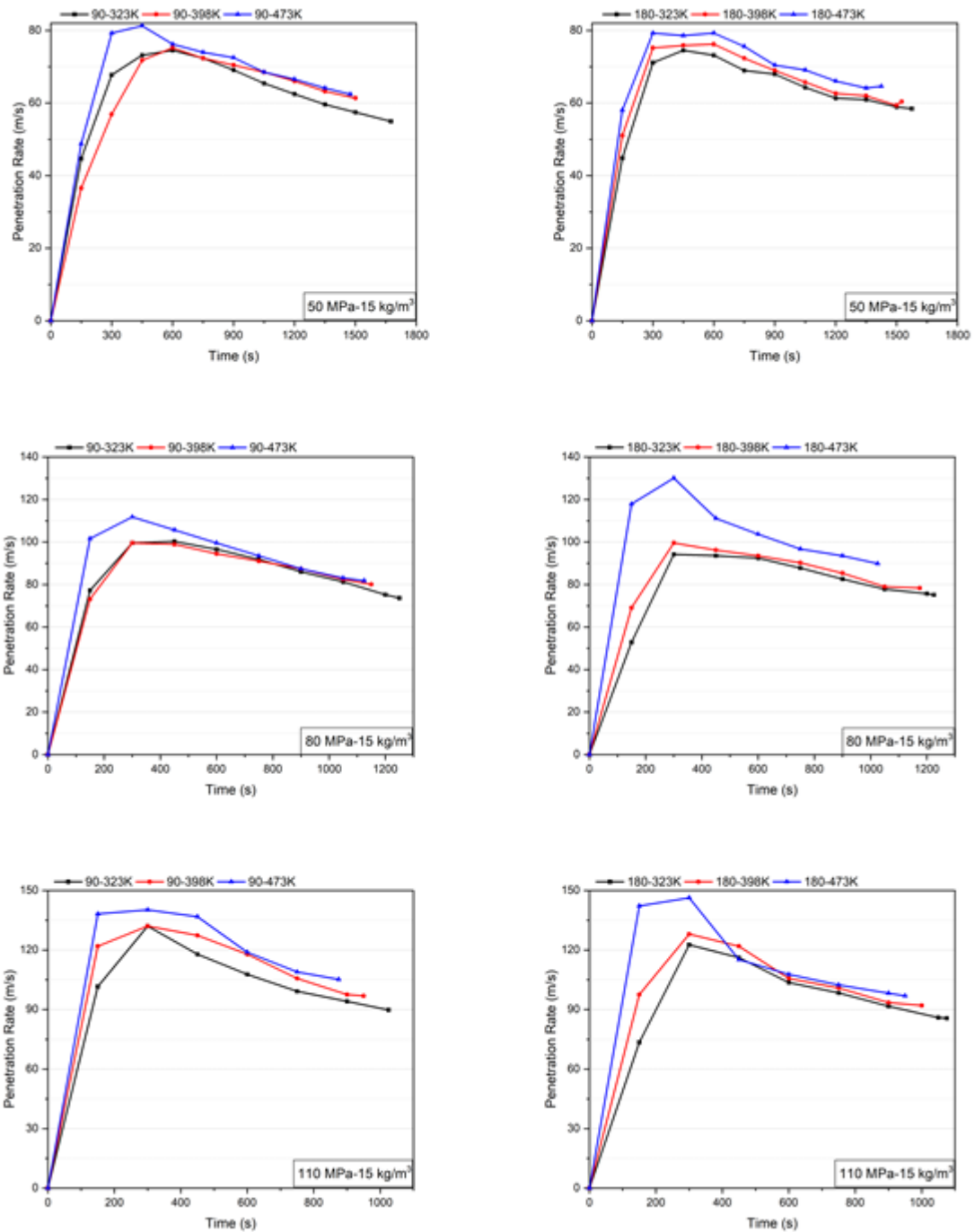


Figure 5.4: Temporal evolution in spray penetration rate for injector angles of 90° and 180° at 15 kg/m³ with 50, 80, and 100 MPa of injection pressure and chamber temperatures of 323K-398K and 423K.

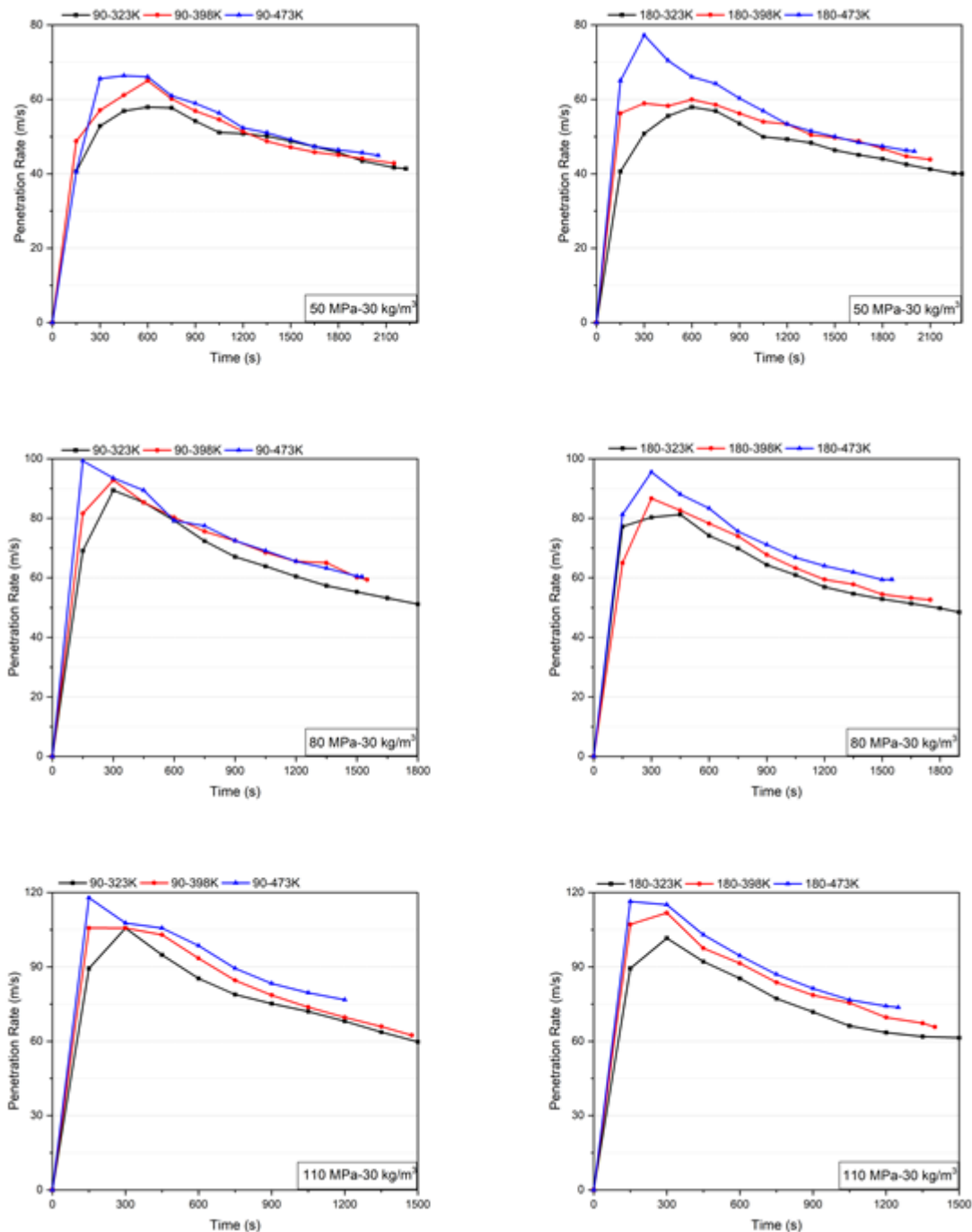


Figure 5.5: Temporal evolution in spray penetration rate for injector angles of 90° and 180° at 30 kg/m³ with 50, 80, and 100 MPa of injection pressure and chamber temperatures of 323K-398K and 423K.

At a high fuel rail pressure, the influence of injector angle between 90° and 180° can be quite acceptable when the jet develops at a rapid rate. In addition, the increased temperature will also help the penetration rate, and spray penetration tends to be perfect for better mixing. However, the possible trade-off of earlier spray impingement will affect the increase in soot

formation. An injection strategy as well as appropriate temperature and pressure regulation are required to reduce soot formation during the time of combustion. The diameter of a single-hole injector or nozzles arrangement on a multi-hole injector will also play an important role in influencing the mixture and emissions throughout the entire combustion process.

5.4 Spray cone angle

The results of the spray cone angle are shown in Figs. 8 and 9. It is shown in turn under the experimental conditions with the variation of ambient gas density, injection pressure, and chamber temperature as aforementioned. The resulting spray cone angle is captured through spray imaging and then processed by MATLAB code to provide an accurate value and is suitable for data analysis with a remarkably large number of images.

The cone angle of the spray decreases over time. When the fuel atomization starts to take place, the high axial velocity and radial momentum together with the impact of the resistance from the external pressure result in a large initial spray cone angle. The result on the graph shows this trend clearly, the spray cone angle has the largest values 47° and 45° for the 90° and 180° injector angles, respectively, at a temperature of 323 K. In addition, reduced surface tension and increased ambient gas momentum lead to some initial moments of formation which accounts for the spray being stalled in the axial direction and tending to diffuse laterally. However, the spray cone angle decreases slightly during the steady-state phase of the spray evolution and becomes very small before reaching the wall. Additionally, the average value of spray cone angle reduction is considered according to the development time of the spray. The maximum reduction at 50 MPa injection pressure is 72% while at 110 MPa injection pressure the reduction is only 55.5% in the case of 323 K- 30 kg/m^3 . This demonstrates a more stable spray formation as well as engine operation at high injection pressure. As the temperature increases, the spray cone angle decreases over the entire range of injection pressure and ambient gas density conditions. Within the period from the time of spraying to $600 \mu\text{s}$, the change is very clear with a difference from 3° to 10° between the temperature levels. After the period from $450 \mu\text{s}$ - $600 \mu\text{s}$, the change in the spray cone angle is not significant because it is determined mainly from the end of the spray beam. Based on the above relationships, the cone injection angle tends to decrease as the chamber temperature increases. A proper explanation for this can be considered the increased temperature of the in-chamber gas, which is capable of evaporating the fuel faster. On the other hand, for the temperature to be uniform at all points of the CVC, a long heating time leads to the tendency of the temperature to propagate in all

directions. The injector temperature tends to increase with the effect of increasing chamber temperature. It can also affect fuel viscosity, spray angle and spray cone angle.

Additionally, the relationships between the pressure of injection and ambient gas density are quite clear. The proof is that the spray cone angle decreases over time after the spray breakup time. It is indisputable the fact that the larger the spray cone angle before impingement on the wall, the better the mixing process will be. One comprehensive theory is that the larger the spray cone angle, the better the mixture, but that can also be prevented by too much fuel being attached to the cylinder walls. Therefore, small diameter injectors are often used for the spray research process to help promote the initial molecularization stage and form a more stable spray.

Fig. 10 shows that the evolution of the penetration length and the cone angle of the fuel blend's spray have a strong correlation. The typical case is shown at a temperature of 473 K and a chamber density of 30 kg/m^3 with the injection pressure levels outlined in the experimental conditions of this paper. The spray cone angle is set to the horizontal axis and the spray penetration length is set to the vertical axis. This graph represents the trade-off of the spray development. It can be seen from the discussion of the previous results that the growth of the jet length will lead to a smaller injection angle. The gradual decrease of the cone injection angle with time is nearly consistent at different injection pressure values. This trade-off relationship can be further optimized to reduce the negative effect of spray impingement on the combustion chamber wall by promoting the air–fuel mixing process with a larger spray cone angle and a suitable spray penetration length for higher engine efficiency. When injection pressure is increased from 50 MPa to 110 MPa, at the initial time when the spray cone angle has the maximum value for each case, the spray penetration length values of the 80 MPa and 110 MPa pressure levels are almost doubled compared to the 50 MPa case. At the beginning of the steady-state phase of spray development, from the first timing since 20° of spray cone angle and below, the increases in spray penetration length were 9.5% and 11.5% of the 80 MPa and 110 MPa pressure levels compared to 50 MPa, respectively. When entering the second half of the spray development, the spray cone angle does not change much, ranging from 13° to less than 20° . However, at this point, the increase of spray penetration length becomes rapid and reaches the finishing touch point, especially for cases with high injection pressure. This is completely consistent with the relevant physical properties of velocity and pressure.

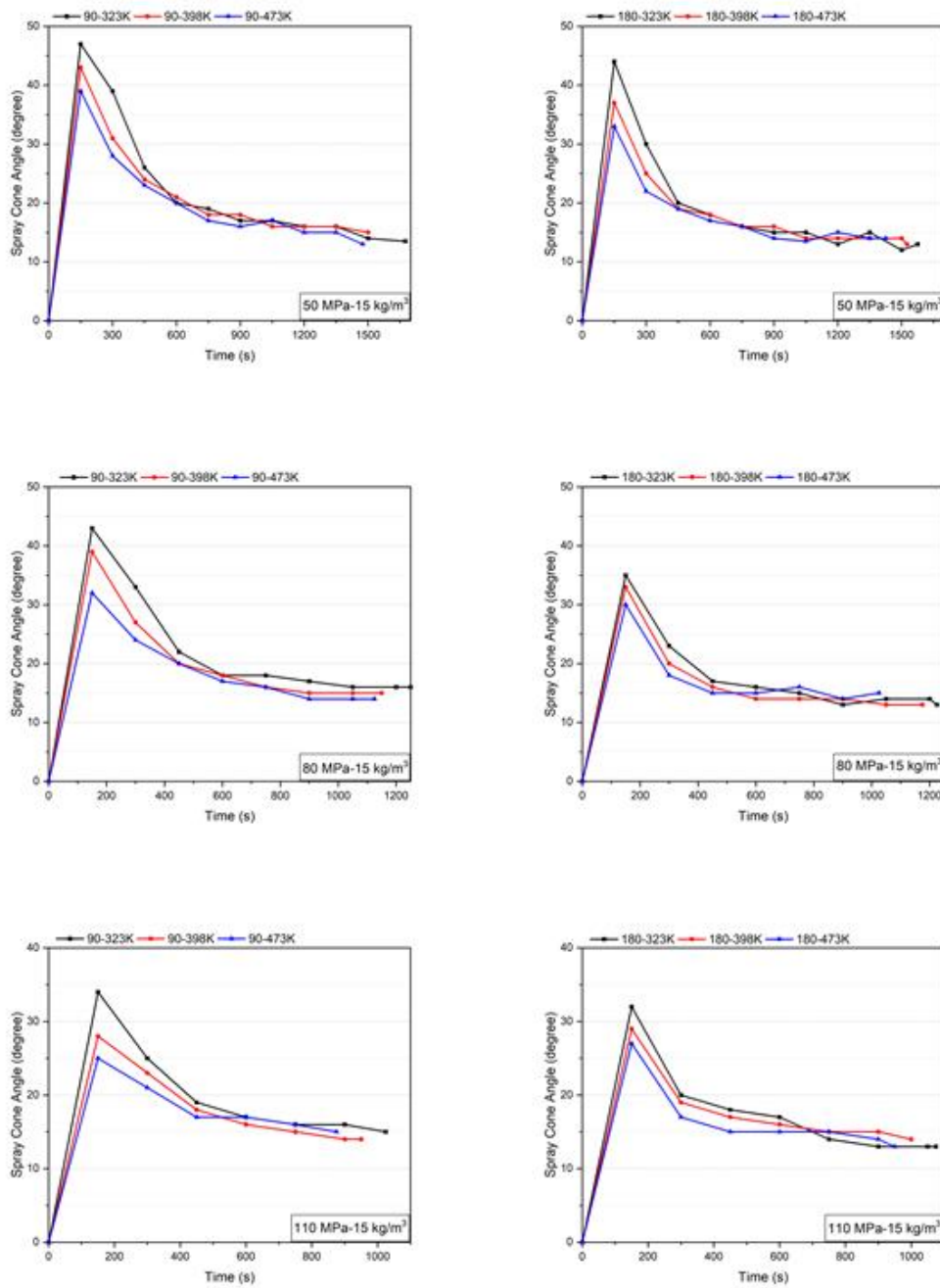


Figure 5.6: Temporal evolution in spray cone angle for injector angles of 90° and 180° at 15 kg/m³ with 50, 80, and 100 MPa of injection pressure and chamber temperatures of 323K-398K and 423K.

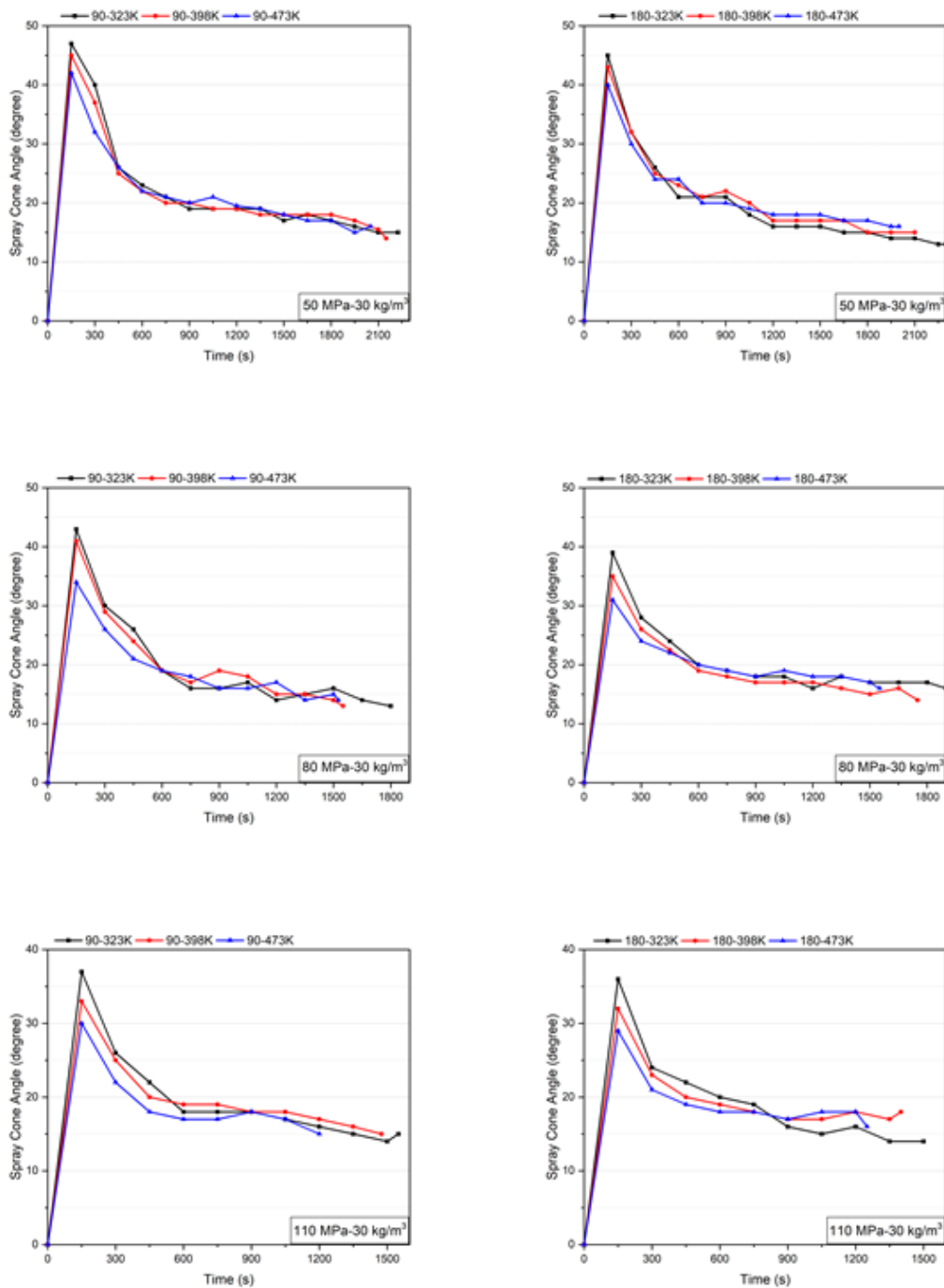


Figure 5.7: Temporal evolution in spray cone angle for injector angles of 90o and 180o at 30 kg/m³ with 50, 80, and 100 MPa of injection pressure and chamber temperatures of 323K-398K and 423K.

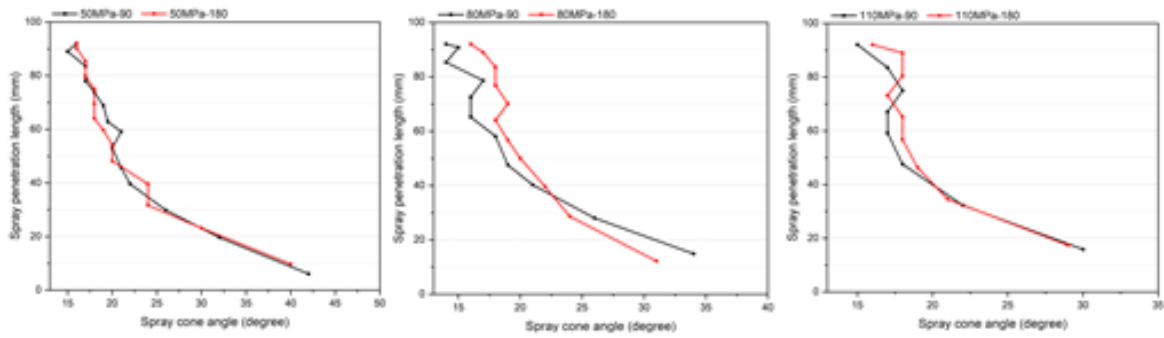


Figure 5.8: The trade-off of spray penetration length and spray cone angle during the spray process at 90° and 180° injector angle and 30 kg/m³ under 50, 80 and 100 MPa of injection pressure at 423K chamber temperature

5.5 Spray area

The spray area is among the crucial parameters used in the spray process evaluation. During the experiment, the spray area is calculated based only on the change in pixel count of the next and first images of 14 the process. The assessment of the spray area is only approximate because the results are only obtained as 2D images while the spray beam is formed in 3D space. During the spray formation process, turbulence within the spray is complex, so the assessment of the spray area is not entirely accurate, but it enables a comparison between different test cases and can highlight the connection between spray penetration and spray cone angle. Figs. 11 and 12 show the trend of the results in terms of spray area with temperature varying from 323 K to 473 K for the experimental matrix described above. The spray area value increases steadily with time and temperature. This is consistent with the spray penetration length and spray cone angle results shown in this paper. In most test cases, the spray area of the 110 MPa injection pressure gives the highest results. However, due to unknown perturbations of the spray beam, in some cases, the result of the average temperature of 398 K in this experimental matrix was higher than that of 423 K. This can be attributed to greater perturbation of the molecules at higher ambient pressure, leading to a large degree of diffusion, making the spray area larger when compared between different temperatures.

Another remarkable feature is that as the gas density increases, the spray area tends to follow the same pattern. This is explained by the spray cone angle, when the gas density increases, it creates greater resistance and causes an imbalance in the spray forming process, making the spray tend to diffuse to the sides and gradually reduce the spray impingement time to reach the wall. In addition, when increasing the temperature from 323 K to 423 K, the spray area also recorded a similar increasing trend. In some cases of 180° injector placement,

although the impingement time is very fast, it is not possible to compensate for the area of the spray. The effect on the 180° injector angle is quite large because the force of gravity tends to be perpendicular to the radial axis of the spray.

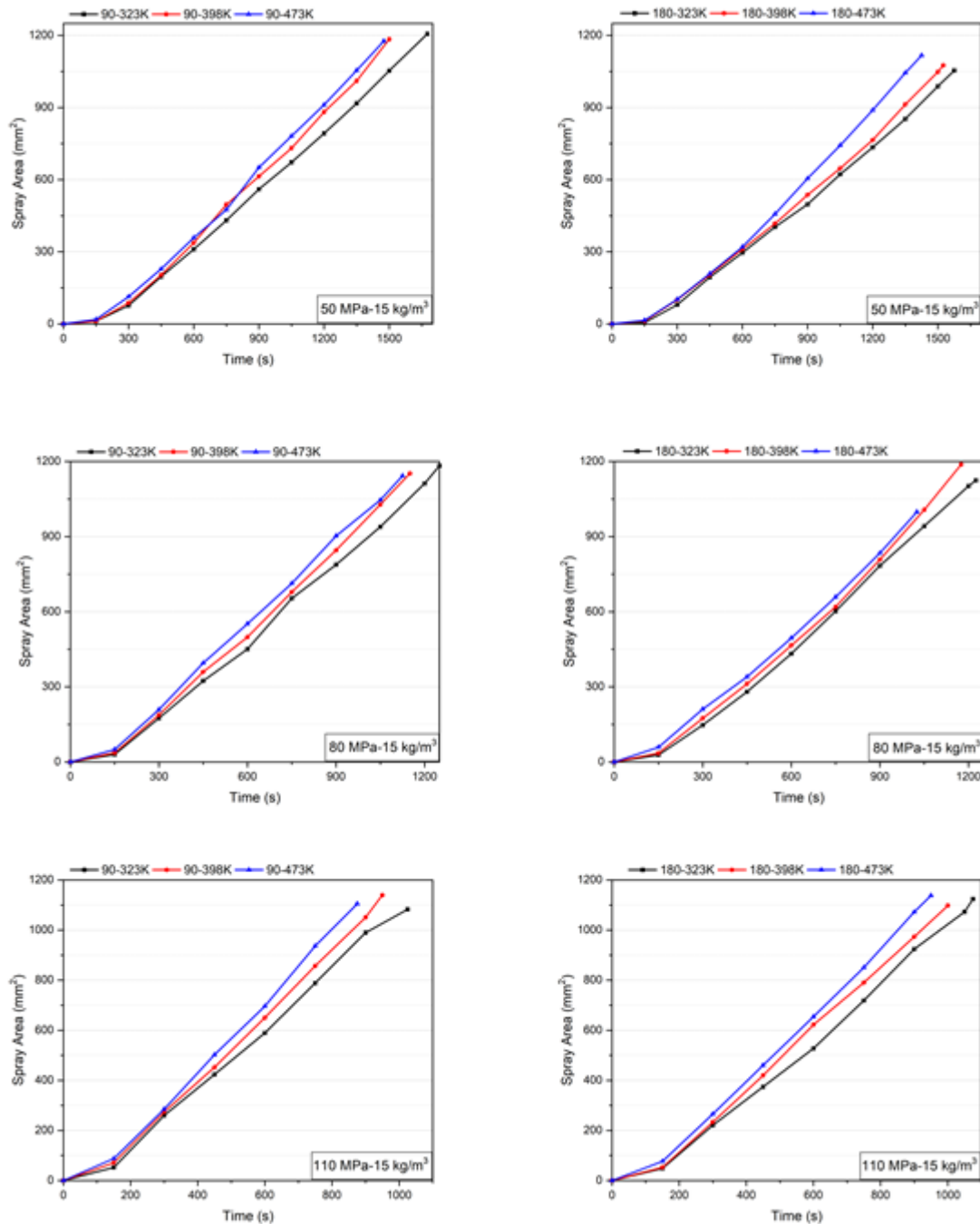


Figure 5.9: Temporal evolution in spray area for injector angles of 90° and 180° at 30 kg/m³ with 50, 80, and 100 MPa of injection pressure and chamber temperatures of 323K-398K and 423K.

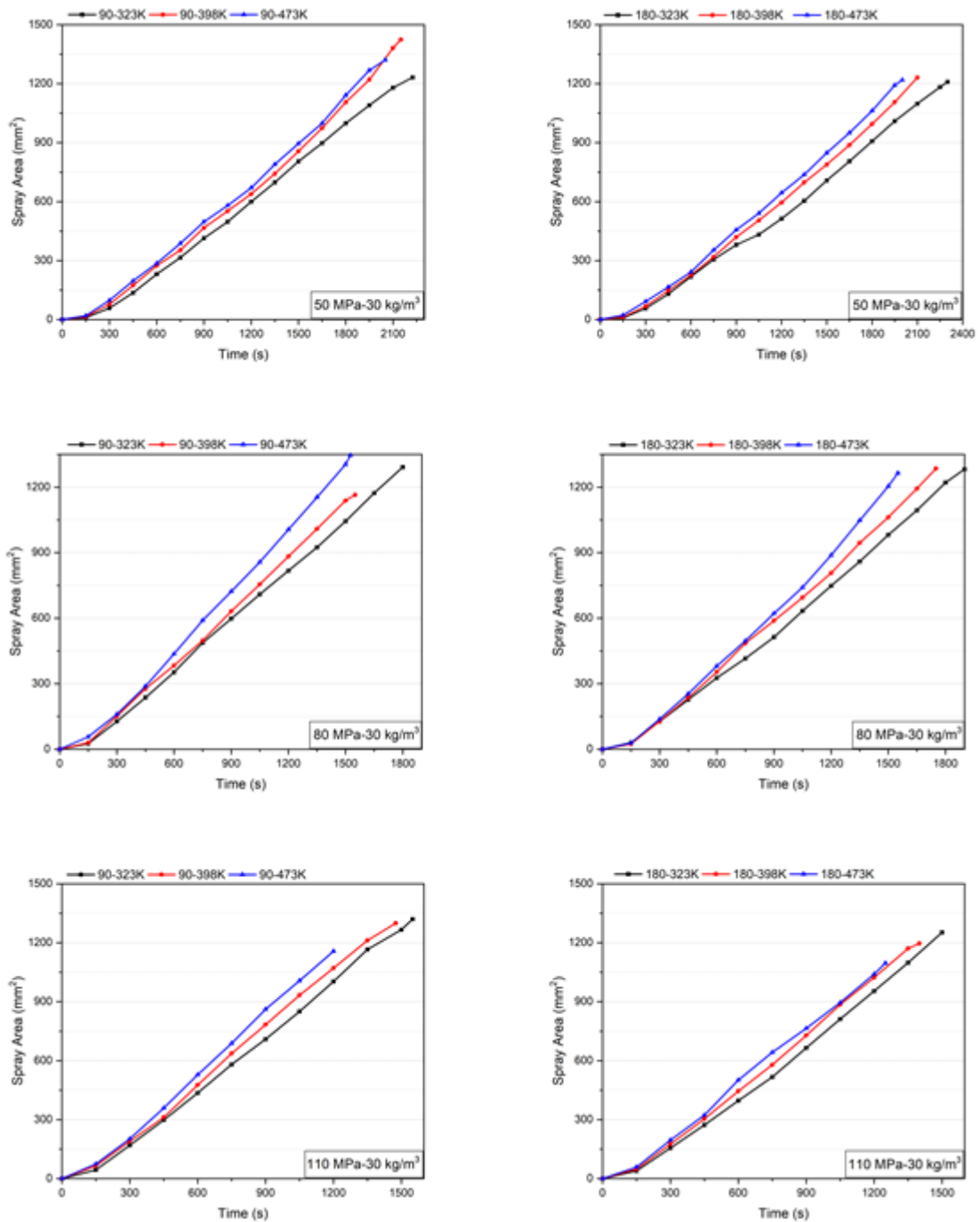


Figure 5.10: Temporal evolution in spray area for injector angles of 90° and 180° at 30 kg/m³ with 50, 80, and 100 MPa of injection pressure and chamber temperatures of 323 K-398 K and 423 K.

5.6 Summary

This current work focuses on studying the spray characteristics of GB blended fuel under GCI conditions. It provides general data and insights related to high-octane fuel injection as well as an established basis for studies on GCI engines. The effect of temperature is the key

factor tested in this study, in addition to injection pressure, chamber density and injector angle. Spray evolution tends to develop more quickly as the chamber temperature increases. Additionally, the results show a decreasing trend in spray cone angle when the temperature is gradually increased under constant conditions of rail pressure and ambient density. Similar to the trend of spray penetration length, the spray penetration rate and spray area also followed the same increasing trend with chamber temperature, stabilizing under the same test conditions. One notable contribution in this study is that the optical setup has overcome the disadvantages from the previous study. The shock wave image is shown more clearly when increasing the injection pressure with larger and denser turbulence. On the other hand, changing the injector angle also evaluates the influence on the result of spray formation. The evidence has always shown that the spray formation process at the 90° injector angle is dominant. This study also provides the necessary reference data for research on fuels using combustion simulation systems such as CVCC or RCEM. Based on the results obtained in this study and the previous study on non-vaporizing spray, it will form the basis for further research on GCI engine conditions through the following stages: vaporization and combustion in the desired temperature ranges. In addition, the spray impingement process and near nozzle experiment can be applied to the platforms that the research has achieved. From there, cross-process data for the condition of the GCI engine when operating with the GB blend is provided comprehensively.

6. Experimental analysis of high-temperature effects on vaporization spray characteristics in GCI engine conditions

This paper presents an experimental study investigating the vaporization spray process to analyze spray characteristics within a CVCC system under simulated conditions resembling Gasoline Compression Ignition (GCI) engines. The research focuses on examining how high ambient temperatures influence spray behavior. The study assesses the vaporization properties of a single-hole injector at varying injection pressures (50 MPa, 80 MPa, and 110 MPa) using two types of fuel, GB20 and GB40. High-speed Schlieren photography captures detailed spray images, distinguishing between liquid and vapor phases. Particularly at elevated temperatures of 800 K and 1000 K, with a constant oxygen concentration of 0%, the separation between liquid and vapor phases becomes more evident. Liquid penetration length decreases as temperatures rise across all injection pressure levels. Observations reveal a rapid expansion of the vaporization zone as temperatures increase from 600 K to 1000 K. Images of GB40 show a broader distribution of liquid compared to GB20, indicating more intricate fuel dispersion in the vapor phase. These findings offer critical insights into air-fuel mixing conditions in GCI engine settings, setting a foundational basis for future theoretical and experimental research in this field.

6.1 Methodology

The experiment utilized a CVCC system to explore how high temperatures affect spray characteristics under vaporization conditions. While previous studies have extensively investigated spray processes under non-vaporizing conditions and combustion dynamics in GCI engines, detailed assessments specifically focusing on vaporization spray characteristics with high-octane gasoline fuel in GCI engine operating conditions have been lacking. This study aims to fill this gap by analyzing the vaporization spray process and its response to temperature levels ranging from 600K to 800K to 1000K. Additionally, it seeks to augment the comprehensive evaluation of GCI engine research using high-octane fuels with additional parameters. In this experimental setup, the injection timing was synchronized with the moment when oxygen concentration in the mixture, after the pre-combustion process, reached 0%, maintaining a calculated density of 10 kg/m³. Throughout this study, the pre-combustion process refers to conditions simulating high temperature and high pressure akin to those found in diesel engines, achieved with a blend of fuel and air. To ensure data integrity and minimize

injection disruptions, the injector remained fully open for 1500 μs per injection event. Injection pressure varied between 50 MPa and 110 MPa in steps of 30 MPa to thoroughly examine the impact of operational conditions on spray characteristics. Detailed specifications for chamber temperature, fuel temperature, and setup parameters for the high-speed camera are provided in Table 6.1.

Table 6.1: Experimental test matrix

Fuel type	GB20-GB40
Injector type	Single hole- 0.33 mm
Injection duration (μs)	1500
Fuel temperature (K)	308
Injection pressure (MPa)	50-80-110
Ambient gas density (kg/m^3)	10 kg/m^3
Chamber body temperature (K)	373 K
Oxygen concentration (%)	0%
Ambient temperature (K)	600-800-1000
Frame rate (frames/sec)	80000
Exposure time	1/900000
Image resolution	256 \times 160 pixels

In experimental research, achieving precise results hinges on meticulous control of system parameters to minimize equipment errors, thereby reducing overall result inaccuracies. Throughout this investigation, stringent measures are employed to maintain consistent boundary conditions across experimental setups involving the CVCC system, associated equipment, and optical systems. It is ensured that variations in these parameters do not exceed 2%, as detailed in Table 6.2, which provides comprehensive information on boundary conditions and permissible error margins. This rigorous approach ensures reliable and comparable data across different experimental instances, enhancing the accuracy and credibility of the research outcomes.

Table 6.2: Experimental boundary conditions and error

Experiment conditions	Average value	Error value (%)
Injection pressure (MPa)	50-80-100	0.68-0.625-0.5
Density (kg/m^3)	15-30	0.1-0.15
Chamber temperature	323K-398K-423K	0.95-1.15-1.3
Fuel temperature (K)	323	1.5

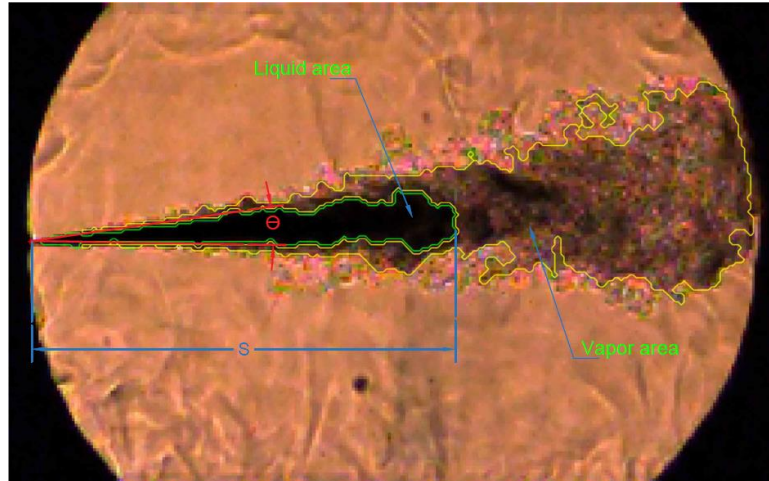


Figure 6.1: Definition of spray vaporization characteristics

6.2 Spray morphology

Figure 6.2 presents a typical vaporization spray image of GB20 and GB40 fuel mixtures at ambient temperatures ranging from 600 K to 1000 K, under a pressure of 110 MPa and density of 10 kg/m³. The image depicts two distinct regions: a dark liquid zone and a surrounding vaporization transition region, maintaining the characteristic jet structure of a single-hole injector. Vaporization images, captured at 300 μs intervals, track the spray from initiation to just before wall impingement, excluding post-impingement outcomes. Initially, the images show consistent liquid phase structures without phase transitions up to 300 μs. The liquid phase's characteristics in the early stages align with previous studies [106]-[109], with its area fraction progressively decreasing over 600 μs until contact with the chamber wall. Despite increasing ambient temperatures accelerating the vaporization process steeply, maintaining stable spray structures up to 1000 K without significant disturbance is confirmed through MATLAB analysis. At temperatures of 800 K and 1000 K, minor liquid remnants are less common around the jet's tail, while the inner liquid core is predominantly surrounded by the vaporization region. High ambient pressure is noted to reduce shear resistance from surrounding gases to the spray, affecting its stability as it forms and reaches a stable state. However, this study primarily focuses on temperature's influence on spray dynamics rather than comparing different ambient pressure levels. As temperature rises, the spray's vaporization boundary becomes smoother, with evaporative streaks disappearing due to entrained hot air, forming a haze at the spray's edge visible via Schlieren imaging. Notably, at 800 K and 1000 K, finely detailed interfacial regions between liquid and gas phases are observed post-600 μs,

indicating decreased surface tension and molecular path, blurring the distinction between liquid and vapor phases.

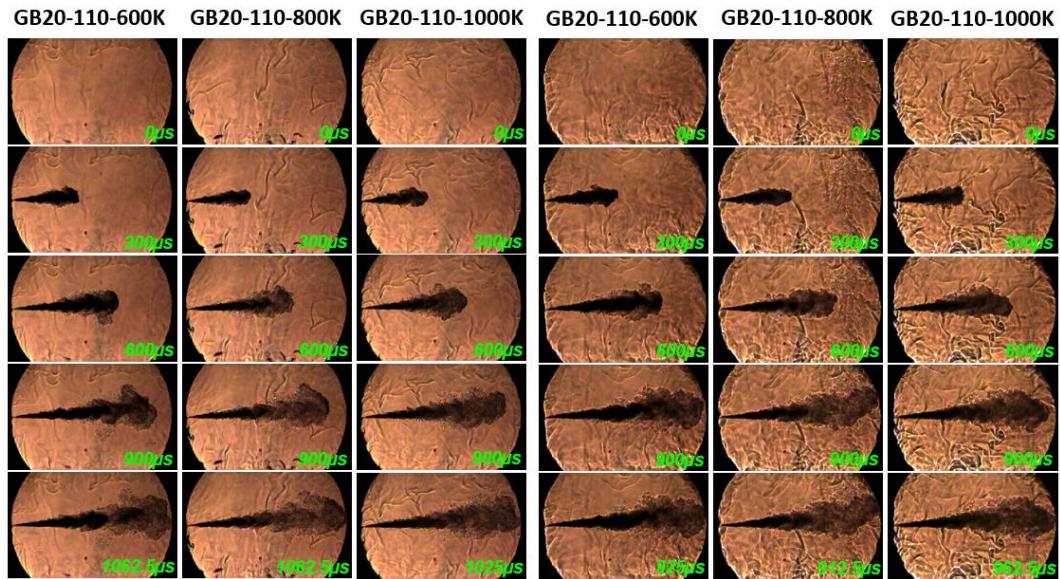


Figure 6.2: Schlieren image sequences for different ambient temperature of GB20 and GB40 at 110 MPa injection pressure and 10 kg/m^3 ambient density

6.3 Liquid penetration length

Figure 6.3 illustrates the results of liquid penetration length under vaporization conditions, examining the influence of high temperatures on injection pressures ranging from 50-80-110 MPa. The graph presents the impact of three temperature levels on liquid penetration length for both GB20 and GB40 fuels. The initial emergence of the spray marks the beginning of spray development, with endpoint measurement taken upon spray profile contact with the combustion chamber wall. This study does not generalize vaporization results beyond 2 milliseconds, focusing on direct comparisons with previous findings for verification. The trend of liquid penetration length exhibits nonlinear growth, differing notably from non-vaporization experiments reported previously. From spray emergence to $600 \mu\text{s}$, a pronounced and gradual increase in liquid penetration length is observed across various temperature and pressure settings. Beyond $700 \mu\text{s}$, minimal changes occur, stabilizing as the vaporization zone nears the wall. Initially, fuel supply from the nozzle controls jet length and velocity through axial momentum. Vaporization subsequently influences liquid penetration length dynamics, resulting in minor changes in later stages. Continuous needle opening allows steady downstream fuel movement, progressively diminishing due to evaporation, especially at higher pressures like 110 MPa. Increased pressure enhances atomization, reducing droplet size and

accelerating evaporation due to heightened surface area-to-volume ratios. While higher injection pressures correlate with increased liquid penetration length at identical time points, the liquid phase shows minimal sensitivity to pressure changes [114].

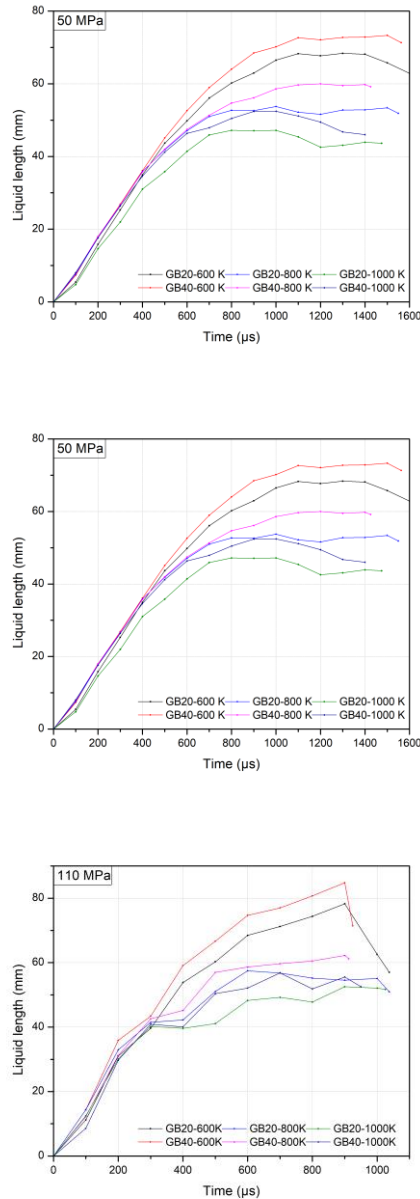


Figure 6.3: Liquid penetration length for GB20 and GB40 at 600 K to 1000 K ambient temperature and 10 kg/m^3 ambient gas density under 50, 80 and to 110 MPa injection pressures.

Moreover, liquid penetration length decreases with rising temperatures controlled by environmental density calculations and adjusted injection timing. Experiments vary temperatures from 600 K to 1000 K, surpassing fuel critical temperatures to favor dual-phase outcomes predominantly of liquid and gas. Similarly, under consistent injection pressures,

liquid penetration length stabilizes downstream where fuel mass flow equals evaporation rate [110][111][112]. Lower injection pressures under the same temperature conditions reduce fuel supply time, where phase transport processes like mass diffusion and heat conduction become evaporation constraints [113]. GB40 fuel, with higher biodiesel content, consistently shows superior liquid penetration length development compared to GB20, attributed to gasoline's faster evaporation rate versus biodiesel. Evaluation across volumetric concentrations reveals GB20's higher evaporation propensity than GB40 under most temperature conditions. These findings underscore the practical significance of gasoline fuels and blends in optimizing combustion systems for GCI engines.

6.4 Liquid area

Figure 6.4 provides an analysis of liquid area results under varying experimental conditions detailed in previous sections. The study examines the impact of ambient temperature on GB20 and GB40 fuels across different injection pressure levels. As ambient temperature rises, there is a corresponding decrease in the liquid area, mirroring trends observed in liquid penetration length. Conversely, differences in injection pressure levels do not significantly affect liquid area results under identical temperature conditions, highlighting the interplay between liquid penetration length and spray angle development. The evolution of the liquid zone during vaporization spray with a single-hole injector is categorized into initial development, a steady-state phase, and eventual decline toward complete vaporization. High-octane gasoline blended with biodiesel demonstrates distinct characteristics compared to diesel or low-octane fuels, particularly relevant for commercial applications and GCI engine objectives. Significant variations in liquid area are observed between temperature cases of 600 K, 800 K, and 1000 K, with less clear differences between 800 K and 1000 K, indicating uneven distribution across scenarios. The vaporization rate, molecule distribution, and atomization process vary with each 200 K temperature increment, influencing spray combustion phenomena, spray break time, and ignition delay in combustion processes. The persistence of faint liquid regions within the vaporization zone is attributed to radial spray momentum and turbulence in the spray core sustained by continuous fuel supply until injector deactivation. Although the vaporization zone reaches the combustion chamber wall before injector deactivation, suggesting potential for liquid region expansion, stabilization and gradual reduction of the liquid region occur as vaporization completes. These observations underscore the rapid acceleration of vaporization

rates in gasoline-biodiesel fuel mixtures under high temperatures, outpacing spray development and fuel supply growth in high-pressure scenarios.

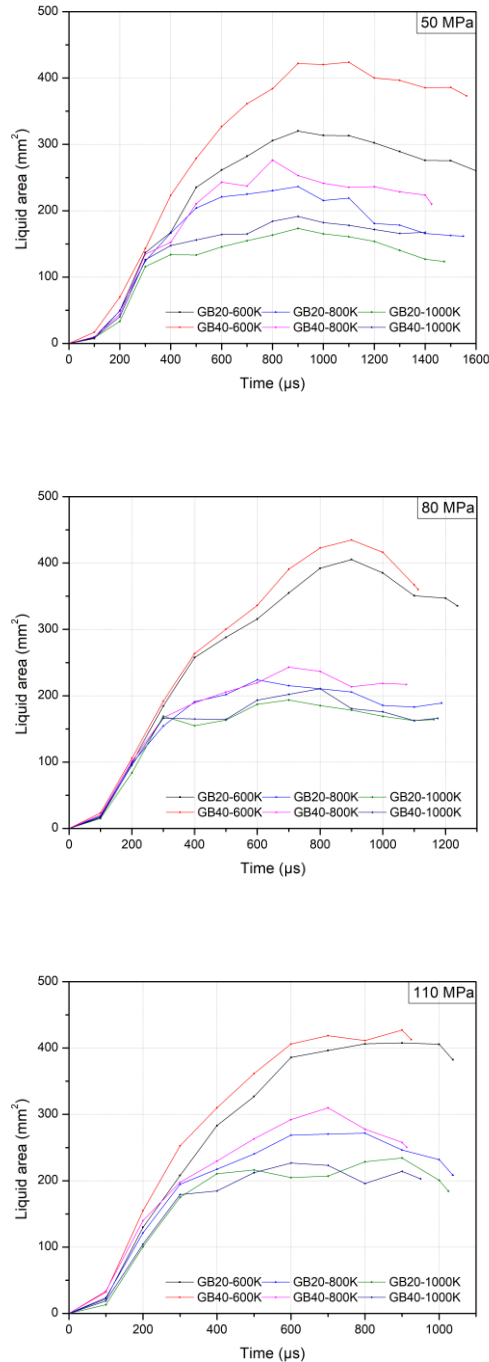


Figure 6.4: Liquid area for GB20 and GB40 at 600 K to 1000 K ambient temperature and 10 kg/m^3 ambient gas density under 50, 80 and to 110 MPa injection pressures.

6.5 Vaporization area

Figure 6.5 illustrates the influence of ambient temperature and injection pressure on the vaporization area formation for GB20 and GB40 fuels. The graphs depict how temperature affects each pressure level and fuel type, distinguishing between liquid and vapor phases within the spray image. Vaporization area determination utilizes MATLAB code for pixel region analysis, converting pixel counts into measured area. This study focuses on defining liquid penetration length and combustion chamber boundaries, not practical vaporization length assessments. Prior research has explored vapor injection for various fuels but lacks thorough investigation into vaporization area evaluation.

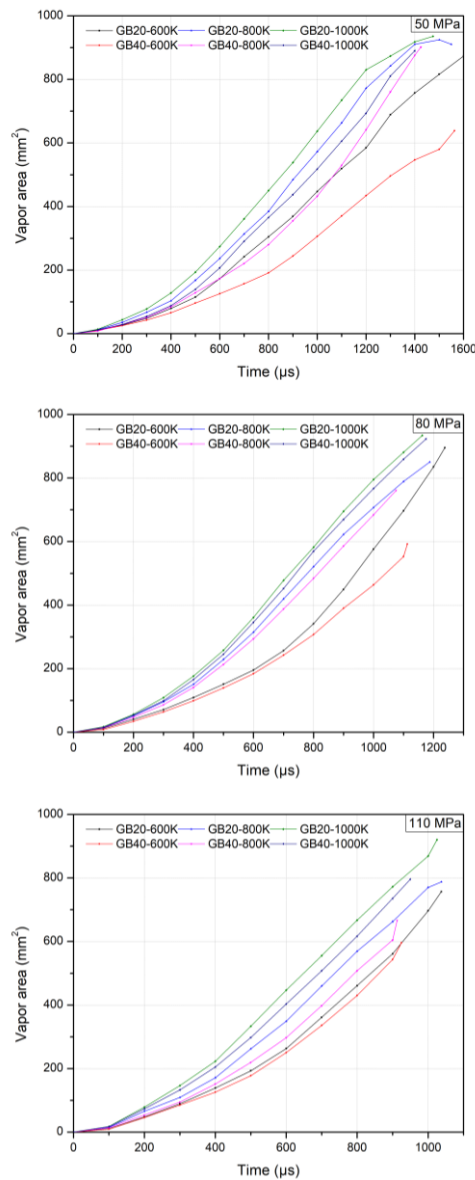


Figure 6.5: Vapor for GB20 and GB40 at 600 K to 1000 K ambient temperature and 10 kg/m^3 ambient gas density under 50, 80 and to 110 MPa injection pressures.

GB20 fuel consistently shows superior vaporization zone development compared to GB40 across all conditions, attributed to its higher gasoline composition. However, GB40, with a higher biodiesel content, does not significantly impact vaporization results. The vaporization zone exhibits an increasing trend as it approaches the combustion chamber wall, following a nonlinear trajectory despite a steep slope. Elevated ambient temperatures accelerate vaporization rates relative to spray speed, particularly noticeable at higher injection pressures. Despite more uniform results across test cases compared to liquid penetration length and other parameters, vaporization area values show minimal variance at different pressure levels. Increased fuel supply under higher injection pressure rapidly develops both liquid and vapor phases. Higher ambient temperatures further stabilize and enhance vaporization, facilitating finer fuel-air mixing in engine conditions. The vaporization process intensifies beyond the chamber wall, potentially affecting liquid phase structure post-contact or after 2 ms, necessitating robust physical and vaporization models for comprehensive evaluation under GCI engine combustion conditions.

6.6 Summary

The investigation into vaporization spray characteristics of gasoline-biodiesel fuel mixtures under GCI engine conditions yielded significant insights. Across varied injection pressures (600-800-1000 K) and fuel types (GB20 and GB40), distinct regions for liquid and vapor phases were consistently observed. The liquid phase gradually decreased from 600 μ s until contact with the chamber wall, with the vaporization boundary becoming apparent after 500 μ s post-spray initiation. Interestingly, differences in injection pressure did not markedly affect the liquid phase area at equivalent temperatures. Initially, GB20 exhibited a lower spray angle than GB40 up to 600 μ s, but this distinction diminished during the vaporization phase. Conversely, the vaporization phase showed an expanding morphology as it approached the chamber wall, accelerated by higher injection pressures across all temperature and fuel type scenarios studied. These findings underscore the complex interplay between injection dynamics, fuel composition, and ambient temperature in influencing vaporization spray behavior in GCI engines.

7. Experimental study of spray combustion phenomena in gasoline-biodiesel blends for GCI engine conditions

This chapter presents the spray and combustion characteristics simulating GCI engine conditions, using a constant volume combustion chamber (CVCC) system with a gasoline-biodiesel blend. The blend's biodiesel content varies from 0 to 20%. Combustion characteristics, including ignition delay, flame development, and heat release rate, were analyzed at an injection pressure of 90 MPa, ambient gas density of 15 kg/m³, and temperatures of 900-1000K. Results show that GB00 exhibits a longer ignition delay compared to GB10 and GB20, reflected in the heat release rates at both 900K and 1000K.

7.1 Spray evolution

Figures 7.1 and 7.2 present a detailed examination of the spray evolution for the fuel blends GB00, GB10, and GB20, subjected to an injection pressure of 70 MPa under two distinct ambient gas densities, 10 kg/m³ and 15 kg/m³. These figures reveal how the shape and behavior of the spray beam change with varying biodiesel content in the fuel mixture, underscoring that biodiesel significantly impacts spray characteristics by enhancing both fuel viscosity and density. In the case of GB00, which is pure gasoline, the spray development is notably slower due to gasoline's higher vaporization characteristics. This slower progression aligns with findings from GCI studies, which have consistently shown that gasoline, under vaporizing conditions, exhibits a shorter liquid length compared to diesel-based fuels. The rapid vaporization of gasoline leads to a quicker transition from liquid to vapor phase, which restricts the overall spray length and influences the spatial distribution of the spray.

As the ambient gas density increases from 10 kg/m³ to 15 kg/m³, the resistance within the combustion chamber rises, affecting the spray formation dynamics. This increased resistance results in a slower progression of the spray towards the chamber wall, as higher density environments impose more significant drag forces on the fuel spray. The images illustrate that at an ambient gas density of 15 kg/m³, the spray angle becomes larger and more comprehensive compared to the scenario with 10 kg/m³. This larger spray angle at higher density indicates more effective fuel-air mixing, which is crucial for achieving efficient combustion.

Combustion theories support the observation that a well-formed fuel-air mixture enhances combustion efficiency, particularly in engines with high compression ratios, where achieving a homogeneous mixture is vital for optimal performance. The trend in spray formation across

different densities demonstrates that spray growth does not follow a simple linear relationship with increasing gas density. Instead, higher ambient density introduces complex interactions that influence the spray's diffusion and mixing characteristics, suggesting that merely increasing density does not proportionally enhance spray development but instead modifies its trajectory and spread.

These findings highlight the intricate balance between biodiesel ratios and ambient conditions required to optimize fuel injection and combustion processes. Adjusting these parameters can significantly influence spray dynamics, leading to better combustion efficiency and overall engine performance. This detailed understanding offers valuable insights into the potential for enhancing GCI engine performance by tailoring fuel composition and operating conditions, ultimately supporting the development of more efficient and reliable engines.

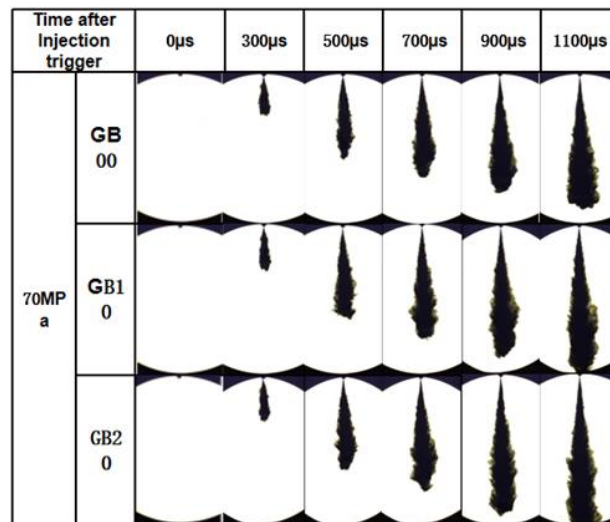


Figure 7.1: Spray evolution under 70 MPa injection pressure of GB00, GB10 and GB20 with 10 kg/m³ of gas density

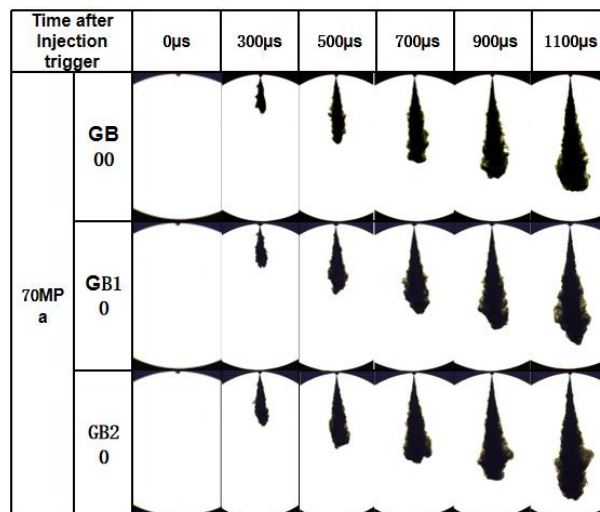


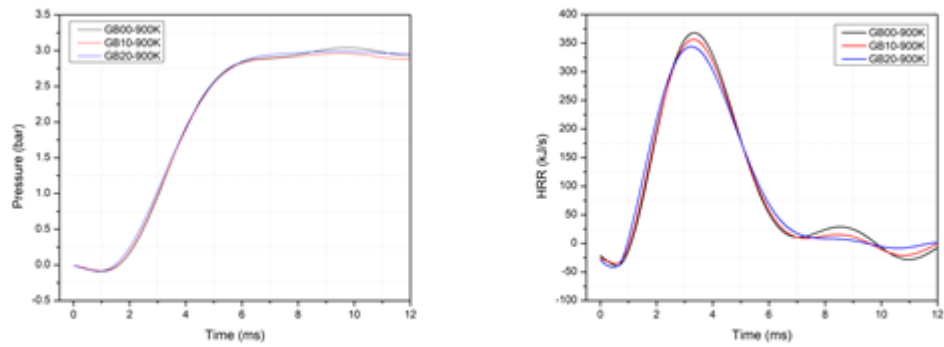
Figure 7.2: Spray evolution under 70 MPa injection pressure of GB00, GB10 and GB20 with 15 kg/m^3 of gas density

Figure 7.2 presents the setup for observation of the natural light emission from spray combustion of gasoline-biodiesel blended fuels. A high-speed CMOS camera (Photron SA3) with a Nikkor lens was used to obtain the natural soot luminosity imaging at 512×128 pixels and rate of 20,000 frames/s, which corresponds to a $40 \mu\text{s}$ increment for each image. The injected signal from the injector triggers the camera to start recording the set of combustion images.

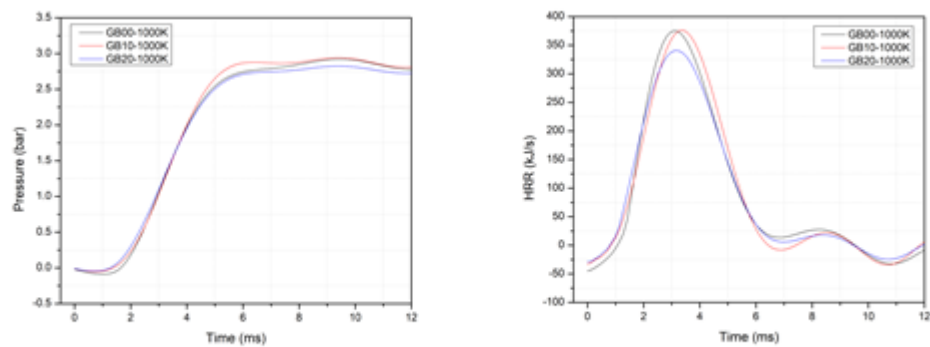
7.2 Pressure and heat released rate

Figure 7.3 presents the combustion pressure and heat release rate characteristics for three fuel types: GB00 (pure gasoline), GB10 (10% biodiesel), and GB20 (20% biodiesel). These measurements were conducted at temperatures ranging from 900 K to 1000 K, with an injection pressure of 90 MPa and an ambient gas density of 15 kg/m^3 , under conditions of 15% oxygen to study combustion mixture control. The results show that all fuels predominantly exhibit single-stage ignition, driven by the primary gasoline component, which leads to rapid chemical reactions across the temperature range. This rapid reaction results in a sharp temperature increase and a corresponding peak in combustion pressure.

As the biodiesel content in the fuel increases, there is a noticeable decrease in the heat release rate at both 900 K and 1000 K. This reduction is attributed to the higher cetane number of biodiesel, which shortens the ignition delay and leads to a more controlled and gradual heat release. Higher cetane numbers indicate that biodiesel ignites more readily and burns more steadily than gasoline, which explains the smoother heat release profile with increased biodiesel content. Moreover, as ambient temperature increases from 900 K to 1000 K, the heat release rate further decreases across all fuel blends tested. This phenomenon occurs because higher ambient temperatures and the volatile nature of the fuel mixture facilitate earlier formation of the mixture, leading to increased heat loss through conduction to the chamber wall and within the diffuse flame. These observations underscore the complex interplay between fuel composition, ignition behavior, and ambient conditions, offering important insights for optimizing combustion processes. Adjusting biodiesel levels and ambient temperatures can effectively control ignition and combustion characteristics, enhancing the performance and efficiency of GCI engines.



(a) 900K, 15% oxygen



(b) 1000K, 15% Oxygen

Figure 7.3: Heat release rate for GB blends fuel at 900 K and 1000 K ambient temperature under ambient density 15 kg/m^3 and 90 MPa injection pressure

7.3 Ignition delay

Figure 7.4 shows the ignition delay values for three different fuels at two ambient temperatures, derived from the heat release rate results. The ignition delay decreases significantly with higher biodiesel content and rising ambient temperatures, aligning with findings in GCI engine combustion studies. The reduction in ignition delay when biodiesel increases from 0 to 20% can be explained by the fuel's properties. Gasoline, the primary component, naturally has high ignition delay characteristics. Adding biodiesel, which has a higher cetane number, lowers the overall ignition delay of the fuel blend. Experimental data confirm that gasoline can be combusted through compression, making it suitable for CI engines. However, its high volatility can lead to the formation of flammable mixtures, causing notable fluctuations in combustion and affecting ignition delay.

Additionally, higher ambient temperatures reduce ignition delay by accelerating fuel evaporation, leading to quicker jet development and earlier mixture formation during

combustion. Despite varying the injection pressure from 40 to 90 MPa, the common rail system pressure remained stable, and the fuel temperature was kept optimal. However, substantial fluctuations in injection pressure could destabilize the system, highlighting the need for further investigation into the impact of such variations.

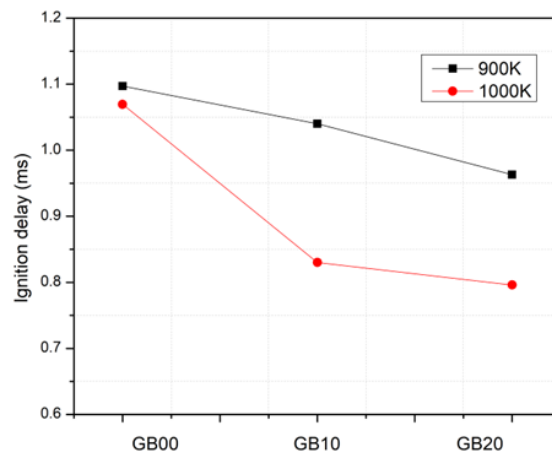


Figure 7.4: Ignition delay of GB fuel blend at 900 K and 1000 K of ambient temperature and 90 MPa injection pressure under 15 kg/m³ ambient density

7.4 Flame development

Figures 7.5 and 7.6 depict the combustion process at ambient temperatures of 900 K and 1000 K. For most fuel mixtures, flame initiation occurs around 1 ms at 900 K and 0.8 ms at 1000 K, with GB20 fuel consistently showing the earliest flame appearance. Once ignited, the flame spreads downstream with multiple ignition points, especially near the wall. Higher biodiesel content in the fuel increases luminous intensity due to the reduced ignition delay. The brightness threshold also rises with increasing ambient temperatures, which promote auto-ignition and affect flame brightness. Comparing ignition delay values from Figures 7.5 and 7.6, those obtained via natural brightness methods show similar trends but are generally higher than those calculated through the heat release rate. Using high-octane gasoline with added biodiesel improves the combustion process, leading to more stable injector operation and enhancing the efficiency and reliability of GCI engines.

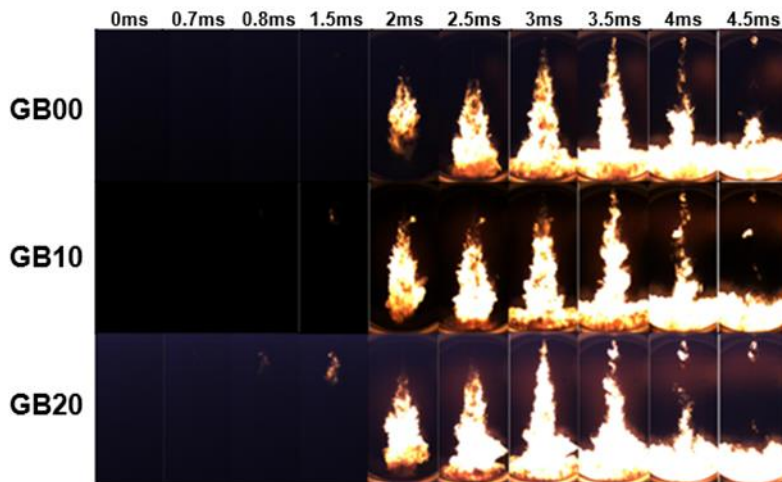


Figure 7.5: Flame development of GB00, GB10 and GB20 under the temperature of 900K and 90MPa of injection pressure under 15kg/m^3 ambient density

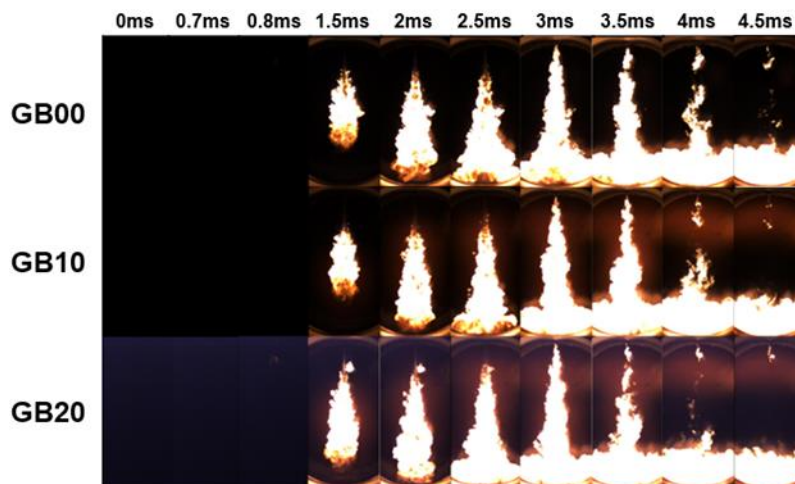


Figure 7.6: Flame development of GB00, GB10 and GB20 under the temperature of 1000K and 90MPa of injection pressure under 15kg/m^3 ambient gas density

7.5 Summary

This study focuses on the combustion dynamics of gasoline-biodiesel (GB) blends under GCI engine conditions. It provides critical data on the non-vaporizing characteristics of high-octane fuel blends by varying injection pressure and ambient gas density. The research examines fundamental spray characteristics, including spray penetration length and cone angle, and offers a detailed view of spray development and morphology.

Key findings reveal that spray penetration length increases with a higher biodiesel ratio, accelerating the penetration rate. Conversely, increased ambient gas density slows down spray development. The spray cone angle decreases gradually as injection pressure and biodiesel

content rise, reflecting injection principles and kinetic trends influenced by environmental density and fuel properties.

The study also explores how ambient temperature within the combustion chamber affects combustion characteristics. Most GB blends ignite once due to gasoline content, with both heat release rate and ignition delay decreasing as biodiesel content increases. Higher ambient temperatures further reduce ignition delay, enhancing fuel vaporization. High-speed camera images confirm this trend with visible flame development. Overall, combining high-octane gasoline with biodiesel improves combustion efficiency and stability, enhancing the performance and reliability of GCI engines and highlighting its potential for advancing engine technology.

8. Conclusions

The purpose of this dissertation is to propose a comprehensive study on the combustion process of gasoline-biodiesel fuel blends under GCI engine conditions. The difference from studies on conventional engines is that this research can create experimental conditions according to predefined objectives and can visually observe the combustion process through optical setups. Observing the combustion process occurring in a very short time is challenging and difficult to achieve on actual engines, and it often requires high costs to experiment on an optical engine. Additionally, the use of high-precision data collection systems helps reduce uncertainty in the results. Measurements of the injection process and fundamental combustion characteristics such as ignition delay are difficult to obtain in LTC engine conditions. In these conditions, ignition delay strongly influences the combustion phase, and small differences can cause the engine to transition to knocking and misfiring states. This high sensitivity hinders reliable ignition delay measurements for different load and speed conditions. Furthermore, the systems also have advantages such as well-controlled (or uncontrolled) flow interactions, powerful tools for measuring low-temperature combustion injection processes, high load, and easily configurable optical techniques.

Based on the experimental results, several main conclusions can be drawn as follows:

- Chapter 1: The concept of the Gasoline Compression Ignition (GCI) engine is introduced in this chapter. Alongside this, the motivation and approach for this research are described sequentially. Additionally, the objectives of this study are detailed with respect to the spray combustion process in GCI engines.
- Chapter 2: The literature review of the spray combustion process in GCI engines is presented according to the stages of research and application in GCI engines. The advantages and existing disadvantages of GCI engines are also detailed. Additionally, the theories of optical research methods and methods for determining combustion characteristics are listed sequentially according to the research trends of this thesis. An overall picture of fuel sources and trends in alternative fuels globally is also covered in this chapter.
- Chapter 3: The research was primarily conducted through experimental investigations of the spray combustion process. The Constant Volume Combustion Chamber (CVCC) system was flexibly applied to the process based on various gas intake methods. The

study also presented algorithm diagrams and developed control program models for these processes. Additionally, different optical methods were applied to compare the suitability and accuracy of each method for specific spray combustion processes. Furthermore, calculation methods and the determination of ignition delay values were also addressed.

- Chapter 4: The evaluation of injection properties for fuel types GB10, GB20, and GB40 under different ambient density conditions and injection durations of 1200 μs and 1500 μs reveals several key findings. The stability of the spraying process, observed from 700 μs onwards, results in minimal fluctuations in spray angle and more stable spray boundaries. Notably, increased biodiesel content in the fuel enhances spray penetration length due to fuel characteristics and changes in injection momentum. However, there's a trade-off as higher biodiesel content leads to faster fuel penetration into the cylinder, which may not efficiently enhance mixing with internal air. Increasing ambient gas density, under similar injection pressure conditions, enlarges the spray cone angle and prolongs spray existence before reaching the chamber wall. This relationship is influenced by injection pressure, duration, and ambient gas density, affecting spray area formation and ultimately the degree of air-fuel mixing. The paper's analysis of spray penetration for each fuel type demonstrates the intricate interplay between injection pressure, ambient gas density, and biodiesel composition, providing valuable insights for research on GCI engines using high-octane fuel with longer ignition delay.
- Chapter 5: The effect of temperature is the key factor tested in this chapter, in addition to injection pressure, chamber density and injector angle. Spray evolution tends to develop more quickly as the chamber temperature increases. Additionally, the results show a decreasing trend in spray cone angle when the temperature is gradually increased under constant conditions of rail pressure and ambient density. Similar to the trend of spray penetration length, the spray penetration rate and spray area also followed the same increasing trend with chamber temperature, stabilizing under the same test conditions. One notable contribution in this study is that the optical setup has overcome the disadvantages from the previous study. The shock wave image is shown more clearly when increasing the injection pressure with larger and denser turbulence. On the other hand, changing the injector angle also evaluates the influence on the result of spray formation. The evidence has always shown that the spray formation process at

the 90° injector angle is dominant. This study also provides the necessary reference data for research on fuels using combustion simulation systems such as CVCC or RCEM. Based on the results obtained in this study and the previous study on non-vaporizing spray, it will form the basis for further research on GCI engine conditions through the following stages: vaporization and combustion in the desired temperature ranges.

- Chapter 6: The evaluation of the vaporization spray process for gasoline-biodiesel fuel mixtures under GCI engine conditions reveals several key findings. Both GB20 and GB40 fuels exhibit distinct regions for the liquid and vapor phases across the entire range of injection pressures and experiment temperatures (600-800-1000 K). The liquid phase gradually decreases from 600 μ s until reaching the chamber wall for both fuels, with the vaporization boundary region appearing after 500 μ s from the spray's initiation. Interestingly, different injection pressure levels show no significant differences in liquid area results at identical temperature levels. While the spray angle of the liquid portion in GB20 fuel tends to be lower than that of GB40 before 600 μ s, the differences diminish as the vaporization phase begins. Furthermore, the vaporization phase exhibits an increasing morphology as it approaches the combustion chamber wall, with higher injection pressures leading to faster development and shorter times across all temperature and fuel type cases considered in this study.
- Chapter 7: Furthermore, the research delves into the influence of ambient chamber temperature on combustion characteristics, revealing that most fuel blends exhibit single-time ignition primarily due to gasoline presence. Heat release rate and ignition delay decrease with increased biodiesel content and rising ambient temperature, facilitated by enhanced fuel vaporization. The study also emphasizes the importance of calculating engine design and refining combustion processes, elucidating the close interplay between non-vaporization, vaporization, and combustion processes. Integration of high-octane gasoline with added biodiesel enhances combustion stability, ensuring more reliable injector operation and improving GCI engine efficiency. These findings, combined with previous studies, provide crucial data for developing and applying GCI engines with high-octane fuel, albeit further investigation into soot formation, NO_x emissions, and exhaust components is warranted for refining experimental matrices and achieving stable GCI operation under varying loads. Tribology experiments and durability tests will further elucidate engine stability when

operating with proposed fuel types, offering insights for direct GCI condition application without altering engine structure.

The contributions of the research are presented as follows:

- The research process applies entirely to high-octane fuel under GCI engine operating conditions.
- It has been proven that GB20 fuel is applicable to low and medium load conditions of GCI engines.
- The comprehensive process from injection, atomization, vaporization and combustion is investigated.
- The relationship between injection process and combustion characteristics is established to evaluate combustion characteristics.
- It is appreciated that chamber temperature and ambient temperature have a profound influence on the characteristics of the spraying process.
- The parameters of the combustion process are fully implemented and provide the necessary data for experimental research on GCI engines using high-octane fuel as well as simulation models of the spray combustion process.

References

- [1] Richard Stone and Jeffren K. Ball, *Automotive Engineering Fundamentals*, Warrendale, USA: SAE Order No, R-199, 2004.
- [2] John B. Heywood, *Internal combustion engine fundamentals*, McGraw-Hill Education: New York, USA, 1988.
- [3] Willard W. Pulkrabek, *Engineering Fundamentals of the internal combustion engine*, Prentice Hall Upper Saddle River, USA: New Jersey 07458, 1997.
- [4] Gautam T Kalghatgi, "The outlook for fuels for internal combustion engines," *International Journal of Engine Research*, vol. 15, no. 4, pp. 383-398, 2014.
- [5] Charles J. Mueller, André L. Boehman, and Glen C. Martin, "An experimental investigation of the origin of increased NO_x emission when fueling a heavy-duty compression ignition engine with soy biodiesel," *SAE international*, vol. 01, no. 1792, p. 28, 2009.
- [6] Reed Hanson, Derek A. Splitter, and Rolf Reitz, "Operating a heavy-duty direct-injection compression-ignition engine with gasoline for low emissions," *SAE Technical Paper*, vol. 01, no. 1442, p. 12, 2019.
- [7] National Research Council, *Technologies and approaches to reducing the fuel consumption of medium-and heavy-duty vehicles*, U.S: National Academies Press, 2010.
- [8] Changming Gong, Xiankai Si, Fenghua Liu, Comparative analysis on combustion and emissions between CO₂ and EGR dilution GDI engine at half-load, stoichiometric and lean-burn conditions, *Fuel*, Volume 309, 2022, 122216, ISSN 0016-2361, <https://doi.org/10.1016/j.fuel.2021.122216>.
- [9] Xiumin Yu, Tianqi Wang, Zezhou Guo, Zhe Zhao, Decheng Li, Yinan Li, Tianyang Gong, Effect of exhaust gas recirculation(EGR) on combustion and emission of butanol/gasoline combined injection engine, *Energy*, Volume 295, 2024, 130940, ISSN 0360-5442, <https://doi.org/10.1016/j.energy.2024.130940>.
- [10] Chang-MingGong, KuoHuang, Jing-Long Jia, Yan Su, Qing Gao, and Xun-JunLiu, "Improvement of fuel economy of a direct-injection spark-ignition methanol engine under light loads," *Fuel*, vol. 90, no. 5, pp. 1826-1832, 2011.
- [11] Jinhua Wang, Zuohua Huang, Chenglong Tang, and Jianjun Zheng, "Effect of hydrogen addition on early flame growth of lean burn natural gas-air mixtures," *International Journal of Hydrogen Energy*, vol. 35, no. 13, pp. 7246-7252, 2010.
- [12] Sage L. Kokjohn, Reed M. Hanson, Derek A. Splitter, and Rolf D. Reitz, "Experiments and Modeling of Dual-Fuel HCCI and PCCI Combustion Using In-Cylinder Fuel Blending," *SAE International Journal of Engines*, vol. 01, no. 2647, p. 51, 2009.
- [13] Wei JefThoo, ArmanKevric, Hoon KiatNg, SuyinGan, PaulShayler, and AntoninoLa Roccab, "Characterisation of ignition delay period for a compression ignition engine operating

on blended mixtures of diesel and gasoline," *Applied Thermal Engineering*, vol. 66, no. 1-2, pp. 55-64, 2014.

[14] Yu Chao, Wang Jian-xin, Wang Zhi, and Shuai Shi-jin, "Comparative study on gasoline homogeneous charge induced ignition (HCII) by diesel and gasoline/diesel blend fuels (GDBF) combustion," *Fuel*, vol. 106, pp. 470-477, 2013.

[15] Shuaiyng Ma, Zunqing Zheng, Haifeng Liu, Quanchang Zhang, and Mingfa Yao, "Experimental investigation of the effects of diesel injection strategy on gasoline/diesel dual-fuel combustion," *Applied Energy*, vol. 109, pp. 202-212, 2013.

[16] Dong Hana, Andrew M.Ickes, Stanislav V.Bohac, Zhen Huang, and Dennis N.Assanis, "HC and CO emissions of premixed low-temperature combustion fueled by blends of diesel and gasoline," *Fuel*, vol. 9, pp. 13-19, 2012.

[17] Reed M. Hanson, Sage L. Kokjohn, Derek A. Splitter, and Rolf D. Reitz, "An Experimental Investigation of Fuel Reactivity Controlled PCCI Combustion in a Heavy-Duty Engine," *SAE international journal of engines*, vol. 01, no. 0864, 2010.

[18] Binbin Yang, Mingfa Yao, Wai K.Cheng, Yu Li, Zunqing Zheng, and Shanju Lia, "Experimental and numerical study on different dual-fuel combustion modes fuelled with gasoline and diesel," *Applied Energy*, vol. 113, p. 722–733, 2014.

[19] Scott Curran, Vitaly Prikhodko, Kukwon Cho, C. Scott Sluder, James Parks, Robert Wagner, Sage Kokjohn, and Rolf D. Reitz, "In-cylinder fuel blending of gasoline/diesel for improved efficiency and lowest possible emissions on a multi-cylinder light-duty diesel engine," *SAE Technical Papers*, vol. 01, no. 2206, 2010.

[20] Xiangang Wang, Zuohua Huang, Olawole AbiolaKuti, Wu Zhang, and Keiya Nishida, "An experimental investigation on spray, ignition and combustion characteristics of biodiesels," *Proceedings of the Combustion Institute*, vol. 33, pp. 2071-2077, 2011.

[21] Xiangang Wang, Olawole Abiola Kuti, Wu Zhang, Keiya Nishida, and Zuohua Huang , "Effect of injection pressure on spray flame characteristics and combustion of biodiesel fuel injected by common rail injection system," *Combustion Science and Technology*, vol. 182, no. 10, pp. 1369-1390, 2010.

[22] Cory A.Adams, Paul Loeper, Roger Krieger, Michael J.Andrie, and David E.Foster, "Effects of biodiesel-gasoline blends on gasoline direct-injection compression ignition (GCI) combustion," *Fuel*, vol. 111, p. 784–90, 2013.

[23] Yanuandri Putrasari, and Ocktaeck Lim, "A study on combustion and emission of GCI engines fueled with gasoline-biodiesel blends," *Fuel* , vol. 189, p. 141–154, 2017.

[24] Yanuandri Putrasari, and Ocktaeck Lim, "A study of a GCI engine fueled with gasoline-biodiesel blends under pilot and main injection strategies," *Fuel*, vol. 221, p. 269–282, 2018.

[25] Decker, *The Use of Synthetic JP-8 Fuels in Military Engines*, MI: RDECOM-TARDEC, 2008.

[26] Peter Schihl and Laura Hoogterp, *On the Ignition and Combustion Variances of Jet Propellant-8 and Diesel Fuel in Military Diesel Engines*, MI: RDECOM-TARDEC, 2008.

- [27] Pickett, L. M., Siebers, D. L., and Idicheria, C. A, "Relationship between ignition processes and the lift-off length of diesel fuel jets," SAE Technical Paper, 2005.
- [28] Siebers, D. L., and Higgins, B., "Flame lift-off on direct-injection diesel sprays under quiescent conditions," SAE Technical Paper, 2001.
- [29] Kalghatgi, G., Agarwal, A.K., Goyal, H., Houidi, M.B. (2022). Introduction to Gasoline Compression Ignition Technology: Future Prospects. In: Kalghatgi, G., Agarwal, A.K., Goyal, H., Houidi, M.B. (eds) Gasoline Compression Ignition Technology. Energy, Environment, and Sustainability. Springer, Singapore. https://doi.org/10.1007/978-981-16-8735-8_1
- [30] WON, Hyun Woo. 2021. "A Method and System for Combining the Advantages of Gasoline Compression Ignition (GCI) Engine Technologies into Hybrid Electric Vehicles (HEVs)" Applied Sciences 11, no. 21: 9934. <https://doi.org/10.3390/app11219934>
- [31] Solanki, V.S., Mustafi, N.N., Agarwal, A.K. (2020). Prospects of Gasoline Compression Ignition (GCI) Engine Technology in Transport Sector. In: Singh, A., Sharma, N., Agarwal, R., Agarwal, A. (eds) Advanced Combustion Techniques and Engine Technologies for the Automotive Sector. Energy, Environment, and Sustainability. Springer, Singapore. https://doi.org/10.1007/978-981-15-0368-9_5
- [32] Raman, V. et al. (2022). Spark Assisted Gasoline Compression Ignition (SAGCI) Engine Strategies. In: Kalghatgi, G., Agarwal, A.K., Goyal, H., Houidi, M.B. (eds) Gasoline Compression Ignition Technology. Energy, Environment, and Sustainability. Springer, Singapore. https://doi.org/10.1007/978-981-16-8735-8_5
- [33] Gautam T. Kalghatgi, Per Risberg, Hans-Erik Ångström, "Advantages of Fuels with High Resistance to Auto-ignition in Late-injection, Low-temperature, Compression Ignition Combustion," SAE International, Vols. 2006-10-16, p. 14, 2006.
- [34] John E. Dec, Wontae Hwang, Magnus Sjöberg, "An Investigation of Thermal Stratification in HCCI Engines Using Chemiluminescence Imaging," SAE International, Vols. 2006-04-03, p. 20, 2006.
- [35] John E. Dec and Wontae Hwang, "Characterizing the Development of Thermal Stratification in an HCCI Engine Using Planar-Imaging Thermometry," SAE International, Vols. 2009-01-0650, 2009.
- [36] John E. Dec and Yi Yang, "Boosted HCCI for High Power without Engine Knock and with Ultra-Low NOx Emissions - using Conventional Gasoline," SAE International, Vols. 2010-01-1086, 2010.
- [37] Adams, "Effects of biodiesel-gasoline blends on gasoline direct-injection compression ignition (GCI) combustion," Fuel, vol. 111, pp. 784-790, 2013.
- [38] Akhilendra Pratap Singh, Nikhil Sharma, Ramesh Agarwal, and Avinash Kumar Agarwal Editors, Advanced Combustion Techniques and Engine Technologies for the Automotive Sector, USA: Department of Mechanical Engineering and Materials Science, 2018.
- [39] R. J. Goldstein, "Fluid Mechanics." Academic Press, 2017.

- [40] G. S. Settles, "Schlieren and Shadowgraph Techniques: Visualizing Phenomena in Transparent Media." Springer, 2011.
- [41] W. Meier and J. H. Frank, "Schlieren and Shadowgraph Techniques: Visualizing Phenomena in Transparent Media," *Experimental Fluid Mechanics*, vol. 55, no. 3, pp. 123-145, 2015.
- [42] M. Raffel et al., "Schlieren and Shadowgraph Techniques: Visualizing Phenomena in Transparent Media." Springer, 2007.
- [43] Yang S, MaZ, Li X, Hung DL, XuM (2020) A review on the experimental non-intrusive investigation of fuel injector phase changing flow. *Fuel* 259.
- [44] Bougie B, Tulej M, Dreier T, Dam NJ, Ter Meulen JJ, Gerber T (2005) Optical diagnostics of diesel spray injections and combustion in a high-pressure high-temperature cell. *Appl Phys B* 80(8):1039–1045
- [45] Ahmed Mohammed Elbanna, Cheng Xiaobei, Yang Can, Medhat Elkelawy, Hagar Alm-Eldin Bastawissi, Hitesh Panchal, Fuel reactivity-controlled compression ignition engine and potential strategies to extend the engine operating range: A comprehensive review, *Energy Conversion and Management: X*, Volume 13, 2022, 100133, ISSN 2590-1745, <https://doi.org/10.1016/j.ecmx.2021.100133>.
- [46] Yu Zhang, Qianchen Peng, Chunmei Wang, Yuhan Huang, Pei Zhou, Yejian Qian, Bin Ye, T.M. Indra Mahlia, Hwai Chyuan Ong, State-of-the-art modeling of two-stage auto-ignition: Turbulence, evaporation and chemistry effects, *Energy Conversion and Management*, Volume 291, 2023, 117269, ISSN 0196-8904, <https://doi.org/10.1016/j.enconman.2023.117269>.
- [47] Rajavasanth Rajasegar, Yoichi Niki, Zheming Li, Jose Maria García-Oliver, Mark P.B. Musculus, Influence of pilot-fuel mixing on the spatio-temporal progression of two-stage autoignition of diesel-sprays in low-reactivity ambient fuel-air mixture, *Proceedings of the Combustion Institute*, Volume 38, Issue 4, 2021, Pages 5741-5750, ISSN 1540-7489, <https://doi.org/10.1016/j.proci.2020.11.005>.
- [48] Phuong X. Pham, Nam V.T. Pham, Thin V. Pham, Vu H. Nguyen, Kien T. Nguyen, Ignition delays of biodiesel-diesel blends: Investigations into the role of physical and chemical processes, *Fuel*, Volume 303, 2021, 121251, ISSN 0016-2361, <https://doi.org/10.1016/j.fuel.2021.121251>.
- [49] Rothamer, D. A., and Murphy, L, "Systematic study of ignition delay for jet fuels and diesel fuel in a heavy-duty diesel engine," *Proceedings of the Combustion Institute*, vol. 34, no. 2, pp. 3021-3029, 2013.
- [50] Caton, P. A., Hamilton, L. J., and Cowart, J. S, "Understanding ignition delay effects with pure component fuels in a single-cylinder diesel engine," *Journal of engineering for gas turbines and power*, vol. 133, no. 3, p. 032803, 2011.
- [51] Assanis DN, Filipi ZS, Fiveland SB, Syrimis M, "A Predictive Ignition Delay Correlation under Steady State and Transient Operation of a Direct Injection Diesel Engine," in *Fall Technical Conference*, 1999.

- [52] Higgins, B., Siebers, D. L., and Aradi, A., "Diesel-spray ignition and premixed-burn behavior," SAE Technical Paper, pp. 0148-7191, 2000.
- [53] Lahiri D, Mehta P, Poola R, Sekar R, "Utilization of Oxygen-Enriched Air in Diesel Engines: Fundamental Considerations.," in ASME Paper No. 97-ICE-72, New York , 1997.
- [54] Hardenberg HO, and Hase, FW, "An empirical formula for computing the pressure rise delay of a fuel from its cetane number and from the relevant parameters of direct-injection diesel engines," SAE International, vol. 790493, p. 12, 1979.
- [55] P. A. Lakshminarayanan, Yogesh V. Aghav, Ignition Delay in a Diesel Engine, Dordrecht: Springer, 2009.
- [56] Shubhra Kanti Das, Kihyun Kim, and OcktaeckLim, "Experimental study on non-vaporizing spray characteristics of biodiesel-blended gasoline fuel in a constant volume chamber," Fuel Processing Technology, vol. 178, pp. 322-335, 2018.
- [57] Peter M. Lillo, Lyle M. Pickett, Helena Persson, Oivind Andersson and Sanghoon Kook, "Diesel spray ignition detection and spatial/temporal correction," SAE International, vol. 5, no. 3, pp. 1330-1346, 2012.
- [58] Chong Cheng, Rasmus Faurskov Cordtz, Troels Dyhr Pedersen, Kim Winther, Niels Langballe Fjørby, Jesper Schramm, Investigation of combustion characteristics, physical and chemical ignition delay of methanol fuel in a heavy-duty turbo-charged compression ignition engine, Fuel, Volume 348, 2023, 128536, ISSN 0016-2361, <https://doi.org/10.1016/j.fuel.2023.128536>.
- [59] Ziming Yang, Chunguang Fei, Yikai Li, Dongfang Wang, Chenhan Sun, Experimental study of the effect of physical and chemical properties of alcohols on the spray combustion characteristics of alcohol-diesel blended fuels, Energy, Volume 263, Part E, 2023, 126158, ISSN 0360-5442, <https://doi.org/10.1016/j.energy.2022.126158>.
- [60] Casey Fuller, Ponnuthurai Gokulakrishnan, Michael S. Klassen, Barry V. Kiel, and Richard Roby, "Investigation of the Effects of Vitiated Conditions on the Autoignition of JP-8," 5th AIAA/ASME/SAE/ASEE Joint Propulsion Conference & Exhibit, no. 4925, 2009.
- [61] S Kobori, T Kamimoto, and A. A. Aradi, "A study of ignition delay of diesel fuel sprays," Int J Engine Research, vol. 1, no. 1, pp. 29-39, 1999.
- [62] Varun Ramesh, Daniel Janecek, David A Rothamer, and Jaal B Ghandhi, "Spray ignition measurements in a constant volume combustion vessel under engine-relevant conditions," in Internal combustion engines, Knoxville, 2016.
- [63] Dung Nguyen and Damon Honnery, "Combustion of bio-oil ethanol blends at elevated pressure," Fuel, vol. 87, no. 2, pp. 232-243, 2008.
- [64] Jinwoo Lee and Choongsik Bae, "Application of JP-8 in a heavy duty diesel engine," Fuel, vol. 90, no. 5, pp. 1762-1770, 2011.
- [65] Lyle M. Pickett and Laura Hoogterp, "Fundamental Spray and Combustion Measurements of JP-8 at Diesel Conditions," SAE International Journal of Commercial Vehicles, vol. 1, pp. 108-118, 2009.

- [66] A. Smith et al., "Visualization of combustion process in gasoline compression ignition (GCI) engines using natural luminosity," *Combust. Sci. Technol.*, vol. 190, no. 4, pp. 753-769, 2018.
- [67] B. Jones and C. Johnson, "Observation of flame development and propagation in gasoline compression ignition (GCI) engines using natural luminosity," *J. Combust. Eng.*, vol. 25, no. 2, pp. 112-126, 2019.
- [68] C. Brown and D. Miller, "Quantification of flame characteristics in gasoline compression ignition (GCI) engines using natural luminosity," *Fuel*, vol. 210, pp. 123-135, 2020.
- [69] D. Gupta et al., "Analysis of flame speed and structure in gasoline compression ignition (GCI) engines using natural luminosity," *J. Eng. Combust.*, vol. 18, no. 3, pp. 209-223, 2017.
- [70] E. Choi and F. Lee, "Correlation of natural luminosity with combustion kinetics in gasoline compression ignition (GCI) engines," *Int. J. Combust. Sci.*, vol. 30, no. 1, pp. 45-57, 2019.
- [71] F. Wang and G. Chen, "Temporal evolution of natural luminosity and its correlation with combustion timing in gasoline compression ignition (GCI) engines," *Combust. Eng.*, vol. 35, no. 4, pp. 301-315, 2018.
- [72] G. Kim and H. Park, "Insights into combustion phenomena in gasoline compression ignition (GCI) engines using natural luminosity," *J. Energy Combust.*, vol. 42, no. 3, pp. 211-225, 2020.
- [73] H. Yang et al., "Investigation of pre-mixed combustion and transition regimes in gasoline compression ignition (GCI) engines using natural luminosity," *Proc. Combust. Inst.*, vol. 37, no. 4, pp. 5001-5010, 2018.
- [74] I. Zhao and J. Liu, "Spatial and temporal evolution of luminous regions in gasoline compression ignition (GCI) engines and their correlation with combustion modes," *Combust. Sci. Technol.*, vol. 198, no. 2, pp. 221-235, 2019.
- [75] Charles Forsberg, What is the long-term demand for liquid hydrocarbon fuels and feedstocks? *Applied Energy*, Volume 341, 2023, 121104, ISSN 0306-2619, <https://doi.org/10.1016/j.apenergy.2023.121104>.
- [76] Muhammed Zafar Ali Khan, Haider Ali Khan, Sai Sudharshan Ravi, James WG Turner, Muhammad Aziz, Potential of clean liquid fuels in decarbonizing transportation – An overlooked net-zero pathway?, *Renewable and Sustainable Energy Reviews*, Volume 183, 2023, 113483, ISSN 1364-0321, <https://doi.org/10.1016/j.rser.2023.113483>.
- [77] Maria Chiara Massaro, Roberta Biga, Artem Kolisnichenko, Paolo Marocco, Alessandro Hugo Antonio Monteverde, Massimo Santarelli, Potential and technical challenges of on-board hydrogen storage technologies coupled with fuel cell systems for aircraft electrification, *Journal of Power Sources*, Volume 555, 2023, 232397, ISSN 0378-7753, <https://doi.org/10.1016/j.jpowsour.2022.232397>.

- [78] Muhammad Yousaf Raza, Fuels substitution possibilities, environment and the technological progress in Bangladesh's transport sector, *Heliyon*, Volume 9, Issue 2, 2023, e13300, ISSN 2405-8440, <https://doi.org/10.1016/j.heliyon.2023.e13300>.
- [79] Lorenc Malka, Flamur Bidaj, Alban Kuriqi, Aldona Jaku, Rexhina Roçi, Alemayehu Gebremedhin, Energy system analysis with a focus on future energy demand projections: The case of Norway, *Energy*, Volume 272, 2023, 127107, ISSN 0360-5442, <https://doi.org/10.1016/j.energy.2023.127107>.
- [80] Rigogiannis, Nick, Ioannis Bogatsis, Christos Pechlivanis, Anastasios Kyritsis, and Nick Papanikolaou. 2023. "Moving towards Greener Road Transportation: A Review" *Clean Technologies* 5, no. 2: 766-790. <https://doi.org/10.3390/cleantechnol5020038>
- [81] ExxonMobil, "Energy and environment," Copyright 2003-2019 Exxon Mobil Corporation, 2012. [Online]. Available: http://www.exxonmobil.co.uk/corporate/files/news_pub_eo2012.pdf. [Accessed accessed 23 July 2013].
- [82] International Energy Agency, "Technology road-map: biofuels for transport," Technology road-map: biofuels for transport, 2013. [Online]. Available: http://www.iea.org/publications/freepublications/publication/Biofuels_Roadmap.pdf. [Accessed 2013].
- [83] Tim Steinweg, Barbara Kuepper, Matt Piotrowski, "Palm Oil Biofuels Market May See Shake-Up in 2020, Heightening Leakage Risks," *Chain reaction research*, p. 11, 2019.
- [84] Wolfgang Vogel, "UFOP Report on Global Market Supply 2017/2018," Chairman of the UFOP Executive Board, Berlin, 2018.
- [85] Masjuki Hj.Hassan and Md. Abul Kalam, "An overview of biofuel as a renewable energy source: Development and challenges," *Procedia Engegy*, vol. 56, p. 39–53, 2013.
- [86] Jin Suk Lee, "Experiences, Challenging Issues and Future Prospects on Biodiesel Implementation on Biodiesel Implementation in Korea," *Bioenergy Research Center*, Daejeon, 2007.
- [87] Daniel C. Oren, Syed Wahiduzzaman, and Colin R. Ferguson, "A Diesel Combustion Bomb: Proof of Concept," *SAE international*, vol. 10, no. 1, 1984.
- [88] Binbin Yang, Shanju Li, Zunqing Zheng, Mingfa Yao, and Wai Cheng, "A comparative study on different dual-fuel combustion modes fuelled with gasoline and diesel," *SAE Technical Papers*, vol. 01, no. 0694, p. 11, 2012.
- [89] Heywood and B. John, *Internal Combustion Engine Fundamentals*, New York, McGraw-Hill (1988).
- [90] S. K. Das, K. Kim and O. Lim, Experimental study on nonvaporizing spray characteristics of biodiesel-blended gasoline fuel in a constant volume chamber, *Fuel Process. Technol.*, 178 (May 2018) 322-335.

- [91] N. A. Henein and D. J. Patterson, Emissions From Combustion Engines And Their Control, Ann Arbor Science Publishers Inc. (1972).
- [92] J. D. Naber and D. L. Siebers, Effects of gas density and vaporization on penetration and dispersion of diesel sprays, SAE Tech. Pap., 412 (1996).
- [93] T. Bohl, G. Tian, A. Smallbone and A. P. Roskilly, Macroscopic spray characteristics of next-generation bio-derived diesel fuels in comparison to mineral diesel, Appl. Energy, 186 (2017) 562-573.
- [94] Z. Wang, X. Chen, D. Vuilleumier, S. Huang and J. Tang, Experimental study on spray characteristics of emulsified diesel blending with water in a constant volume chamber, Atomization and Sprays, 26 (2016) 513-533.
- [95] Yuan W, Liao J, Li B, Zhong W. Experimental study on spray characteristics of gasoline/hydrogenated catalytic biodiesel under GCI conditions. J Chem 2020; 2020:4285460. 9 pages.
- [96] Hiroyasu H, Arai M, Structures of Fuel Sprays in Diesel Engines, (1990), 10.4271/900475.
- [97] Das SK, Kim K, Lim O. Experimental study on non-vaporizing spray characteristics of biodiesel-blended gasoline fuel in a constant volume chamber. Fuel Process Technol 2018;178(May):322–35. <https://doi.org/10.1016/j.fuproc.2018.05.009>.
- [98] Vu DN, Lim O. Experimental study on ignition characteristic of gasoline-biodiesel blended fuel in a constant-volume chamber. J Mech Sci Technol 2019;33(10): 5073–83. <https://doi.org/10.1007/s12206-019-0946-1>.
- [99] Medina M, Fatouraie M, Wooldridge M. High-Speed Imaging Studies of Gasoline Fuel Sprays at Fuel Injection Pressures from 300 to 1500 bar, SAE Tech. Pap., vol. 2018-April, no. Cvc, pp. 1–18, 2018, 10.4271/2018-01-0294.
- [100] Medina M, Zhou Y, Fatouraie M, Wooldridge M. High-Speed Imaging Study on the Effects of Internal Geometry on High-Pressure Gasoline Sprays, SAE Technical Paper 2020-01-2111, 2020, 10.4271/2020-01-2111.
- [101] Nguyen Ho Xuan Duy, Ocktaeck Lim, An investigation of the effect of chamber temperature on macroscopic spray characteristic under GCI engine conditions, Fuel, Volume 346, 2023, 128239, ISSN 0016-2361, <https://doi.org/10.1016/j.fuel.2023.128239>.
- [102] J. Yang, O. Lim, An investigation of the spray characteristics of diesel-DME blended fuel with variation of ambient pressure in a constant volume combustion chamber, J. Mech. Sci. Technol. 28 (2014) 2363–2368, <http://dx.doi.org/10.1007/s12206-014-0528-1>.
- [103] Barabás I, Todorut, I-A. Predicting the temperature dependent viscosity of biodiesel–diesel–bioethanol blends, energy. Fuel 2011;25:5767–74. <https://doi.org/10.1021/ef2007936>
- [104] Y. Bao, Q.N. Chan, S. Kook, E. Hawkes, Spray Penetrations of Ethanol, Gasoline and Iso-Octane in an Optically Accessible Spark-Ignition Direct-Injection Engine, SAE Int. J. Fuels Lubr. 7 (2014) 1010–1026, <http://dx.doi.org/10.4271/2014-01-9079>.

- [105] Shu Q, Wang J, Peng B, Wang D, Wang G. Predicting the surface tension of biodiesel fuels by a mixture topological index method, at 313K. *Fuel* 2008;87: 3586–90. <https://doi.org/10.1016/j.fuel.2008.07.007>.
- [106] Cheng Zhan, Shangqing Tong, Chenglong Tang, Zuohua Huang, The spray vaporization characteristics of gasoline/diethyl ether blends at sub-and super-critical conditions, *Applied Thermal Engineering* 164 (2020) 114453, <https://doi.org/10.1016/j.applthermaleng.2019.114453>
- [107] Jianguo Du, Balaji Mohan, Jaeheon Sim, Tiegang Fang, William L. Roberts, Experimental and analytical study on liquid and vapor penetration of high-reactivity gasoline using a high-pressure gasoline multi-hole injector, *Applied Thermal Engineering* 163 (2019) 114187.
- [108] Jianguo Du, Balaji Mohan, Jaeheon Sim, Tiegang Fang, William L. Roberts, Macroscopic non-reacting spray characterization of gasoline compression ignition fuels in a constant volume chamber, *Fuel* 255 (2019) 115818, <https://doi.org/10.1016/j.fuel.2019.115818>.
- [109] Tzanetakis T, Johnson J, Schmidt H, Atkinson W and Naber J (2022) Non-Reacting Spray Characteristics of Gasoline and Diesel With a Heavy-Duty Single-Hole Injector. *Front. Mech. Eng* 8:887657. doi:10.3389/fmech.2022.887657
- [110] R. Payri, F.J. Salvador, P. Martí-Aldaraví, D. Vaquerizo, Ecn spray g external spray visualization and spray collapse description through penetration and morphology analysis, *Appl. Therm. Eng.* 112 (2017) 304–316.
- [111] Siebers, D. L. (1998). Liquid-Phase Fuel Penetration in Diesel Sprays. SAE Tech. Paper 980809. doi:10.4271/980809
- [112] Siebers, D. L. (1999). Scaling Liquid-phase Fuel Penetration in Diesel Sprays Based on Mixing-Limited Vaporization. SAE Tech. Paper 1999-01-0528. doi:10.4271/1999-01-0528
- [113] Naber, J., and Siebers, D. L. (1996). Effects of Gas Density and Vaporization on Penetration and Dispersion of Diesel Sprays. SAE Tech. Paper 960034. doi:10.4271/960034

Appendices

List of Publications

Duy, N. H. X., Lim, O. (2022). A study on spray characteristic of gasoline-biodiesel blended under gci engines condition performed on constant volume combustion chamber system. **Journal of Mechanical Science and Technology** 36 (4) (2022) 2095~2106.<http://doi.org/10.1007/s12206-022-0343-z>

Nguyen Ho Xuan Duy, Ocktaeck Lim, An investigation of the effect of chamber temperature on macroscopic spray characteristic under GCI engine conditions, **Fuel**, Volume 346, 2023, 128239, ISSN 0016-2361,<https://doi.org/10.1016/j.fuel.2023.128239>.

Nguyen Ho Xuan Duy, Tran Quang Khai and Ocktaeck Lim, “An investigation on characteristics of spray combustion under GCI engine conditions using gasoline-biodiesel blends”, **International Journal of Energy Research – under review round 2 (status date 2024-05-20)**

Nguyen Ho Xuan Duy, Tran Quang Khai and Ocktaeck Lim, “Experimental study of the effect of high temperature on vaporization spray characteristics under GCI engine conditions”, **Energy, Elsevier, under review (status date 2024-05-20)**

Cahyani Windarto, Ardika Setiawan, **Nguyen Ho Xuan Duy,** Ocktaeck Lim, Investigation of propane direct injection performance in a rapid compression and expansion machine: Pathways to diesel marine engine efficiency parity with spark discharge duration strategies, **International Journal of Hydrogen Energy**, Volume 48, Issue 87, 2023, Pages 33960-33980, ISSN 0360-3199, <https://doi.org/10.1016/j.ijhydene.2023.05.131>.

Khoa, N.X., Putrasari, Y., Vu, D.N., **Duy, N.H.X.,** Lim, O. (2022). The Effect of Control Strategies on the Gasoline Compression Ignition (GCI) Engine: Injection Strategy, Exhaust Residual Gas Strategy, Biodiesel Addition Strategy, and Oxygen Content Strategy. In: Kalghatgi, G., Agarwal, A.K., Goyal, H., Houidi, M.B. (eds) Gasoline Compression Ignition Technology. **Energy, Environment, and Sustainability. Springer, Singapore.** https://doi.org/10.1007/978-981-16-8735-8_3

List of conferences

International conferences

Nguyen Ho Xuan Duy and Ocktaeck Lim, 13th International Conference of Applied Energy (ICAE) 2021, Bangkok, Thailand, 2021.

Nguyen Ho Xuan Duy and Ocktaeck Lim, 14th International Conference of Applied Energy (ICAE) 2022, Bochum, Germany, 2022.

Nguyen Ho Xuan Duy and Ocktaeck Lim, 15th International Conference of Applied Energy (ICAE) 2023, Doha, Qatar, 2023.

Domestic conferences

Nguyen Ho Xuan Duy and Ocktaeck Lim, 2019 KSAE Annual Spring Conference, Ramada hotel, Jeju, Korea, 2019.

Nguyen Ho Xuan Duy and Ocktaeck Lim, KSAE 2019 Annual Autumn Conference & Exhibition, Hwabaek International Convention Center, Gyeongju, Korea, 2019.

Nguyen Ho Xuan Duy and Ocktaeck Lim, 2019 KSAE Annual Spring Conference, Ramada hotel, Jeju, Korea, 2020.

Nguyen Ho Xuan Duy and Ocktaeck Lim, KSAE 2019 Annual Autumn Conference & Exhibition, Hwabaek International Convention Center, Gyeongju, Korea, 2020.

Nguyen Ho Xuan Duy and Ocktaeck Lim, KSAE, Annual Autumn Conference, Bexco, Busan, 2022.

Nguyen Ho Xuan Duy and Ocktaeck Lim, KSAE, Annual Spring Conference, Shinhwa World, Jeju, 2022.

Nguyen Ho Xuan Duy and Ocktaeck Lim, KSAE, KSAE Spring 2023 Conference Chapter Busan, Changwon and Ulsan, Ulsan, Korea, 2023.

Image processing code

```
clear; clc; close all;

px2mm = 0.609756;
nozzle_x = 7;
nozzle_y = 80;
nozzle_position = [nozzle_y, nozzle_x];
meaningful_length = 2/3;
background = imread('GB20-10-500-1500-400-1_00001.png');
img_name = 'GB20-10-500-1500-400-1_00033.png';
fig_name = 'fig_000.png';

gray2bin_threshold_full = 30000;
gray2bin_threshold_liquid = 6000;
small_size = 10;

se = strel('disk', 1);
sigma = 0.9;
background = rgb2gray(background);
background = imgaussfilt(background, sigma);
background_full = (background(:, :) >= gray2bin_threshold_full);
background_full = bwareaopen(background_full, small_size);
background_full = imcomplement(background_full);
background_full = bwareaopen(background_full, small_size);
background_liquid = (background(:, :) >= gray2bin_threshold_liquid);
background_liquid = bwareaopen(background_liquid, small_size);
background_liquid = imcomplement(background_liquid);
background_liquid = bwareaopen(background_liquid, small_size);
result2csv = [];
csvtitle = {'Img name', 'Liquid length', 'Liquid angle', 'Liquid area', 'Vapor area'};
```



```

for i = 50:-1:45
    img_name(26) = num2str(uint8(floor(i/100)));
    img_name(27) = num2str(uint8(floor(mod(i,100)/10)));
    img_name(28) = num2str(uint8(mod(i,10)));
    fig_name(5) = num2str(uint8(floor(i/100)));
    fig_name(6) = num2str(uint8(floor(mod(i,100)/10)));
    fig_name(7) = num2str(uint8(mod(i,10)));

    raw_img = imread(img_name);
    img = rgb2gray(raw_img);
    img = imgaussfilt(img, sigma);
    img_full = (img(:,:,) >= gray2bin_threshold_full);
    img_full = bwareaopen(img_full, small_size);
    img_full = imcomplement(img_full);
    img_full = bwareaopen(img_full, small_size);
    img_full = (bitxor(img_full, background_full));
    img_full = imopen(img_full, se);
    img_full = bwareaopen(img_full, small_size);
    img_liquid = (img(:,:,) >= gray2bin_threshold_liquid);
    img_liquid = bwareaopen(img_liquid, small_size);
    img_liquid = imcomplement(img_liquid);
    img_liquid = bwareaopen(img_liquid, small_size);
    img_liquid = (bitxor(img_liquid, background_liquid));
    img_liquid = imopen(img_liquid, se);
    img_liquid = bwareaopen(img_liquid, small_size);
    liquid_stat = regionprops(img_liquid, 'Centroid', 'Area');
    [B_liquid, L_liquid, N_liquid, A_liquid] = bwboundaries(img_liquid);
    liquid_particle = 0;
    for j = 1:length(liquid_stat)

```

```

    dist = sqrt((liquid_stat(j).Centroid(1) - nozzle_x)^2 + (liquid_stat(j).Centroid(2) -
nozzle_y)^2);
    if (dist < liquid_stat(j).Area)
        liquid_particle = j;
        temp_boundary = B_liquid{j};
        temp_min_x = min(temp_boundary(:, 2));
        temp_y = [];
        for k = 1:length(temp_boundary)
            if (temp_boundary(k, 2) == temp_min_x)
                temp_y = [temp_y temp_boundary(k, 1)];
            end
        end
        bot_px = max(temp_y);
        top_px = min(temp_y);
        for j = nozzle_x:(temp_min_x - 1)
            y_min = round(nozzle_y + (j - nozzle_x)/(temp_min_x - nozzle_x)*(top_px -
nozzle_y));
            y_max = round(nozzle_y + (j - nozzle_x)/(temp_min_x - nozzle_x)*(bot_px -
nozzle_y));
            for k = y_min:y_max
                img_full(k, j) = 1;
            end
        end
        break;
    end
end

if (liquid_particle ~= 0)
    liquid_x_min = min(B_liquid{liquid_particle}(:,2));
    img_liquid(:, 1:liquid_x_min) = (bitor(img_liquid(:, 1:liquid_x_min), img_full(:,
1:liquid_x_min)));
end

```

```

end
liquid_stat = regionprops(img_liquid, 'Centroid', 'Area');
liquid_particle = 0;
for j = 1:length(liquid_stat)
    dist = sqrt((liquid_stat(j).Centroid(1) - nozzle_x)^2 + (liquid_stat(j).Centroid(2) -
nozzle_y)^2);
    if (dist < liquid_stat(j).Area)
        liquid_particle = j;
        break;
    end
end
liquid_length = 0;
liquid_angle = 0;
top_ray = nozzle_position;
bot_ray = nozzle_position;
[B_liquid, L_liquid, N_liquid, A_liquid] = bwboundaries(img_liquid);
fg = figure('Name', img_name, 'Units', 'normalized', 'Position', [0 0 1 1], 'WindowState',
'maximized');
imshow(raw_img); hold on;
if (liquid_particle ~= 0)
    boundary = B_liquid{liquid_particle};

    plot(boundary(:,2), boundary(:,1), 'g', 'LineWidth', 1);

    L_max_liquid = max(B_liquid{liquid_particle}(:,2));
    liquid_length = L_max_liquid - nozzle_x;
    for j = (nozzle_x + 1):(nozzle_x + liquid_length/3*2)
        for k = 1:length(boundary)
            if ((boundary(k, 2) == j)&&(boundary(k, 1) < nozzle_y))
                top_ray = [top_ray; boundary(k,:)];
            elseif ((boundary(k, 2) == j)&&(boundary(k, 1) > nozzle_y))

```

```

        bot_ray = [bot_ray; boundary(k,:)];
    end
end
end
y_vec_1 = top_ray(:, 1);
y_vec_2 = bot_ray(:, 1);
x_vec_1 = top_ray(:, 2);
x_vec_2 = bot_ray(:, 2);
if ((length(x_vec_1)) > 0)
    x_vec_1 = x_vec_1 - nozzle_x;
    y_vec_1 = y_vec_1 - nozzle_y;
    if ((y_vec_1(:)\x_vec_1(:)) ~= 0)
        k_vec_1 = 1/(y_vec_1(:)\x_vec_1(:));
    else
        k_vec_1 = -9999;
    end
    x_vec_2 = x_vec_2 - nozzle_x;
    y_vec_2 = y_vec_2 - nozzle_y;
    if ((y_vec_2(:)\x_vec_2(:)) ~= 0)
        k_vec_2 = 1/(y_vec_2(:)\x_vec_2(:));
    else
        k_vec_2 = 9999;
    end
    liquid_angle = 180 - (abs(atan(1/k_vec_1)) + abs(atan(1/k_vec_2)));
end
top_ray = nozzle_position;
bot_ray = nozzle_position;
for j = (nozzle_x + 1):(nozzle_x + liquid_length/3*2)
    top_ray = [top_ray; [int8((j - nozzle_x)*k_vec_1) + nozzle_y, j]];
    bot_ray = [bot_ray; [int8((j - nozzle_x)*k_vec_2) + nozzle_y, j]];
end

```

```

    end
end

img_vapor = (bitxor(img_liquid, img_full));
[B_vapor, L_vapor, N_vapor, A_vapor] = bwboundaries(img_vapor);
vapor_particle = 0;
vapor_stat = regionprops(img_vapor, 'Centroid', 'Area');
area = [];
area = [vapor_stat.Area];
[M,I] = max(area);
if (M > 100)
    vapor_particle = I;
end
if (vapor_particle == 0)
    if (liquid_particle ~= 0)
        for j = 1:length(vapor_stat)
            if ((abs(vapor_stat(j).Centroid(2) - liquid_stat(liquid_particle).Centroid(2)) <
30)&&(abs(vapor_stat(j).Centroid(1) - liquid_stat(liquid_particle).Centroid(1)) < 40))
                vapor_particle = j;
                break;
            end
        end
    end
end
else
    area = [vapor_stat.Area];
    [M,I] = max(area);
end
if (vapor_particle ~= 0)
    boundary = B_vapor{vapor_particle};
    plot(boundary(:,2), boundary(:,1), 'b', 'LineWidth', 1);

```

```

end
plot(nozzle_x, nozzle_y, 'r*');
plot(bot_ray(:,2), bot_ray(:,1), 'r', 'LineWidth', 2);
plot(top_ray(:,2), top_ray(:,1), 'r', 'LineWidth', 2);

rectangle('Position', [48 2 60 23], 'Curvature', 0.1, 'FaceColor' ,[0 0 0], 'EdgeColor', 'b');
text_length_L = ['Liquid length: ' num2str(liquid_length*px2mm,'%0.2f') 'mm'];
text(50, 5, text_length_L, 'FontSize', 10, 'Color' , 'r');
if (liquid_particle ~= 0)
    area_L = liquid_stat(liquid_particle).Area*px2mm*px2mm;
else
    area_L = 0;
end
text_angle_L = ['Liquid angle: ' num2str(liquid_angle,'%0.2f') '^o'];
text(50, 10, text_angle_L, 'FontSize', 10, 'Color' , 'r');
text_area_L = ['Liquid area: ' num2str(area_L,'%0.2f') 'mm^2'];
text(50, 15, text_area_L, 'FontSize', 10, 'Color' , 'r');
if (vapor_particle ~= 0)
    area_V = vapor_stat(vapor_particle).Area*px2mm*px2mm;
else
    area_V = 0;
end
text_area_V = ['Vapor area: ' num2str(area_V,'%0.2f') 'mm^2'];
text(50, 20, text_area_V, 'FontSize', 10, 'Color' , 'r');

result2csv = [result2csv; i (liquid_length*px2mm) liquid_angle area_L area_V];
saveas(fig, fig_name);

% close(img_name);
end

```

```
T = array2table(result2csv);  
T.Properties.VariableNames = csvtitle;  
writetable(T, 'result.csv')
```